Optical parametric oscillators for precision IR spectroscopy and metrology

DISSERTATION

zur Erlangung des akademischen Grades
doctor rerum naturalium
(Dr. rer. nat.)
im Fach Physik

eingereicht an der
Mathematisch-Naturwissenschaftlichen Fakultät I
Humboldt-Universität zu Berlin

von
Herr Dipl.-Phys. Evgeny Kovalchuk
geboren am 12.11.1964 in Tschernovtsy, Ukraine

Präsident der Humboldt-Universität zu Berlin:
Prof. Dr. Dr. h.c. Christoph Markschies

Dekan der Mathematisch-Naturwissenschaftlichen Fakultät I:
Prof. Dr. Christian Limberg

Gutachter:

1. Prof. Achim Peters, PhD
2. Prof. Dr. Thomas Elsässer
3. Prof. Dr. Andreas Wicht

eingereicht am: 22. Dezember 2006
Tag der mündlichen Prüfung: 27. April 2007

Abstract

This thesis presents a continuous-wave optical parametric oscillator (cw OPO), specially developed for high-resolution Doppler-free molecular spectroscopy and metrology. The basic objective was to solve the long-standing problem of controlled access to any desired wavelength in the wide emission range of OPOs, including the ability to precisely tune the output frequency over the molecular and atomic transitions of interest. The system implemented during this work fully achieves these goals and its performance was demonstrated in various measurements and applications. Furthermore, this cw OPO was integrated with a femtosecond optical frequency comb to realize a new concept for a coherent link between the visible and infrared spectral ranges. The specific achievements include:

• *The design and development of a reliable cw OPO system with narrow linewidth output radiation and well defined frequency tuning characteristics.* For this, a new design for the OPO cavity with an intracavity etalon was implemented, extending the concept of a cw singly resonant OPO with resonated pump wave. The newly developed device, operating in the spectral ranges from 1.50 μm to 1.82 μm and from 2.56 μm to 3.66 μm, demonstrates very good long-term stability and spectral properties, which were determined in direct beat frequency measurements with a methane infrared optical frequency standard. Thus, an idler radiation linewidth of $\sim$ 12 kHz and mode-hop-free operation of the OPO over several days were observed. Furthermore, it was shown for the first time that an OPO can be phase locked to a highly stable optical reference and thus much more precisely controlled and tuned.

• *The first successful implementation of Doppler-free spectroscopy using an OPO.* This work pioneered the application of OPOs in Doppler-free spectroscopy. To detect and study nonlinear Doppler-free resonances in methane, a frequency modulation spectroscopy setup was implemented and resonances were observed in a wide range of methane pressures.

• *Invention and realization of a new concept for a direct coherent link between the visible and infrared spectral ranges.* In this concept, the cw OPO serves as a bidirectional coherent bridge between the infrared and the visible. When initially referenced to an infrared methane optical frequency

standard and combined with a femtosecond Ti:Sapphire laser comb, the OPO can be used for precise frequency measurements in the visible. On the other hand, the combination of cw OPO and comb can also take advantage of the new developments in visible optical frequency standards to synthesize highly-stable infrared radiation. As a first demonstration of this new technique, a direct absolute frequency comparison between an iodine stabilized laser at 532 nm and a methane stabilized laser at 3.39 μm was performed.

Zusammenfassung

In der vorliegenden Doktorarbeit wird ein Dauerstrich Optisch Parametrischer Oszillator (cw OPO) vorgestellt, der speziell für die hochauflösende Dopplerfreie Molekülspektroskopie und Metrologie entwickelt wurde. Der kontrollierte Zugang zu jeder beliebigen Wellenlänge im breiten Emissionsspektrum von OPOs wie auch das präzise Abstimmen seiner Ausgangsfrequenz über zu untersuchende molekulare und atomare Übergänge stellten lange Zeit Probleme dar, deren Lösung die Grundzielsetzung dieser Arbeit war. Das im Laufe dieser Arbeit entwickelte System hat diese Ziele vollständig erreicht, was durch verschiedene Messungen und Anwendungen demonstriert wurde. Weiterhin, wurde dieser cw OPO mit einem femtosekunden optischen Frequenzkamm kombiniert, um eine neue Idee für eine kohärente Verbindung zwischen dem sichtbaren und dem infraroten Spektralbereich zu realisieren. Die besonderen Leistungen dieser Arbeit sind:

• *Entwicklung und Aufbau eines zuverlässigen OPO Systems mit schmaler Linienbreite und wohldefinierter Durchstimmbarkeit der Frequenz.* Zu diesem Zweck wurde ein neues OPO-Design mit einem Intracavity-Etalon entwickelt und aufgebaut, wobei der OPO auf dem Konzept eines – schon früher in unserer Arbeitsgruppe entwickelten – einfach-resonanten cw OPOs mit resonanter Pumpwelle basiert. Die OPO-Ausgangsstrahlung liegt im Spektralbereich zwischen 1.50 μm und 1.82 μm, sowie zwischen 2.56 μm und 3.66 μm, und zeigt eine sehr gute Langzeitstabilität und sehr gute Spektraleigenschaften, welche durch direkte Frequenzvergleichsmessungen mit einem optischen Methan-Frequenzstandard im Infraroten bestimmt wurden. Eine Idler-Linienbreite von $\sim$ 12 kHz und ein Modensprung-freier Betrieb des OPOs über einen Zeitraum von einigen Tagen wurde beobachtet. Zum allerersten Mal wurde gezeigt, dass ein OPO zu einer hochstabilen optischen Referenz phasengelockt und somit seine Frequenz sehr genau kontrolliert und durchgestimmt werden kann.

• *Realisierung der ersten Dopplerfreien Spektroskopie mittels eines OPOs.* Hier wurde Pionierarbeit auf dem Gebiet der Anwendung eines OPOs in der Dopplerfreien Spektroskopie geleistet. Um nichtlineare Dopplerfreie Resonanzen in Methan aufzeichnen und untersuchen zu können, wurde ein

Aufbau zur Frequenz-Modulationsspektroskopie realisiert. Die Resonanzen wurden in einem weiten Bereich von Methan-Drücken beobachtet.

● *Idee und Realisierung eines neuen Konzepts für eine direkte kohärente Frequenzverbindung zwischen infrarotem und sichtbarem Spektralbereich.* Bei diesem Konzept dient der cw OPO als eine bidirektionale kohärente Brücke zwischen dem infraroten und dem sichtbaren Spektralbereich. Nachdem der OPO in Kombination mit einem femtosekunden Ti:Saphir-Laser Frequenzkamm zu einem IR optischen Methan-Frequenzstandard referenziert wurde, kann der OPO für hochgenaue Frequenzmessungen im Sichtbaren verwendet werden. Anderseits kann man auch die Vorteile von neuen Entwicklungen im Bereich von optischen Frequenzstandards im Sichtbaren ausnutzen und hochstabile Strahlung im Infraroten innerhalb des OPO Signal– und Idler–Durchstimmbereiches erzeugen. Als erste Demonstration dieser neuen Technologie wurde ein direkter absoluter Frequenzvergleich zwischen einem Jod-stabilisierten Laser bei 532 nm und einem Methan-stabilisierten Laser bei 3.39 μm durchgeführt.

Schlagwörter:
Optisch Parametrischer Oszillator, Femtosekunden Ti:Saphir-Laser Frequenzkamm, Präzisionsexperimente, Metrologie

for Anna

and my parents

Valentina and Vasily

Contents

List of Figures

Chapter 1

Introduction

The invention of lasers in 1960 opened up a new era in many fields of natural and applied sciences, as well as in daily life. Coming into use in practical spectroscopy, tunable laser sources called forth improvements by many orders of magnitude in sensitivity, in spectral as well as temporal resolution. Today it has become possible to resolve optical spectra at the sub-Hertz level, to manipulate and address individual atoms as well as ions and to study the intra-atomic and molecular dynamics down to attosecond timescales. Scientists now have powerful tools to look more deeply into the structure of atoms and molecules. Using lasers for trapping and cooling of neutral atoms enabled the creation of a new artificial state of ultra-cold matter in the form of atomic—and recently also molecular—Bose–Einstein condensates and Fermi gases.

An old dream of scientists investigating spectroscopical properties of different materials has been an universal laser source analogous to a radio frequency synthesizer, the very desirable properties of which are high power, narrow linewidth and wide tunability, as well as ease of use and high reliability. Contrary to many expectations, several widely tunable coherent sources, such as dye-lasers in the visible and color-center lasers in the near and mid-infrared spectral ranges, did not fulfil this desire. They are comparatively cumbersome and require bulky and ineffective Argon-ion or Krypton-ion pump lasers. Only after extensive developments in solid-state lasers, periodically poled nonlinear crystals and, recently, in femtosecond optical frequency metrology, the concept of optical synthesizers has once again moved into the focus of scientific interest.

Continuous wave Optical Parametric Oscillators (cw OPOs) can in prin-
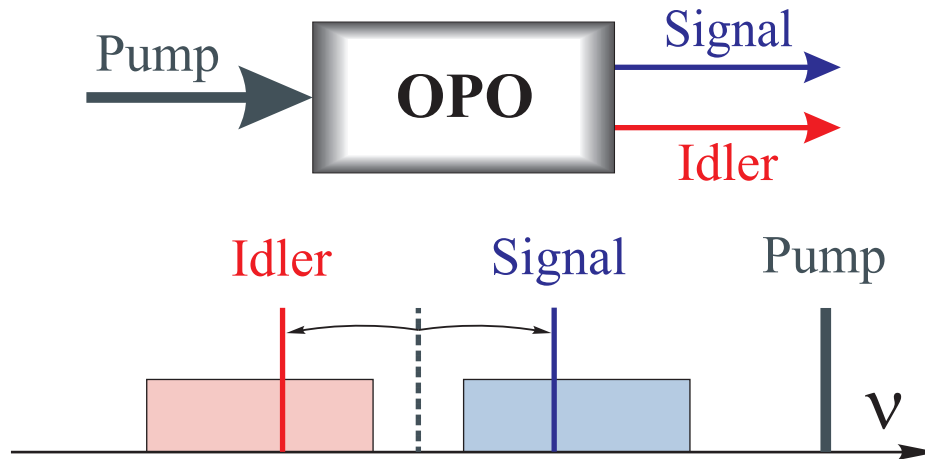
Figure 1.1: *Principle of operation of an optical parametric oscillator. Down conversion of pump photons into two lower energy photons under condition of the energy conservation: $\nu_P = \nu_S + \nu_I$. The frequencies ν_S and ν_I are determined by the phase-matching condition: $\vec{k}_P = \vec{k}_S + \vec{k}_I$.*

ciple meet all the requirements to become reliable and universal sources for optical frequency synthesis and high-resolution spectroscopy. In the last decade, several laboratories have developed such cw OPOs based on various nonlinear materials and many different designs for numerous customized spectroscopic applications were invented.

A simple depiction of the operation principle of an OPO is shown in Fig. 1.1. An OPO consists of a nonlinear crystal placed inside an optical resonator. Illumination of the crystal with a highly intense laser pump beam of frequency ν_P causes the generation of two new waves, the signal and the idler radiation with frequencies ν_S and ν_I, respectively, with $\nu_S \geq \nu_I$. In this parametric process, the law of energy conservation must hold: $\nu_P = \nu_S + \nu_I$. The net result is that a pump photon is annihilated while two other, signal and idler photons are created.

The efficiency of optical parametric amplification and generation depends directly on the phase-matching condition, which corresponds to the conservation of the momentum during such photon splitting: $\vec{k}_P = \vec{k}_S + \vec{k}_I$. Providing the phase-matching for different wavelengths results in broadly tunable optical radiation. The phase-matching condition can in particular be fulfilled for collinearly interacting waves by choosing certain polarization combinations and propagation directions in birefringent nonlinear crystals.

Alternatively, the phase mismatch due to the crystal dispersion can be compensated by preparing a micro-structured crystal with a periodically inverted polarity of the crystal domains. One way to achieve this is to use the permanent periodical poling of a ferroelectric crystal. This modern method of quasi-phase-matching in a bulk crystal was first implemented about ten years ago and subsequently initiated substantial growth in the development of new and highly efficient nonlinear materials.

To achieve self-sustained oscillations on both parametric waves, an optical resonator has to be set up around the nonlinear crystal, providing optical feedback at least for one wave. The oscillations arise after reaching some threshold level of the pump intensity, corresponding to the balance between round-trip losses and parametric gain.

There are several types of OPOs featuring different configurations of the resonant waves. In a doubly resonant OPO (DRO), the signal and idler waves both resonate in the optical cavity, while in a singly resonant OPO (SRO) only one of them is resonant. Despite of the low threshold levels, DROs are less commonly used due to their instability and mode-hop sensitivity. Such internal instability is not present in SROs. The SRO threshold, though, is comparatively high, at the level of several Watts of pump power for practical devices. However, lowering of the SRO threshold is possible by providing the resonant conditions also for the pump wave.

A cw pump resonant SRO (PR-SRO), also denoted as a pump enhanced SRO, can benefit directly from the implementation of intrinsically stable single-frequency pump sources. According to a concept, recently invented in our laboratory, the cavity length of the PR-SRO is controlled to permanently stay in resonance condition with the pump wave [1, 2, 3]. Such OPOs feature high spectral purity of output radiation and are resistant to mode hops.

1.1   OPOs as new spectroscopic tools

Coherent optical sources based on periodically poled nonlinear materials find more and more new applications in the field of broadband optical frequency conversion between the visible and the mid-infrared spectral ranges. Among them, cw OPOs have considerable utility in medicine and biology, in precise chemical analysis and in the study of molecular dynam-

OPOs pumped by 1064 nm Nd:YAG

OPOs pumped by 532 nm doubled Nd:YAG

advanced OPO systems

350   500   700   1000 1400   2000 2800   4000
Wavelength (nm)
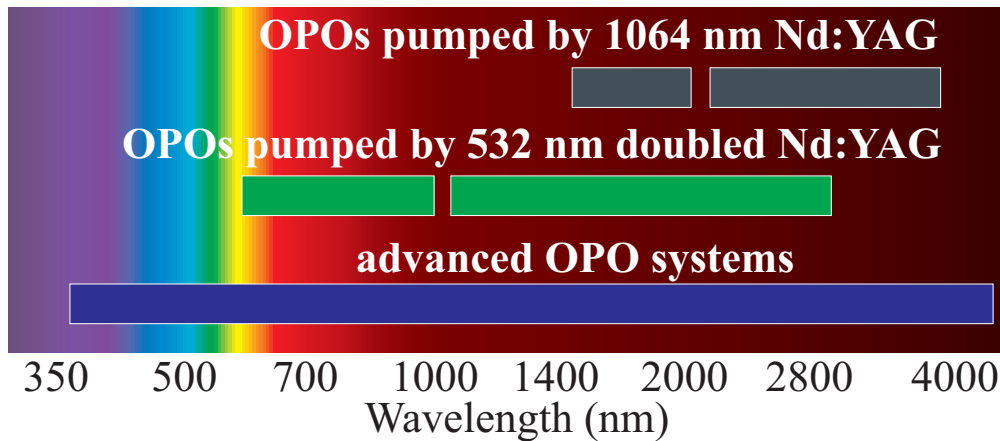
Figure 1.2: *Spectral coverage of infrared and green pumped OPO systems, developed in our laboratory. Future advanced OPO systems can use an additional stage for the second harmonic generation of the signal and idler radiation.*

ics. They have been broadly used for highly sensitive environmental monitoring and in real-time gas imaging systems operating in the mid-infrared spectral region.

Trace-gas-detection and, specifically, photoacoustic spectroscopy have become one of the main fields of practical use of OPOs [4, 5, 6]. Here, one can observe some general trends. First of all, since the detection limit of the photoacoustic spectroscopy directly depends on the applied laser power, scientists have tried to achieve more and more output power from cw OPOs.

Then, while the spectra of interest are extremely wide, spectroscopists are interested in rapidly tuning the OPO output frequency over hundreds of gigahertz, despite of discontinuity in tuning and mode hops which usually occur in this case. For these applications it is often enough to broadly tune OPOs simply by mode hopping between neighboring longitudinal cavity modes.

In contrast to the usual practice of linear Doppler-limited spectroscopy, methods of Doppler-free spectroscopy deal with very narrow optical spectra. Using this technique it is possible to resolve spectral features with extremely narrow linewidths of less than a few hundreds of Hertz. Thus, to do high-resolution Doppler-free molecular spectroscopy with OPOs, one needs to precisely tune the signal or idler wave to the desired wavelength and then to perform accurate mode-hop-free frequency sweeps over the spectral lines of interest.

The implementation of optical parametric oscillators for Doppler-free spectroscopy has been suggested for a long time. However, many such attempts undertaken by several scientific groups in the past have failed.

Technological progress in the fabrication of periodically poled nonlinear crystals, durable optical coatings and ultra-stable solid-state pump lasers have recently led to a new generation of continuous-wave optical parametric oscillators with single frequency output. Cw OPOs became one of the most promising infrared devices for high-resolution and Doppler-free molecular spectroscopy.

Recently, our research group demonstrated the successful Doppler-free spectroscopic applications of cw OPOs in the infrared and the visible spectral ranges [7, 8].

1.2 OPOs for high-resolution spectroscopy

Several cw singly resonant OPO systems covering a very wide range of the optical spectrum from the visible to the mid-infrared ($0.66 - 4.0$ μm) have been developed in our laboratory as depicted in Fig. 1.2. These OPOs provided substantial amounts ($10 - 250$ mW) of coherent radiation with narrow linewidth (< 160 kHz), continuous tunability (several GHz) and excellent long-term stability [1, 2, 9, 10, 11]. In the meantime, other groups have also demonstrated DROs with narrow linewidth signal radiation (< 13 kHz) and phase locking the beat frequency between signal and idler in a nearly degenerated DRO [12, 13].

This unique combination of features makes optical parametric oscillators very attractive tools for high-resolution molecular spectroscopy. Especially, they are one of few coherent sources available in the mid-infrared spectral region around 3 μm, where many fundamental molecular transitions occur. Several Doppler-limited spectroscopic applications of single frequency cw OPOs in the near– and mid–infrared spectral ranges have been demonstrated since 1998 [11, 14, 15, 16, 17, 18]. However, at the beginning of the research work presented here, the question about the feasibility of Doppler-free spectroscopy using OPOs was still open.

Until recently, one of the remaining challenges in using cw OPOs for spectroscopic applications has been to prevent gaps in the spectral coverage and thereby to guarantee access to every atomic and molecular transition

of interest. Such gaps were generally caused by irregularities in the non-linear crystal and etalon effects due to residual reflectivity of AR-coatings, resulting in spurious modulation of the wide OPO gain profile. While OPOs showed excellent performance at fixed output wavelengths [19, 20, 21] corresponding to local gain maxima, attempts to tune them to a desired wavelength led to unpredictable frequency hops between neighboring maxima.

To avoid these problems, it is desirable to provide additional mode selection. To this end, we have departed from a compact semi-monolithic cavity design developed previously in our laboratory for a new type of singly resonant OPO with resonated pump [1, 19, 20, 21]. We implemented an extended cavity setup with a specially designed intracavity etalon. Unlike the etalons that are commonly used in single-frequency lasers and also in a variety of singly resonant OPOs [14, 15, 22], this one is located inside a cavity with two resonated waves, of which it should only affect one (signal) and not the other (pump). It is therefore antireflection coated for the pump wave. The performance of this coating is crucial for the proper operation of the OPO.

Fig. 1.3 shows two variations of the OPO setup. In the original semi-monolithic version (a) the OPO cavity is formed by a single external mirror and a second mirror coated directly onto one face of the nonlinear crystal. To incorporate the intracavity etalon we changed the setup to an extended cavity design (b). This cavity contains the second broad beam waist at the surface of the plane output mirror, nearby which the etalon is placed.

Using the configuration with an intracavity etalon we achieve very reliable and well-predictable tuning behavior of the OPO output frequency (Fig. 1.4). All wavelengths which may be required for high-resolution spectroscopy have become immediately available. We also obtain very good long-term stability of the idler radiation with low frequency drift rates and mode-hop-free operation over several days. The OPO can be continuously tuned over several gigahertz by synchronously tuning the pump frequency and tilting the etalon or changing its temperature. The range of continuous tuning is principally limited only by that of the pump laser. We demonstrated a linewidth of the idler radiation of 12 kHz and the possibility of phase locking of the idler frequency to an optical reference.

We proved the performance of our new OPO setup, for the first time, by successfully applying an OPO in the high-resolution Doppler-free spectroscopy of methane at 3.39 μm. To record and study narrow nonlinear reso-
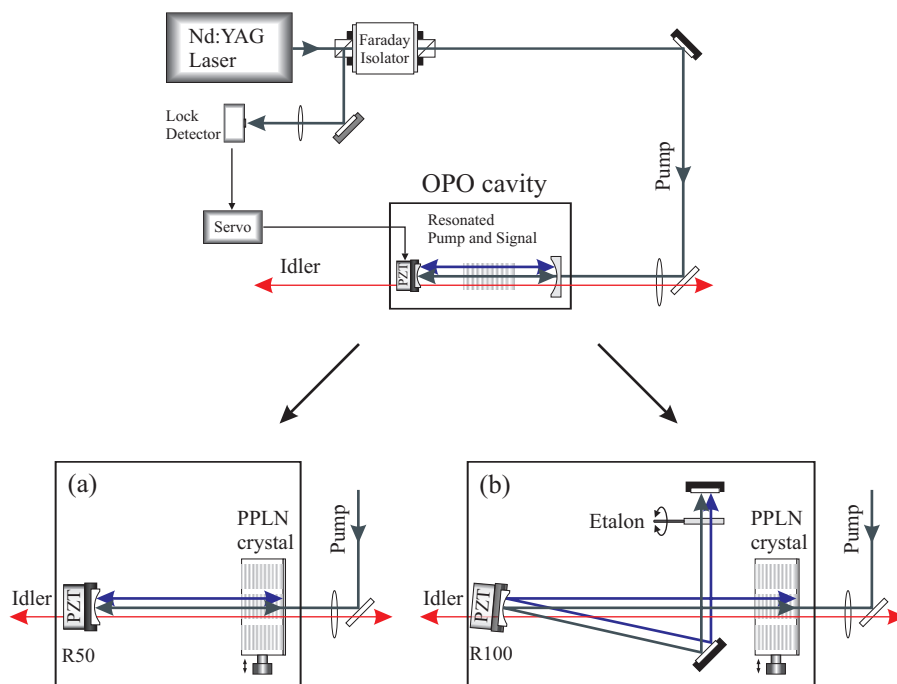
Figure 1.3: *Two variations of a pump resonant SRO: (a), semi-monolithic cavity and (b), extended cavity design with an intracavity etalon.*
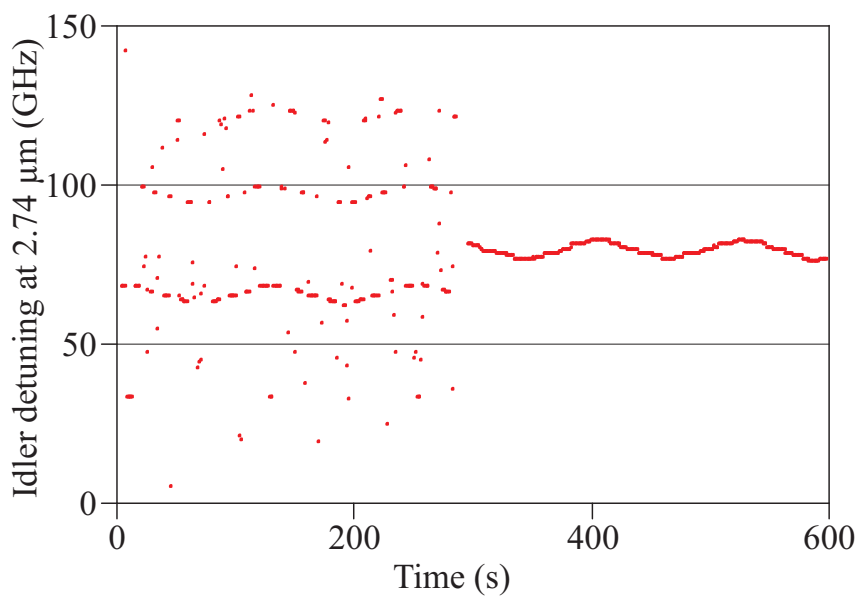
Figure 1.4: *An example of the tuning behavior of the OPO idler output without (left) and with (right) an intracavity etalon which suppresses unpredictable frequency hops. The OPO is tuned by varying the pump frequency.*
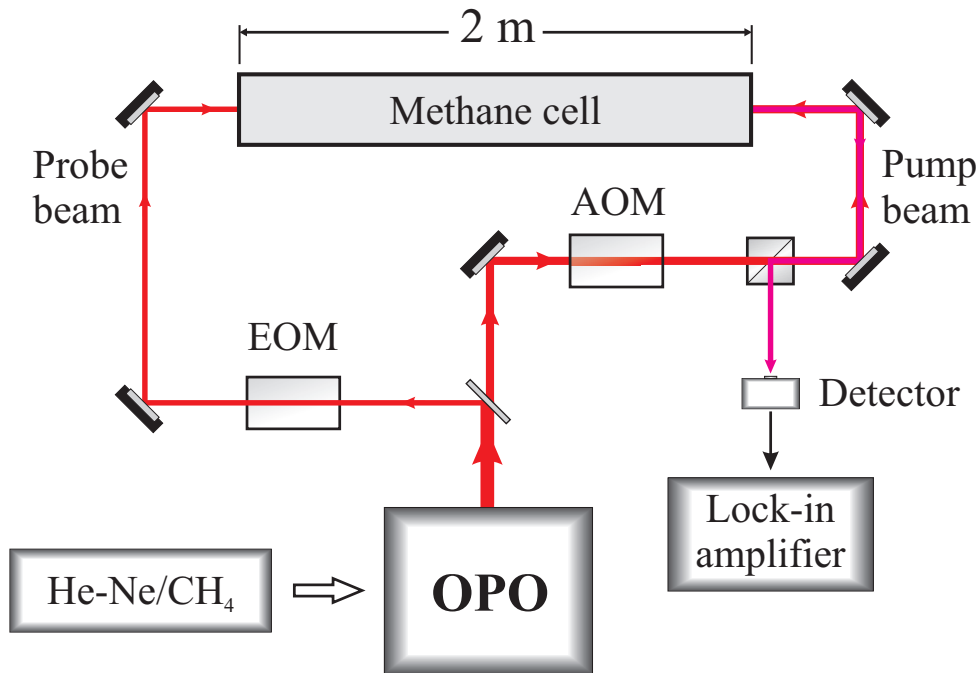
Figure 1.5: *First application of the OPO in high-resolution Doppler-free molecular spectroscopy of methane at 3.39 µm. A frequency modulation spectroscopy setup is implemented to detect Doppler-free resonances. The OPO idler frequency can be referenced to a He–Ne/CH$_4$ optical frequency standard [23, 24, 25, 26].*

nances, a frequency modulation spectroscopy setup has been implemented (Fig. 1.5). We observed Doppler-free resonances in a wide range of methane pressures and determined their pressure broadening.

Following our design of the pump-enhanced singly resonant OPO with an intracavity etalon, Stothard *et al.* [27] at the university of St. Andrews, UK, built an OPO serving as a reliable coherent source of a scanning system for an active real-time hyperspectral gas imaging under atmospheric pressure conditions. They developed an OPO which enables fine tuning of the output wavelength to the selected methane line by controllable mode hopping and then holding this wavelength during the imaging process.

It is also worth noting that the setup of our OPO with extended resonator containing an intracavity etalon became a prototype of the first commercially available cw OPO (OS 4000, LINOS Photonics), dozens of which are presently in use in spectroscopical and metrological practice.
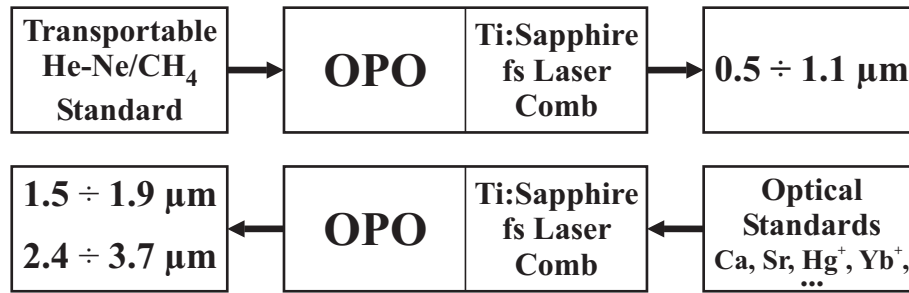
Figure 1.6: *OPO-comb tandem as a bidirectional coherent link between IR and visible spectral ranges.*

1.3 OPOs for optical metrology

Cw OPOs are of great practical significance for optical frequency metrology and give hope for the development of new infrared molecular clocks. Operating at 3.39 μm, methane stabilized Helium-Neon lasers are proven secondary mid-infrared standards with an accuracy and reproducibility of the output frequency at the level of $10^{-13} - 10^{-14}$. Traditionally, they are based on saturated absorption/dispersion resonances of the $F_2^{(2)}$ component of the P7 rotation-vibrational transition of the methane molecule. The implementation of appropriate tunable laser sources such as cw OPOs however makes it possible to use much stronger transitions from low-lying rotational levels as new references. At cryogenic temperatures, this would increase the spectroscopic signal by 2–3 orders of magnitude and thus lead to the creation of molecular optical frequency standards of higher performance [28, 29].

Consequently, it is clear that cw OPOs have very high application potential due to their excellent spectral and tuning characteristics, and the ability to be phase locked to stable optical references. Combining them with the recently developed optical frequency combs based on femtosecond lasers [30, 31, 32, 33] opens up new perspectives in optical metrology. In such a system the special properties of the OPO allow it to serve as a bidirectional coherent bridge linking the IR and visible spectral ranges (see Fig. 1.6) [34, 35].

For example, an infrared methane optical frequency standard [23, 24, 25, 26] can be used as a highly stable reference for an OPO and a visible frequency comb, to do high-resolution spectroscopy in the visible and near-infrared. Alternatively, an OPO phase locked to a femtosecond frequency
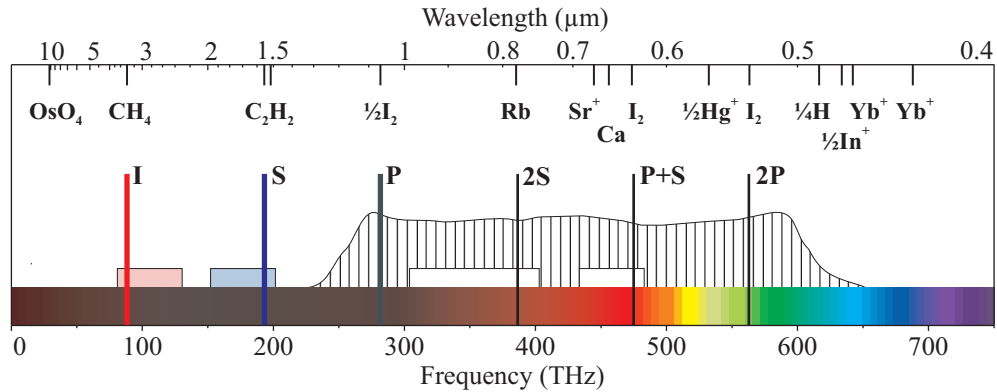
Figure 1.7: *Schematic of spectra of a Ti:Sapphire femtosecond laser frequency comb and OPO output lines alongside the molecular, ion and atomic reference lines employed in the present-day optical frequency standards.*

comb, which itself is referenced to a high performance microwave or optical clock, can provide very stable and tunable emission with known absolute frequency in both the mid-IR and telecom spectral ranges. This thesis presents this new idea and its first implementation for direct frequency comparisons between methane and iodine stabilized lasers.

Such kind of metrological applications of OPOs become possible by the following considerations. It is well known that femtosecond lasers produce combs of equidistant optical lines. Less well known is the fact that OPOs also generate a comb-like spectrum, although widely spaced, as depicted in Fig. 1.7. The OPO emits not only the signal and idler waves, but also a variety of linear combinations of these two frequencies in the visible spectral range also covered by a Ti:Sapphire femtosecond laser comb. These mixing products of the signal and pump waves, resonated in the OPO cavity, are generally not phase-matched and therefore very week with power levels of the order of several microwatts or less. They are however strong enough to perform frequency beat measurements with adjacent comb lines.

The OPO output spectrum has two degrees of freedom, the pump and idler frequencies. The comb spectrum is determined by two microwave frequencies as well, the spacing between comb lines and the offset frequency of the whole comb. Suppose, we know one absolute frequency, be it either the idler or the pump frequency of the OPO, the spacing of the comb or the position of only one of its components. Now, if we simultaneously measure 3 beats between the OPO output lines with nearby comb lines, then we

possess the full information about all OPO and comb frequencies.

Thus, the Ti:Sapphire femtosecond laser frequency comb can be referenced to an infrared optical frequency standard using the OPO and then be involved into absolute frequency measurements within its frequency coverage. Or if the comb is stabilized to a visible optical clock and the OPO is phase locked to the comb, the stability of the clock can be transferred to any infrared frequency generated by the OPO and used for optical metrology in the mid-infrared and telecom spectral ranges. Providing such a coherent link between widely separated optical frequencies can simplify direct absolute comparisons between optical standards of different nature and lead to new fundamental tests of physics [36, 37, 38, 39, 40, 41, 42].

1.4 Overview of the thesis

This thesis presents a continuous wave singly resonant OPO with resonated pump which was specially developed for high-resolution spectroscopy, using a new design of the OPO cavity with an intracavity etalon. The very first application of this OPO in Doppler-free spectroscopy of the methane molecule at 3.39 μm is demonstrated. I introduce a new method of the measurement of optical frequencies by combining a cw optical parametric oscillator with a Ti:Sapphire femtosecond laser frequency comb. This combination can be used to provide the coherent link between the visible and the infrared spectral ranges. To illustrate the metrological potential of this method, a direct frequency comparison of two different molecular optical frequency standards was performed.

Chapter 1 first outlines the state of the art in the field of cw optical parametric oscillators and gives an overview of their spectroscopic applications. It then introduces the novel design of an extended OPO cavity and summarizes the main features of such an OPO with an intracavity etalon. Furthermore, the concept of combining an OPO and a femtosecond laser frequency comb for optical frequency metrology is also introduced.

Chapter 2 of this thesis is devoted to the theoretical basics associated with an optical parametric oscillator. First, some useful treatments concerning nonlinear conversion processes and OPO principles are provided. Then, other aspects closely related to OPOs, such as quasi-phase-matching, domain structure and periodical poling of lithium niobate are considered.

Finally, some important formulae describing a singly resonant OPO with resonated pump are given.

In Chapter 3, I describe in detail our OPO with an intracavity etalon specially developed for high-resolution Doppler-free molecular spectroscopy. Thereafter, Chapter 4 presents the main features of the OPO and the results of phase locking of the OPO idler frequency to a methane optical frequency standard.

The capability of the new OPO design is demonstrated in Chapter 5. I present a frequency modulation spectroscopy setup used for detection of Doppler-free resonances in methane.

In Chapter 6, I first review the experimental methods of the optical metrology using femtosecond laser frequency combs. Then, our new concept of optical frequency measurements based on combination of a cw OPO and a femtosecond comb is explained. Thereafter, setup of a Ti:Sapphire femtosecond laser comb and its referencing to a methane infrared optical frequency standard are described. Finally, the results of an absolute optical frequency comparison between methane and iodine stabilized lasers are presented.

Chapter 7 finally summarizes the main results of this thesis and gives an outlook.

Chapter 2

Optical Parametric Oscillator

Following the invention of lasers, nonlinear optics emerged as a rapidly growing branch of modern physics. It deals with phenomena caused by strong optical fields. When the amplitude of the electric field component of the light wave becomes comparable with inter-atomic electric fields that act inside dielectric solids or molecular bounds, the response of the medium becomes dependent upon the intensity of the light. Interaction of intense laser light with a dielectric medium does not follow the laws of classical optics anymore. The demonstration of second-harmonic generation in 1961 by P. A. Franken et al. [43] was the starting point for investigation of many exciting manifestations of nonlinear optics.

The first experimental realization of a tunable coherent optical parametric oscillator (OPO) was reported more than 40 years ago by J. A. Giordmaine and R. C. Miller at the Bell Telephone Laboratories, USA [44]. At the same time, optical parametric amplification was demonstrated by the group of S. A. Akhmanov and R. V. Khokhlov at the Moscow University, Russia [45]. These two experiments were conducted using different nonlinear crystals and pulsed lasers as pump sources.

Since that time a variety of OPO devices based on new efficient nonlinear materials and solid-state laser pump sources has been developed in many laboratories around the world. Modern OPOs can provide high power continuous wave radiation as well as work in the ultra-fast femtosecond regime. Their operation range spreads between the near-ultraviolet and the mid-infrared spectral ranges.

In this chapter, we consider theoretical aspects of parametric amplification and OPO principles. Thereafter, we describe the technique of quasi-

phase-matching and domain structure of a periodically poled lithium nio-bate. Finally, we examine main features of a singly resonant OPO with res-onated pump wave.

2.1 Nonlinear frequency conversion

Let us consider interactions of intense optical fields with transparent ho-mogeneous dielectric media. We will follow the treatment similar to that presented in [46, 47] and summarized in [48]. We will use the convention regarding the units of susceptibility in SI (or MKS) system [47, 49], such that the first nonlinear term of the dielectric polarization becomes $P_{NL} = \varepsilon_0 \chi^{(2)} E^2$, where $\varepsilon_0 = 8.85 \cdot 10^{-12}$ C/(V·m) is the permittivity of the vacuum, $\chi^{(2)}$ is the nonlinear second-order susceptibility, and E is the field strength. In this case $\chi^{(2)}$ is measured in [m/V], since the units of E and P are [V/m] and [C/m^2], respectively.

Generally, the components of the polarization vector $\vec{P}$ in a dielectric medium can be expressed as a power series in the components of the electric field $\vec{E}$:

$$P_i = \varepsilon_0 \, \chi_{ij}^{(1)} \, E_j + \varepsilon_0 \, \chi_{ijk}^{(2)} \, E_j E_k + \varepsilon_0 \, \chi_{ijkl}^{(3)} \, E_j E_k E_l + \dots \, , \qquad (2.1)$$

where the indices i, j, k, l are related to the rectangular reference frame (X, Y, Z), $\chi_{ij}^{(1)}$ is the linear susceptibility, $\chi_{ijk}^{(2)}$ and $\chi_{ijkl}^{(3)}$ are the tensors of second- and third-order nonlinear optical susceptibilities. The second-order term describes sum- and difference-frequency generation, second-harmonic generation, parametric amplification and up-conversion of optical frequen-cies. The $\chi^{(3)}$-nonlinearity is responsible for effects such as third-harmonic generation, self-focusing of the light, four-wave mixing, optical phase con-jugation and others.

2.1.1 Properties of the second-order polarization

In our next consideration, we will restrict our attention to the second-order susceptibility. We will consider nonlinear interactions in crystals of certain symmetry, where the polarization of the medium contains a nonlinear term $\vec{P}_{NL}$, which is proportional to the intensity of the light $\vec{P}_{NL}(\vec{E}) \propto (\vec{E})^2$.

The second-order polarization is only inherent in crystals without inversion symmetry. In a centrosymmetric medium the polarization must reverse the direction and have the same absolute value for a reversed direction of the electric field: $\vec{P}_{\mathrm{NL}}(\vec{E}) = -\vec{P}_{\mathrm{NL}}(-\vec{E}) \equiv -\vec{P}_{\mathrm{NL}}(\vec{E})$, which is only fulfilled for vanishing second-order nonlinearity.

Usually, the tensor $d_{ijk} = \chi^{(2)}_{ijk}/2$ is used in practice rather than $\chi^{(2)}_{ijk}$, so that we can represent the second-order polarization with respect to the crystallographic axes X, Y, Z, as

$$(P_{\mathrm{NL}})_i = P_i^{(2)} = 2\,\varepsilon_0\,d_{ijk}\,E_j E_k \ . \tag{2.2}$$

As a rule, the optical frequencies involved in nonlinear optical interactions in crystals are at least one order of magnitude lower than the frequencies of the electronic transitions and much higher than those related to ionic motion. Thus, the absorption of light by the crystal lattice is negligible and such nonlinear crystals are transparent over the entire optical range. The mechanism of the nonlinear susceptibility in crystals has been analyzed by Kleinman in Ref. [50]. It is based on electronic polarization and does not include absorption. In this case second-order susceptibility has to obey additional properties of symmetry.

For an absorption-free medium all components of the d_{ijk}-tensor are real and independent of the frequency. Moreover, the response of the medium to the applied optical field is instantaneous, so that the nonlinear polarization can be expressed in the time domain by $P_i^{(2)}(t) = 2\,\varepsilon_0\,d_{ijk}\,E_j(t)E_k(t)$. Because of the symmetry to an exchange of $E_j(t)$ and $E_k(t)$ in this expression, the d_{ijk}-tensor is also symmetric in its last two indices, i.e., $d_{ijk} = d_{ikj}$. In practice, a contracted 3×6 matrix d_{il} is used to describe second-order susceptibility according to the notation

$$\begin{array}{ccccccc} jk\colon & 11 & 22 & 33 & 23, 32 & 13, 31 & 12, 21 \\ l\colon & 1 & 2 & 3 & 4 & 5 & 6 \end{array} \tag{2.3}$$

For example, following this notation we can rewrite the expression of nonlinear polarization (2.2) for the process of second-harmonic generation

in the matrix form

$$
\begin{pmatrix} P_x^{(2)} \\ P_y^{(2)} \\ P_z^{(2)} \end{pmatrix} = 2\,\varepsilon_0 \begin{pmatrix} d_{11} & d_{12} & d_{13} & d_{14} & d_{15} & d_{16} \\ d_{21} & d_{22} & d_{23} & d_{24} & d_{25} & d_{26} \\ d_{31} & d_{32} & d_{33} & d_{34} & d_{35} & d_{36} \end{pmatrix} \begin{pmatrix} E_x^2 \\ E_y^2 \\ E_z^2 \\ 2E_y E_z \\ 2E_x E_z \\ 2E_x E_y \end{pmatrix}. \tag{2.4}
$$

An additional symmetry condition, which is known as Kleinman's conjecture [50], is applicable to the electronic polarization of lossless media, which is independent of the optical frequency. It allows free permutations of the indices of the d_{ijk} tensor. Using notation (2.3) one can find that

$$
\begin{aligned}
d_{21} &= d_{16}, & d_{23} &= d_{34}, & d_{24} &= d_{32}, \\
d_{26} &= d_{12}, & d_{31} &= d_{15}, & d_{35} &= d_{13}, \\
d_{36} &= d_{14}, & d_{25} &= d_{14}.
\end{aligned} \tag{2.5}
$$

Kleinman's conjecture reduces the number of independent d_{il} coefficients to 10:

$$
d_{il} = \begin{pmatrix} d_{11} & d_{12} & d_{13} & d_{14} & d_{15} & d_{16} \\ d_{16} & d_{22} & d_{23} & d_{24} & d_{14} & d_{12} \\ d_{15} & d_{24} & d_{33} & d_{23} & d_{13} & d_{14} \end{pmatrix}. \tag{2.6}
$$

This contracted tensor and the piezoelectric tensor, describing the piezoelectric effect, have both the same form for the crystals of a given point-group symmetry. They both also fulfil the same symmetry restrictions. For example, the LiNbO$_3$ crystal belongs to the trigonal $3m$ point-group, with the tensor d_{il} having three independent coefficients with the following representation:

$$
d_{il} = \begin{pmatrix} 0 & 0 & 0 & 0 & d_{31} & -d_{22} \\ -d_{22} & d_{22} & 0 & d_{31} & 0 & 0 \\ d_{31} & d_{31} & d_{33} & 0 & 0 & 0 \end{pmatrix}. \tag{2.7}
$$

For congruent LiNbO$_3$ crystals, which are mainly used for production of Periodically Poled Lithium Niobate (PPLN) chips, the values for these coef-

ficients are [51, 48]:

$$
\begin{aligned}
d_{22} &= 2.10 \pm 0.21 \,\mathrm{pm/V}\,, \\
d_{31} &= -4.35 \pm 0.44 \,\mathrm{pm/V}\,, \\
d_{33} &= -27.20 \pm 2.70 \,\mathrm{pm/V}\,.
\end{aligned}
\tag{2.8}
$$

It is easy to see that the nonlinear interactions making use of the largest d_{33} coefficient in $\mathrm{LiNbO_3}$ are possible for all three waves polarized along the Z-axis. This is only feasible for quasi-phase matched materials, as will be shown later.

2.2 OPO principles

As mentioned before, the second-order polarization is responsible for second harmonic generation as well as for optical parametrical amplification. A nonlinear crystal with a nonvanishing second-order susceptibility placed into an optical resonator are two constituent parts of an Optical Parametric Oscillator (OPO). Focusing an intense laser beam into the crystal gives rise to an oscillation of the electronic polarization at a noise-like continuum of optical frequencies within the transparency band of the crystal. This oscillating polarization in turn supplies a continuum of secondary optical waves at these frequencies. If the frequency of the pump wave is ω_P, then in this continuum two complementary waves always exist. These are so called signal and idler waves, of frequencies $\omega_\mathrm{S} \geq \omega_\mathrm{I}$, such that

$$
\omega_\mathrm{P} = \omega_\mathrm{S} + \omega_\mathrm{I}
\tag{2.9}
$$

This relation can be interpreted as energy conservation during the splitting of a pump photon into two photons of lower energy. Only that wave pair of this manifold can be effectively amplified whose wave vectors satisfy the phase matching condition:

$$
\Delta k = k_\mathrm{P} - k_\mathrm{S} - k_\mathrm{I} \; = \; (\, n_\mathrm{P}\,\omega_\mathrm{P} - n_\mathrm{S}\,\omega_\mathrm{S} - n_\mathrm{I}\,\omega_\mathrm{I} \,) \, / \, c \stackrel{!}{=} 0,
\tag{2.10}
$$

where k_P, k_S, and k_I are the wave vectors, n_P, n_S, and n_I are the refraction indices at the frequencies of the pump, signal and idler waves, and c is the speed of light in vacuum. The expression for the wave vector mismatch

Δk is given for the collinear propagation of these three interacting waves, mainly taking place in OPOs, second harmonic generators, and other non-linear devices.

The refraction indices in a crystal generally depend on many factors, such as temperature, orientation of the crystal axes, electric field and pressure. Changing any of these parameters gives the ability to tune the OPO output frequencies. So, we see that in this parametric process only those frequencies become observable which obey momentum conservation of the interacting photons. Fulfilment of the condition (2.10) for the different wavelengths can provide a broadly and continuously tunable source of optical radiation.

Phase matching of the interacting waves can be achieved using two main approaches. The traditional way is to select a nonlinear birefringent crystal in which the phase matching condition can be obtained for the beams with orthogonal polarization making use of the difference in refractive index for an ordinary and an extra-ordinary wave [52]. Two types of birefringent phase matching can be distinguished. For type I phase matching the polarizations of the signal and idler waves are the same, whereas for type II phase matching they are orthogonal. The conversion efficiency of the birefringent phase matching critically depends on the crystal temperature and the angle between interacting waves and the crystal axes.

Another more progressive type of a non-critical and more effective phase matching becomes possible by implementing quasi-phase matched (QPM) materials. They offer the possibility to employ interactions with the highest nonlinearities which are normally unreachable by use of birefringent phase matching. The phase-mismatch between the pump, signal and idler waves is in this case compensated by periodical inversion of the sign of the effective nonlinearity. Since we use this type of phase matching in a Periodically Poled Lithium Niobate (PPLN) crystal, we will describe some principles of the QPM later in Section 2.2.2.

Under phase matched condition the amplification of the signal and idler waves in the nonlinear crystal works like in an active laser medium. Placing such a crystal inside an optical resonator provides strong coupling into a cavity mode and leads to an effective buildup of the signal and idler waves.

After reaching the threshold level of the pump radiation, where the parametric gain becomes equal to the losses of the parametric waves, the signal and idler simultaneously start to oscillate. Far above this threshold

more and more pump photons are converted into the signal and idler ones, asymptotically reaching 100% of quantum efficiency in an ideal case. To reduce the threshold of the parametric oscillation one can use different types of optical cavities.

In a singly resonant OPO (SRO), the optical cavity is resonant to one of the arising waves, signal or idler. Typical values of the SRO threshold are in the range of several Watts of pump power. In a doubly resonant OPO (DRO) the signal and idler waves are both resonant, with the pump threshold being at a level of tens to hundreds of milliwatts. Another effective way to further reduce the threshold of an SRO is to resonate the pump wave in the same cavity which also resonates either for the signal or the idler wave. Such a singly resonant OPO with resonated pump (PR-SRO) shows similar threshold levels as a DRO, but is less sensitive to changes of external parameters as the later.

In Section 2.3 we will consider the properties of a PR-SRO in more detail. Just before we are going to give some basic equations describing the process of parametric amplification. For simplicity, we will deal with plane waves analogous to the treatment in Ref. [46] and Ref. [47]. In case of interaction of Gaussian beams, the solutions of interest have the same form, so that we will only have to modify the constant factors by introducing some coupling parameters depending on the beam geometry, as it has been done in References [53] and [54].

2.2.1 Parametric amplification

In the following we will consider a propagation of three traveling plane waves with frequencies ω_S, ω_I and $\omega_P = \omega_S + \omega_I$ in a transparent lossless nonlinear medium along an arbitrary chosen direction z:

$$E_{P_i}(z,t) = \frac{1}{2}\left(A_{P_i}(z)\sqrt{\frac{\omega_P}{n_P}}\, e^{i(\omega_P t - k_P z)} + \text{c.c.} \right),$$

$$E_{S_j}(z,t) = \frac{1}{2}\left(A_{S_j}(z)\sqrt{\frac{\omega_S}{n_S}}\, e^{i(\omega_S t - k_S z)} + \text{c.c.} \right), \tag{2.11}$$

$$E_{I_k}(z,t) = \frac{1}{2}\left(A_{I_k}(z)\sqrt{\frac{\omega_I}{n_I}}\, e^{i(\omega_I t - k_I z)} + \text{c.c.} \right),$$

where indices i, j, and k refer to Cartesian coordinates and can each take on values x and y [46]. The normalized amplitudes of the electric fields introduced here are:

$$A_l(z) = \sqrt{\frac{n_l}{\omega_l}} E_l(z), \text{ with } l = \text{P, S, I.} \tag{2.12}$$

The normalization is chosen so that

$$|A_l(z)|^2 = \frac{2I_l}{c\varepsilon_0\omega_l} = \frac{2\hbar}{c\varepsilon_0} \cdot (I_l/\hbar\omega_l) \tag{2.13}$$

is always proportional to the flux of photons $I_l/\hbar\omega_l$ of frequency ω_l in $[1/(\text{s}\cdot\text{m}^2)]$, where $I_l = c\,\varepsilon_0\,n_l E_l^2/2$ is the intensity of the optical wave at ω_l in $[\text{W}/\text{m}^2]$, and $\hbar$ is the Planck constant divided by 2π.

As a starting point for characterizing the nonlinear parametric interaction we take the wave equation

$$\nabla^2\vec{E} = \frac{n^2}{c^2}\frac{\partial^2}{\partial t^2}\vec{E} + \mu_0\frac{\partial^2}{\partial t^2}\vec{P}_{\text{NL}}\,, \tag{2.14}$$

derived from the Maxwell equations in SI units

$$\begin{aligned}
\nabla \times \vec{E} &= -\mu_0\frac{\partial\vec{H}}{\partial t}\,, \\
\nabla \times \vec{H} &= \vec{J} + \frac{\partial\vec{D}}{\partial t}\,, \\
\nabla \cdot \vec{D} &= \rho\,, \\
\nabla \cdot \vec{H} &= 0\,,
\end{aligned} \tag{2.15}$$

for a dielectric nonmagnetic medium which contains neither free charges ($\rho = 0$) nor free currents ($\vec{J} = 0$), where $\mu_0 = 4\pi \cdot 10^{-7}\text{ N}/\text{A}^2$ is the permeability of the vacuum, and $c = (\varepsilon_0\mu_0)^{-1/2}$. The nonlinearity of the medium is included in the expression for the electric displacement vector using relations (2.1) and (2.2) as:

$$\vec{D} = \varepsilon_0\vec{E} + \vec{P} = \varepsilon_0\left(1 + \chi^{(1)}\right)\vec{E} + \vec{P}_{\text{NL}} = \varepsilon_0 n^2\vec{E} + \vec{P}_{\text{NL}}\,. \tag{2.16}$$

For simplicity, we have restricted (2.16) to the scalar field approximation, where $n = (1 + \chi^{(1)})^{1/2}$ is the refractive index corresponding to the electric

field polarization state of the relevant wave.

In case of definite propagation direction and fixed electric field polarizations of the three interacting waves (2.11), the nonlinear polarizations driving the pump, signal and idler waves in the lossless medium can also be expressed as the scalar relations:

$$
\begin{aligned}
(P_{\text{NL}})_{\text{P}} &= 2\,\varepsilon_0\,d_{\text{eff}}\,E_{\text{S}}E_{\text{I}}\,, \\
(P_{\text{NL}})_{\text{S}} &= 2\,\varepsilon_0\,d_{\text{eff}}\,E_{\text{P}}E_{\text{I}}^*\,, \\
(P_{\text{NL}})_{\text{I}} &= 2\,\varepsilon_0\,d_{\text{eff}}\,E_{\text{P}}E_{\text{S}}^*\,,
\end{aligned}
\tag{2.17}
$$

with the effective nonlinear coefficient d_{eff} being the same in all equations. This coefficient can be calculated from the tensor d_{ijk} of (2.2) by transformation from the crystal frame X, Y, Z to the chosen propagation frame x, y, z [52, 47, 49].

The wave equation (2.14) solved for the pump, signal and idler waves in the slowly-varying envelope approximation ($d^2 A_l(z)/dz^2 \ll k_l \cdot d A_l(z)/dz$) by using relations (2.11) and (2.17) results in the following propagation equations:

$$
\frac{dA_{\text{P}}}{dz} = -i\kappa A_{\text{S}} A_{\text{I}} e^{i\Delta kz}\,,
\tag{2.18}
$$

$$
\frac{dA_{\text{S}}}{dz} = -i\kappa A_{\text{P}} A_{\text{I}}^* e^{-i\Delta kz}\,,
\tag{2.19}
$$

$$
\frac{dA_{\text{I}}}{dz} = -i\kappa A_{\text{P}} A_{\text{S}}^* e^{-i\Delta kz}\,,
\tag{2.20}
$$

where $\Delta k = k_{\text{P}} - k_{\text{S}} - k_{\text{I}}$ is the phase mismatch parameter and κ is the coupling constant:

$$
\kappa = \frac{d_{\text{eff}}}{c} \cdot \sqrt{\frac{\omega_{\text{P}}\omega_{\text{S}}\omega_{\text{I}}}{n_{\text{P}}n_{\text{S}}n_{\text{I}}}}\,.
\tag{2.21}
$$

These so called coupled-wave equations describe parametric interaction of the plane pump, signal and idler waves in a dielectric lossless medium with second-order nonlinearity. They define the energy conversion between these three waves along the direction of propagation through the nonlinear medium. The evolution of the parametric conversion is determined by the phase matching and the initial intensities of the interacting waves.

The coupled-wave equations (2.18)-(2.20) are universally used not only

to study parametric amplification, but also for the characterization of all other three-wave mixing processes, sum- and difference-frequency generation and second harmonic generation. They can be solved analytically in some approximations.

Nondepleted pump approximation

In the approximation of the nondepleted pump, where it is assumed that the amplitude of the pump wave remains constant, $A_P(z) = A_P(0)$, the coupled-wave equations describing parametric interaction can be rewritten in the form:

$$\frac{dA_S}{dz} = -i\kappa A_P(0)A_I^* e^{-i\Delta kz} , \tag{2.22}$$

$$\frac{dA_I}{dz} = -i\kappa A_P(0)A_S^* e^{-i\Delta kz} . \tag{2.23}$$

For arbitrary initial signal and idler field amplitudes, $A_S(0)$ and $A_I(0)$ respectively, the solution of (2.22) and (2.23) is [46, 47]:

$$A_S(z) = \left[A_S(0) \left(\cosh(gz) + \frac{i\Delta k}{2g} \sinh(gz) \right) \right.$$
$$\left. - \frac{i\kappa A_P(0)}{g} A_I^*(0) \sinh(gz) \right] e^{-i\Delta kz/2} , \tag{2.24}$$

$$A_I(z) = \left[A_I(0) \left(\cosh(gz) + \frac{i\Delta k}{2g} \sinh(gz) \right) \right.$$
$$\left. - \frac{i\kappa A_P(0)}{g} A_S^*(0) \sinh(gz) \right] e^{-i\Delta kz/2} , \tag{2.25}$$

where

$$g = \sqrt{\left(\kappa A_P(0) \right)^2 - \left(\Delta k/2 \right)^2} . \tag{2.26}$$

These solutions can be reduced in case of exact phase matching $\Delta k = 0$. If the idler radiation is not present at the input ($A_I(0) = 0$) we can find simple expressions for the parametric gain of the signal amplitude and the rising amplitude of the idler wave along the propagation direction:

$$A_S(z) = A_S(0)\cosh(gz)\,,$$
$$A_I(z) = -iA_S^*(0)\sinh(gz)\,. \tag{2.27}$$

The above amplitudes asymptotically reach in the high-gain systems, when $gz \gg 1$, the values:

$$A_S(z) = -iA_I^*(z) = \frac{1}{2}A_S(0)\exp(gz)\,, \tag{2.28}$$

with an amplitude gain coefficient becoming $g = \kappa A_P(0)$.

In the practical situation of continuous wave OPOs the parametric gain is very low, so that the value gz is $\ll 1$. In this case the solution (2.27) can be represented in the low-gain limit up to the second order of the nonlinear parameter g:

$$\begin{aligned} A_S(z) &= A_S(0)\left(1 + \frac{1}{2}(gz)^2\right) \\ &= A_S(0) + \frac{1}{2}(\kappa z)^2|A_P(0)|^2 A_S(0)\,, \end{aligned} \tag{2.29}$$

$$A_I(z) = -iA_S^*(0)\cdot gz = -i\,\kappa z\, A_P(0)A_S^*(0)\,. \tag{2.30}$$

We see that in the low-gain regime the amplitude of the signal wave which is present at the input of the nonlinear medium grows quadratically with the interaction length. Simultaneously, the amplitude of the idler wave which is absent at the input grows linearly.

Pump depletion in the low-gain limit

The same behavior of the signal and idler waves in the low-gain regime can also be achieved by searching the first order solution for the depleted pump wave. We begin to integrate equation (2.20) assuming that to first

order we can substitute the initial values $A_P(0)$ and $A_S(0)$ at the input of the nonlinear medium for the pump and signal field amplitudes:

$$\frac{dA_I}{dz} = -i\kappa A_P(0) A_S^*(0) e^{-i\Delta kz} \,. \tag{2.31}$$

Using boundary conditions for the idler wave, $A_I(0) = 0$, as previously, we obtain the solution for its amplitude:

$$A_I(z) = -i\,\kappa\,A_P(0) A_S^*(0) \left(e^{-i\Delta kz} - 1 \right) / (-i\Delta k) \,, \tag{2.32}$$

which can be easily rewritten as

$$A_I(z) = -i\,\kappa z\,A_P(0) A_S^*(0)\, \mathrm{sinc}(\Delta kz/2)\, e^{-i\Delta kz/2} \,. \tag{2.33}$$

We now substitute (2.32) into the coupled-wave equations (2.18) and (2.19), and integrate both using the boundary conditions for the pump and signal waves. We have to seek the first order solutions in the low-gain limit up to the second order in the nonlinearity κ. In the case of exact phase matching $\Delta k = 0$, which is more relevant to our application, we achieve the following expressions for the pump, signal and idler wave amplitudes:

$$A_P(z) = A_P(0) - \frac{1}{2}(\kappa z)^2 |A_S(0)|^2 A_P(0) \,, \tag{2.34}$$

$$A_S(z) = A_S(0) + \frac{1}{2}(\kappa z)^2 |A_P(0)|^2 A_S(0) \,, \tag{2.35}$$

$$A_I(z) = -i\,\kappa z\,A_P(0) A_S^*(0) \,. \tag{2.36}$$

It is thus seen that, as long as the pump wave undergoes depletion, its amplitude decreases quadratically with the interaction length. Using these relations we can already write some equations for the threshold and efficiency of an optical parametric oscillator. Before we do this in the next section we are going to deduce formulae for the conversion efficiency and signal amplification in the low-gain regime.

Conversion efficiency

Let us consider a single-pass parametric interaction of the three collinear pump, signal and idler waves along the direction of their propagation in a

nonlinear crystal of length l. Using equations (2.33) and (2.13) we can write the expression for the conversion efficiency of the pump wave into the idler wave power in the presence of the signal wave of intensity $I_S = I_S(0)$:

$$\eta_I = \frac{I_I(l)}{I_P(0)} = \frac{\omega_I}{\omega_P} \frac{|A_I(l)|^2}{|A_P(0)|^2} = \frac{2\kappa^2 \omega_I}{c\varepsilon_0 \omega_P \omega_S} I_S l^2 \operatorname{sinc}^2(\Delta kl/2). \qquad (2.37)$$

Substituting (2.21) into (2.37) results in:

$$\eta_I = \frac{2\mu_0 \omega_I^2 d_{\text{eff}}^2}{c\, n_P n_S n_I} I_S l^2 \operatorname{sinc}^2(\Delta kl/2), \qquad (2.38)$$

or in terms of wavelengths:

$$\eta_I = \frac{2^3 \pi^2 d_{\text{eff}}^2}{c\varepsilon_0\, n_P n_S n_I \lambda_I^2} I_S l^2 \operatorname{sinc}^2(\Delta kl/2). \qquad (2.39)$$

Thus, the conversion efficiency is maximal in the special case of perfect phase matching $\Delta k = 0$ and is proportional to the square of the effective nonlinearity, to the square of the interaction length and to the intensity of the signal wave. The last term indicates the influence of the phase mismatch which we will discuss later after deriving the equation for the signal wave parametric gain.

Signal amplification

The expression for the amplification of the signal wave in the approximation of the nondepleted pump wave amplitude can be found from equation (2.24). For a non-vanishing initial signal amplitude $A_S(0)$ and absence of the idler radiation at the input of a nonlinear crystal, the output amplitude of the signal wave after an interaction length l is

$$A_S(l) = A_S(0) \left(\cosh(gl) + \frac{i\Delta k}{2g} \sinh(gl) \right) e^{-i\Delta kl/2}. \qquad (2.40)$$

Taking into account (2.13) and (2.26), the parametric amplification of the signal power is given by

$$G_S = \frac{I_S(l)}{I_S(0)} - 1 = \kappa^2 |A_P(0)|^2 l^2 \left(\frac{\sinh(gl)}{gl} \right)^2. \qquad (2.41)$$

Using (2.21) and (2.13) for the intensity of the pump wave $I_P = I_P(0)$ we obtain

$$G_S = \Gamma^2 l^2 \frac{\sinh^2\left[\Gamma^2 l^2 - (\Delta k l/2)^2\right]^{1/2}}{\Gamma^2 l^2 - (\Delta k l/2)^2} , \tag{2.42}$$

where

$$\Gamma^2 = \frac{2^3 \pi^2 d_{\text{eff}}^2}{c \varepsilon_0 \, n_P n_S n_I \, \lambda_S \, \lambda_I} \, I_P \tag{2.43}$$

is the gain factor (see for example [55]).

If the gain factor is small compared to the phase mismatch, $\Gamma \ll \Delta k/2$, the gain coefficient g becomes imaginary and the hyperbolic sine transforms into an ordinary sine, so that combining (2.42) and (2.43) we can write the equation for the parametric gain of the signal wave

$$G_S = \frac{2^3 \pi^2 d_{\text{eff}}^2}{c \varepsilon_0 \, n_P n_S n_I \, \lambda_S \, \lambda_I} \, I_P \, l^2 \, \text{sinc}^2(\Delta k l/2) . \tag{2.44}$$

We see that the signal parametric gain and the idler conversion efficiency in the low-gain limit have the same behavior and the corresponding expressions (2.44) and (2.39) differ only by the constant factor $\frac{\lambda_I I_P}{\lambda_S I_S}$. The both parameters show strong dependence on the value of the phase mismatch Δk. They reach maxima for perfect phase matching and rapidly decrease with increasing Δk.

The parametric gain and conversion efficiency of a nonlinear crystal of length l drop to half of its maximum value if $\Delta k = \pm 0.886 \, \pi/l = \pm 2.78 \, /l$ and then, after the first zeros at $\Delta k = \pm 2\pi/l$, begin to oscillate with the period $2\pi/l$ and decreasing amplitude. This expression can be used for an estimation of the width of the parametric gain curve. Typical values of the parametric gain width for infrared OPOs based on lithium niobate are in the order of hundreds of Gigahertz.

If the phase mismatch Δk is fixed during the parametric interaction , the intensities of the signal and idler waves increase to their maximum values at the interaction length which is equal to the coherence length $l_c = \pi/\Delta k$. If the crystal length $l \gg l_c$, spacial oscillations of conversion efficiency, which is proportional to $(1/\Delta k)^2 \sin^2(\Delta k l/2)$, occur along the propagation direc-

tion in the crystal with the period $2l_c = 2\pi / \Delta k$. In this case the maximum intensity of the parametric radiation, which can be reached, drops inversely proportional to the square of the phase mismatch Δk.

There are two commonly used methods providing phase matching. The traditional one works in birefringent crystals compensating for the dispersion by choosing the appropriate polarization of the interacting waves. The second technique is the quasi-phase-matching based on periodically poled nonlinear crystals. Some very useful considerations and discussions concerning the optical parametric gain, properties of mid-infrared nonlinear materials and different OPO devices can be found for example in an overview paper [55]. Let us now consider the basics of the quasi-phase-matching and then finish this section by characterizing the periodically poled lithium niobate.

2.2.2 Quasi-phase-matching

The idea of quasi-phase-matching (QPM) was independently proposed by Armstrong *et al.* [56] and Franken *et al.* [57]. As we have seen from equations (2.39) and (2.44) the phase mismatch Δk of the interacting pump, signal and idler waves results in appearance of the characteristic coherence length $l_c = \pi / \Delta k$, where the parametric conversion takes place effectively. Thereafter the energy accumulated in the amplified signal and idler waves flows back to the pump wave as long as the parametric waves are out of phase with the nonlinear polarization driving them, as shown in Fig. 2.1. Periodical compensation of such phase walk-off along the propagation direction can prevent this reversal of energy flow and provide effective parametric conversion at the whole crystal length.

The quasi-phase-matching condition is implemented by alternating the direction of a nonlinear crystal optical axis with a period Λ equal to twice the coherence length l_c. This leads to a periodical inversion of the sign of the effective nonlinear coefficient d_{eff} which can be represented as the square-wave function

$$d(z) = d_{\text{eff}} \, \text{sign}[\cos(2\pi z \, / \, \Lambda)], \tag{2.45}$$

or as a Fourier series with the grating vectors $k_m = \pm 2\pi m \, / \, \Lambda$ and amplitudes equal to $G_m = (2/\pi m) \sin(m\pi/2)$, where m denotes the order of the
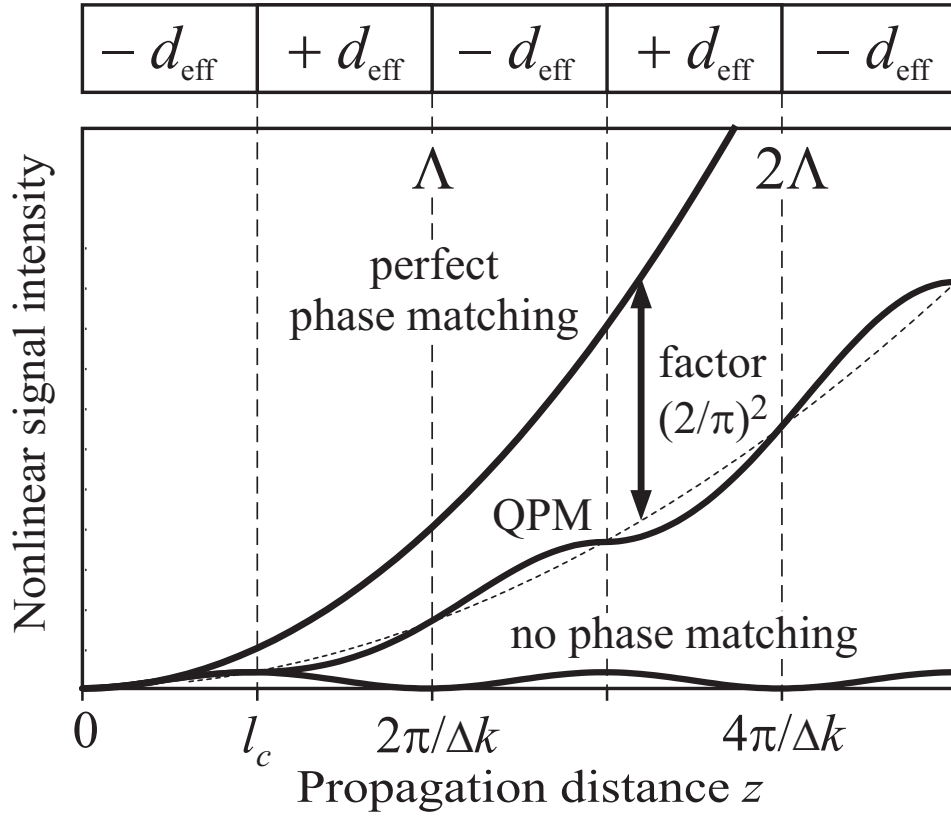
Figure 2.1: *Principle of quasi-phase-matching (adapted from Ref. [58]).*

QPM interaction [47]. The fundamental component ($m = 1$) is given by

$$d_{\mathrm{QPM}}(z) = (2/\pi)\, d_{\mathrm{eff}}\, \exp\left(i\, \frac{2\pi}{\Lambda}\, z\right). \tag{2.46}$$

Let us consider only the first-order QPM interaction now. It is mostly used because its amplitude is larger than that of the higher-order interactions. In this case the expression for the nonlinear polarizations driving pump, signal and idler waves (2.17) has to be modified by substituting $d_{\mathrm{QPM}}(z)$ for the effective nonlinear coefficient d_{eff}. Thus, the coupled-wave equations (2.18)-(2.21) of the previous subsection and the theoretical considerations following them are also valid for QPM interactions. The effective nonlinear coefficient for the first-order QPM

$$|d_{\mathrm{eff}}|_{\mathrm{Q}} = (2/\pi)\, d_{\mathrm{eff}} \tag{2.47}$$

and the phase mismatch parameter

$$\Delta k_Q = k_P - k_S - k_I - 2\pi/\Lambda \tag{2.48}$$

have to be used instead of d_{eff} and Δk respectively. The QPM periods can be found from the condition $\Delta k_Q = 0$:

$$\Delta k_Q = 2\pi \left(n_P/\lambda_P - n_S/\lambda_S - n_I/\lambda_I - 1/\Lambda \right) = 0. \tag{2.49}$$

Proper choice of Λ permits to efficiently convert a very wide range of optical wavelengths. It becomes possible to choose the highest effective nonlinearity of crystals, because the same polarization can be used for all interacting waves. Since the quasi-phase-matching is non-critical, the frequencies of the output waves can be varied by changing the crystal temperature.

2.2.3 Periodically Poled Lithium Niobate

Lithium Niobate (LiNbO$_3$) has been recognized as an efficient nonlinear optical crystal since the early sixties (see Ref. [59] and references therein). It has the largest nonlinear coefficient $|d_{33}| \approx 27\,\text{pm/V}$ (2.8) among QPM materials. Quasi-phase-matching in LiNbO$_3$ as well as in other ferroelectrics is based on the alternate poling of the crystal by periodical inverting the electric dipole domains along the propagation direction of the interacting beams.

To get an impression about the nature of the ferroelectricity in a LiNbO$_3$ crystal let us look at its structure. A summary of physical properties and the crystal structure of lithium niobate can be found in Ref. [60]. In the ferroelectric phase below the Curie temperature (about 1210 °C) a LiNbO$_3$ crystal belongs to the $3m$ point group. Its crystal structure can be characterized by either a hexagonal or rhombohedral unit cell. In the conventional hexagonal unit cell, the crystal exhibits three-fold rotational symmetry about its c axis. The $+c$ axis can be defined by cooling of the crystal [59]. It is directed out of the c face which becomes positive in this test. The optical $+z$ axis coincides with the crystallographic $+c$ axis.

The absolute arrangement of the atoms in LiNbO$_3$ has been determined by X-rays diffraction [63]. The oxygen atoms form planar layers building an octahedral structure as shown in Fig. 2.2. In the ferroelectric phase, the Nb
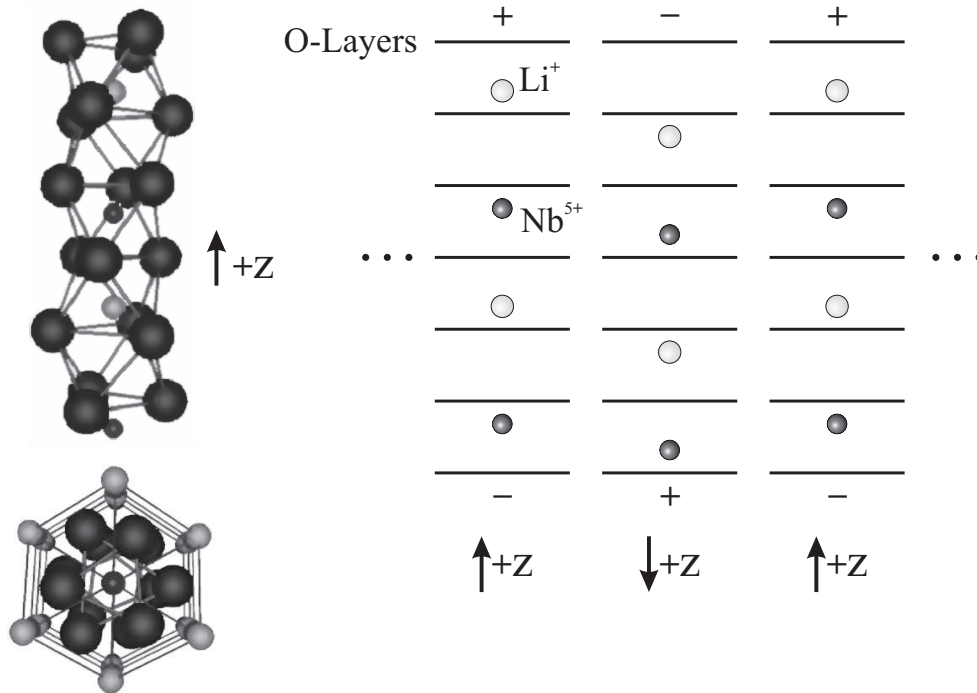
Figure 2.2: *Left: octahedral crystal structure of the lithium niobate and view along the +z axis (adapted from Ref. [61]). Right: schematic of the reversal ferroelectric domain structure in a periodically poled lithium niobate. (adapted from Ref. [62])*

and Li atoms are situated between the oxygen layers, each of them inside its own octahedron. The Nb and Li octahedra are arranged along the optical axis in pairs which are separated by one vacancy octahedron. The metal ions of each octahedron pair are displaced along the crystal optical axis from the centers of octahedra towards the external oxygen layers. This displacement is responsible for the spontaneous polarization of $LiNbO_3$.

There are two stable ferromagnetic domain configurations, inverted with respect to each other. By applying some external perturbation it is possible to reverse the domain polarity. The transition between these states can occur if the impact is able to move the metal ions through the potential energy barrier and then to fix their new position.

This reversing of the ferroelectric domains in a nonlinear crystal has been used for a long time for the effective quasi-phase-matched interactions. Initially, such a periodical structure of inversely poled domains has been produced in waveguide devices and in miniature crystal rods using different

techniques (see for example Ref. [64] and references therein). The first results of periodical poling of a nonlinear bulk material have been achieved in LiNbO$_3$ by using direct electron beam lithography [65] and by electric-field poling using a periodical mask of electrodes [66]. This new method has been applied to realize efficient second-harmonic generation of blue light in waveguides [66] and bulk [67] devices.

The first implementation of a bulk Periodically Poled Lithium Niobate (PPLN) for OPOs has been reported by L. E. Myers *et al.* in Ref. [68]. In the last several years, multi-grating PPLN chips with interaction length up to 60 mm have become commercially available. Now it is one of the mostly used QPM materials for optical frequency conversion and optoelectronic applications.

To make use of the highest nonlinear coefficient d_{33} in LiNbO$_3$ the polarizations of three interacting optical fields have to be parallel to the *z*-axis of the crystal (extraordinary polarization). The required quasi-phase-matching periods can be calculated in any special case by solving equation (2.49), with the indices of refraction for the interacting waves being substituted from Sellmeier equations [69, 70] which empirically describe the temperature dependence of the crystal dispersion.

For the congruent melt (mole ratio Li/Nb = 0.946) of LiNbO$_3$ the temperature-dependent Sellmeier equation for the extraordinary index of refraction is:

$$n_e(\lambda, T) = \sqrt{a_1 + b_1 f(T) + \frac{a_2 + b_2 f(T)}{\lambda^2 - (a_3 + b_3 f(T))^2} + \frac{a_4 + b_4 f(T)}{\lambda^2 - (a_5)^2} - a_6 \lambda^2} \; . \tag{2.50}$$

Here $f(T) = (T - 24.5)(T + 570.82)$, with the temperature T expressed in degrees Celsius and the vacuum wavelength λ in μm. The coefficients

$$a_1 = 5.35583 \qquad\qquad b_1 = 4.629 \cdot 10^{-7}$$
$$a_2 = 0.100473 \qquad\qquad b_2 = 3.862 \cdot 10^{-8}$$
$$a_3 = 0.20692 \qquad\qquad b_3 = -0.89 \cdot 10^{-8}$$
$$a_4 = 100 \qquad\qquad b_4 = 2.657 \cdot 10^{-5}$$
$$a_5 = 11.34927$$
$$a_6 = 1.5334 \cdot 10^{-2}$$

were found from the experimental data [70].

At higher temperatures, the thermal expansion of a nonlinear crystal and thus the corresponding increase of poling periods should be taken in to account. Using the thermal expansion coefficients α and β and referencing to the LiNbO$_3$ crystal length of $l(25)$ at 25 °C, the temperature dependence of the crystal length can be expressed as:

$$l(T) = l(25) \left[1 + \alpha(T - 25) + \beta(T - 25)^2 \right], \qquad (2.51)$$

where $\alpha = 1.54 \cdot 10^{-5}$ K^{-1} and $\beta = 5.3 \cdot 10^{-9}$ K^{-2}.

The poling periods of the first order QPM for the mid-infrared and the visible parametric interactions are in the range of several to tens of μm. In the case relevant to our OPO based on the PPLN crystal which is pumped at 1064 nm and for the extraordinary polarizations of all three interacting waves, the first order QPM periods are around 30 μm.

2.3 Singly resonant OPO with resonated pump

Providing the phase matching conditions in a nonlinear crystal determines the maximum parametric gain of the generated signal and idler. Placing the crystal into an optical resonator causes the simultaneous oscillation of both parametric waves. The oscillation threshold is defined by the parity of round-trip losses and the parametric gain of the resonated waves.

Singly and doubly resonant cavities are generally used in optical parametric oscillators. Doubly resonant OPOs (DROs) have mirrors highly reflecting at both the signal and idler wavelengths, whereas the mirrors of singly resonant OPOs (SROs) are highly reflecting at only one of them. Although DROs have a substantially lower threshold than SROs, they are not intrinsically stable and require sophisticated cavity designs with high mechanical and thermal stability as well as single-frequency pump sources. Owing to very moderate stability requirements, continuous wave SROs have received wide acceptance compared to DROs.

To enhance the pump power and reduce the SRO threshold, one can use an optical cavity which is additionally resonant at the pump wavelength. In this case the OPO is named as a singly resonant OPO with resonated pump wave (PR-SRO).

In this work we deal with PR-SRO, the cavity of which is resonant at

both the signal and pump waves. One of the main advantages of such a pump-enhanced SRO is that the OPO cavity length can be stabilized to the pump laser frequency. If the pump laser is intrinsically stable, its frequency characteristics can be transferred to the signal and idler waves via the stabilized cavity, provided that the temperature of the nonlinear crystal is also stable. Compared to doubly resonant OPOs, pump enhanced SROs are less subjected to mode hops and demonstrate practically the same threshold levels.

The basics of parametric oscillators are discussed in text-books on quantum electronics and nonlinear optics [46, 47, 71] for a simple case of interacting plane waves. Some general equations are given there for the threshold and efficiency of singly and doubly resonant OPOs. The frequency tuning and output power properties of a singly, doubly and triply resonant OPO are reviewed in Ref. [72].

The main theoretical studies concerning an SRO with a resonant pump, which shares a common cavity with one of the parametric waves, are presented in Ref. [54]. This paper considers a realistic case of the TEM_{00} Gaussian modes. It is based on the mean-field approximation, where the round-trip gain and losses are small. Simple expressions for the nonlinearity, threshold and the output powers of the signal and idler are given for both ring and standing-wave resonators.

In this section, we consider the main features of a pump resonant SRO which is resonated at the signal wavelength. We deduce some expressions for threshold and conversion efficiency in the plane-wave approximation similar to what has been done in Ref. [19] and thereafter compare them with more exact solutions for the Gaussian modes of the OPO resonator from Ref. [54]. Finally, we examine the frequency stability of this kind of OPOs.

2.3.1 Threshold and efficiency

A singly resonant OPO with resonated pump consists of a nonlinear crystal of length l with effective nonlinear coefficient d_{eff} which is placed into a standing-wave Fabry-Perot resonator. For simplicity, we will consider a resonator which is built up from two mirrors. This is schematically shown in Fig. 2.3.

Cavity mirrors are both highly reflecting the pump and signal waves and highly transmitting the idler wave. They are separated from the crystal by
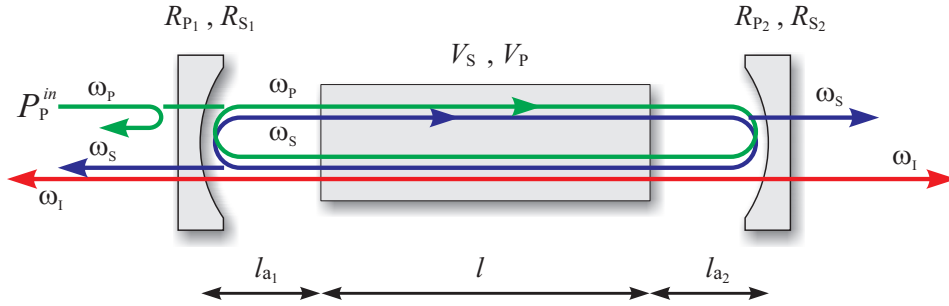
Figure 2.3: *Scheme of a singly resonant OPO with resonated pump (adapted from Ref. [62]). A nonlinear crystal of length l is placed inside an optical cavity. Cavity mirrors are highly reflecting at both pump (ω_P) and signal (ω_S) frequencies and highly transmitting at the idler (ω_I) frequency. R_{P_1}, R_{S_1} and R_{P_2}, R_{S_2} are the corresponding reflectivities of both mirrors; V_P and V_S are the total linear round-trip losses at the pump and signal frequencies. The optical length of the OPO resonator is locked to the pump frequency. The incident pump beam of power P_P^{in} always stays on resonance with the OPO cavity, which guarantees an effective buildup of the intracavity pump power.*

distances l_{a_1} and l_{a_2}. Thus, the optical length L_{res} of the OPO resonator for both the pump and signal waves is $L_{res\,P,S} = l_a + n_{P,S}\,l$, where $l_a = l_{a_1} + l_{a_2}$, and $n_{P,S}$ is the refraction index for the pump or the signal wavelength.

The input mirror has reflectivities $R_{P_1} = 1 - T_{P_1}$ and $R_{S_1} = 1 - T_{S_1}$ for the pump and signal wavelengths, respectively. For the second mirror these reflectivities are $R_{P_2} = 1 - T_{P_2}$ and $R_{S_2} = 1 - T_{S_2}$. Parameters $T_{P_{1,2}}$ and $T_{S_{1,2}}$ denote the corresponding transmission of the mirrors.

Total linear round-trip power losses for the pump and signal waves are described by absorption-like coefficients V_P and V_S, respectively. They consolidate all distributed and local losses in the nonlinear crystal and that of intermediate surfaces in the OPO resonator. V_P and V_S can also include transmissions of supplementary intracavity mirrors or even frequency dependent losses due to spurious etalon effects and additional selective elements as well. Sometimes it is convenient to combine the transmission of the second mirror T_{P_2} and T_{S_2} with coefficients V_P and V_S.

In the following treatment we suppose that the transmissions of the OPO cavity mirrors and the round-trip losses for the pump and signal are small: $V_P, T_P = T_{P_1} + T_{P_2} \ll 1$ and $V_S, T_S = T_{S_1} + T_{S_2} \ll 1$, so that the cavity finesse is relatively high. Assuming that the parametric gain is also small, we can use the coupled-wave equations (2.18)-(2.21) which are obtained in

the slowly-varying envelope approximation. We will consider here only the special case of the exact phase matching and that the idler wave is completely coupled out at both ends of the OPO cavity.

We start with expressions (2.34)-(2.36) which have been deduced in the previous section from the coupled-wave equations in the low-gain limit. In the case that the idler radiation is absent at the input of the the nonlinear crystal ($A_I(0) = 0$), the amplitudes of the pump, signal and idler waves after propagation through the crystal are:

$$A_P(l) = A_P(0)\left(1 - \frac{1}{2}(\kappa l)^2 |A_S(0)|^2\right), \tag{2.52}$$

$$A_S(l) = A_S(0)\left(1 + \frac{1}{2}(\kappa l)^2 |A_P(0)|^2\right), \tag{2.53}$$

$$A_I(l) = -i(\kappa l)A_P(0)A_S^*(0). \tag{2.54}$$

We assume that the OPO cavity length is locked to the frequency of the pump wave, so that the pump radiation is always resonant with the cavity. At the same time, the oscillation of the OPO signal wave occurs at one of the longitudinal cavity modes as soon as the threshold is reached.

To find the self-consistency condition for the pump and signal waves after a round-trip in the OPO resonator, we have to consider the wave propagation of both waves. We can choose a starting point of a forward path at the input face of the nonlinear crystal. Taking into account the double-path parametric amplification of the signal in the crystal, using equations (2.52) and (2.53), and considering contributions up to the second order in the nonlinear parameter κ we can write:

$$A_S(0) = A_S(0)\left(1 + \frac{1}{2}(\kappa l)^2 |A_P(0)|^2\right)^2 \sqrt{R_{S_2}}\sqrt{1 - V_S}\sqrt{R_{S_1}}, \tag{2.55}$$

$$\begin{aligned} A_P(0) = A_P(0)&\left(1 - \frac{1}{2}(\kappa l)^2 |A_S(0)|^2\right)^2 \sqrt{R_{P_2}}\sqrt{1 - V_P}\sqrt{R_{P_1}} \\ &+ A_P^{in}\sqrt{T_{P_1}}. \end{aligned} \tag{2.56}$$

These equations can further be simplified in the limit of low gain, small losses and small mirror transmissions (high-finesse cavity):

$$A_S(0) = A_S(0)\left(1 + (\kappa l)^2|A_P(0)|^2\right)\left(1 - \frac{1}{2}(T_{S_1} + T_{S_2} + V_S)\right), \quad (2.57)$$

$$A_P(0) = A_P(0)\left(1 - (\kappa l)^2|A_S(0)|^2\right)\left(1 - \frac{1}{2}(T_{P_1} + T_{P_2} + V_P)\right) \\ + A_P^{in}\sqrt{T_{P_1}}. \quad (2.58)$$

Threshold and intracavity power of the pump and signal waves

From equation (2.57) we find that the amplitude of the pump wave, which circulates in the OPO resonator above the threshold ($A_S(0) > 0$), in this approximation remains constant regardless of the pump power:

$$|A_P(0)|^2 = \frac{T_{S_1} + T_{S_2} + V_S}{2(\kappa l)^2} \quad (2.59)$$

This is the so-called optical limiting effect. It can be used for power stabilization of the pump radiation. It is easy to see that equation (2.59) implies a balance between the amplification factor and total losses of the signal wave.

With the help of relations (2.13) and (2.21) and introducing a single-pass nonlinearity

$$E_{NL} = \frac{2\mu_0}{c} \frac{d_{\text{eff}}^2\omega_S\omega_I}{n_P n_S n_I} \frac{l^2}{\text{Area}}, \quad (2.60)$$

we can find the pump power circulating in the resonator from (2.59):

$$P_P(0) = \frac{T_{S_1} + T_{S_2} + V_S}{2E_{NL}}. \quad (2.61)$$

The threshold condition for the external pump power P_P^{in} coupled into the OPO resonator can be deduced from equations (2.58) and (2.61) substi-

tuting $A_S(0) = 0$:

$$P_{P\,th}^{in} = \frac{(T_{P_1} + T_{P_2} + V_P)^2}{T_{P_1}} \frac{T_{S_1} + T_{S_2} + V_S}{8E_{NL}}.$$ (2.62)

It is clear that the OPO threshold is minimal in case of 100% reflective mirrors for the signal wave ($T_{S_1} = T_{S_2} = 0$) and if the transmission of the input mirror for the pump wave is equal to its round-trip losses ($T_{P_1} = T_{P_2} + V_P$). The latter is also known as the impedance matching condition.

The signal power circulating in the resonator can be evaluated from equations (2.58) using (2.59) and (2.62):

$$|A_S(0)|^2 = \frac{4T_{P_1}}{T_{P_1} + T_{P_2} + V_P} \frac{|A_{P\,th}^{in}|^2}{T_{S_1} + T_{S_2} + V_S} \left(\sqrt{\frac{P_P^{in}}{P_{P\,th}^{in}}} - 1 \right).$$ (2.63)

Conversion efficiency

Finally we can find conversion efficiencies for the signal and idler waves which are emitted by the OPO. They are defined as the ratios of the signal and idler powers outcoupled from the OPO to the incident pump power P_P^{in}. The total signal power is distributed between both outputs proportionally to the mirror transmissions T_{S_1} and T_{S_2}. The idler power is emitted equally in both directions.

The signal conversion efficiency η_S results from equation (2.63), taking into account equation (2.13) and that in the low-gain limit according to equation (2.53) $|A_S(0)|^2 \approx |A_S(l)|^2$. The conversion efficiency of the idler wave η_I can thereafter be obtained from equations (2.54) and (2.59):

$$\eta_S = (T_{S_1} + T_{S_2}) \frac{|A_S(0)|^2}{|A_P^{in}|^2} \frac{\hbar\omega_S}{\hbar\omega_P}$$

$$= \frac{\omega_S}{\omega_P} \frac{4T_{P_1}}{T_{P_1} + T_{P_2} + V_P} \frac{T_{S_1} + T_{S_2}}{T_{S_1} + T_{S_2} + V_S} \left(\sqrt{\frac{P_{P\,th}^{in}}{P_P^{in}}} - \frac{P_{P\,th}^{in}}{P_P^{in}} \right),$$ (2.64)

$$\eta_{\mathrm{I}} = \frac{|A_{\mathrm{I}}(l)|^2}{|A_{\mathrm{P}}^{in}|^2} \frac{\hbar\omega_{\mathrm{I}}}{\hbar\omega_{\mathrm{P}}} = \frac{\omega_{\mathrm{I}}}{\omega_{\mathrm{P}}} \frac{4T_{\mathrm{P}_1}}{T_{\mathrm{P}_1} + T_{\mathrm{P}_2} + V_{\mathrm{P}}} \left(\sqrt{\frac{P_{\mathrm{P}\,th}^{in}}{P_{\mathrm{P}}^{in}}} - \frac{P_{\mathrm{P}\,th}^{in}}{P_{\mathrm{P}}^{in}} \right)$$

$$= \frac{T_{\mathrm{S}_1} + T_{\mathrm{S}_2} + V_{\mathrm{S}}}{T_{\mathrm{S}_1} + T_{\mathrm{S}_2}} \frac{\omega_{\mathrm{I}}}{\omega_{\mathrm{S}}} \eta_{\mathrm{S}} . \tag{2.65}$$

From these equations it can be easily shown that the conversion efficiencies η_{S} and η_{I} are maximal for a pump power level which is four times higher than the threshold pump power. Optimization of the different OPO parameters such as crystal length, threshold and conversion efficiencies of resonant and non-resonant waves are discussed in Ref. [19, 54].

Nonlinearity in case of Gaussian beams

In the case of a Gaussian beams, the expressions for the OPO threshold and for the internal power of the pump and signal take the same form as deduced above for interacting plane waves. The single-pass nonlinearity (2.60) should only be modified correspondingly. The expressions (2.64) and (2.65) for the conversion efficiencies for the signal and idler waves remain valid.

Here we provide the results obtained in Ref. [54] for the case of a real PR-SRO pumped with a focused Gaussian beam which is matched to the TEM$_{00}$ mode of the OPO Fabry-Perot resonator. Since the pump and signal waves share the same cavity, they have the same waist position and the same Rayleigh range,

$$z_R = \frac{n_{\mathrm{P}}\omega_{\mathrm{P}}}{2c} w_{0\mathrm{P}}^2 = \frac{n_{\mathrm{S}}\omega_{\mathrm{S}}}{2c} w_{0\mathrm{S}}^2 . \tag{2.66}$$

The single pass nonlinearity can be expressed as:

$$E_{\mathrm{NL}} = \frac{4\mu_0}{\pi c^2} \frac{d_{\mathrm{eff}}^2 \omega_{\mathrm{S}}^2 \omega_{\mathrm{I}}^2}{n_{\mathrm{P}}^2 \omega_{\mathrm{P}}} \, l \cdot h , \tag{2.67}$$

where h is a dimensionless focusing function similar to the Boyd-Kleinman integral [53]. The value of h is < 1.1 and is determined by several parameters such as the ratio of the wave vectors k_{R} and k_{P} of the resonant and the pump waves respectively, $\zeta = k_{\mathrm{R}}/k_{\mathrm{P}} = (n_{\mathrm{R}}\omega_{\mathrm{R}})/(n_{\mathrm{P}}\omega_{\mathrm{P}})$, and by the OPO resonator geometry. The h-function possesses a broad maximum at the fo-

cusing parameter z_R/l between 0.2 and 0.5 depending on the focus position and resonant wave frequency.

In the special case of a singly resonant OPO with resonated pump and signal waves, which is pumped at $\lambda_P = 1064$ nm and which emits a signal wave near $\lambda_S = 1550$ nm ($\zeta \approx 0.7$), having the focus at the end of the nonlinear crystal, the value of h reaches a maximum of ≈ 0.7 at the optimum focusing parameter $z_R/l \approx 0.4$.

2.3.2 Frequency stability

The frequency stability of a singly resonant OPO with resonated pump is examined in Ref. [19] similarly to the model used in Ref. [73] for a doubly resonant OPO. Since the length of the OPO cavity is locked to the frequency of the intrinsically stable pump laser, the signal wave circulates in the same stable cavity.

In an ideal case, the relative stability of both the signal and idler waves is the same as the one of the pump wave, provided that the the cavity lock is tight enough to follow the pump laser frequency and to suppress fast fluctuations of the cavity length. At the same time, the OPO has to be pumped with a stable narrow linewidth, single-frequency radiation. In practice the OPO frequency stability is determined by the quality of the electronics for the cavity length feedback loop and for the stabilization of the nonlinear crystal temperature.

Here, we provide the result obtained in Ref. [19, 1] for the tuning coefficients of the signal frequency due to variations of the crystal temperature T_{cr} and the pump frequency ν_P:

$$
\left(\frac{\partial \nu_S}{\partial T_{cr}} \right)_{\nu_P} = -\nu_S \frac{\left(\frac{\partial n_S}{\partial T_{cr}} - \frac{\partial n_P}{\partial T_{cr}} \right) + \alpha \left(n_S - n_P \right)}{n_S + \frac{l_a}{l} + \frac{\partial n_S}{\partial \nu_S} \nu_S} , \tag{2.68}
$$

$$
\left(\frac{\partial \nu_S}{\partial \nu_P} \right)_{T_{cr}} = \frac{\nu_S}{\nu_P} \frac{n_P + \frac{l_a}{l} + \frac{\partial n_P}{\partial \nu_P} \nu_P}{n_S + \frac{l_a}{l} + \frac{\partial n_S}{\partial \nu_S} \nu_S} . \tag{2.69}
$$

Here, $\alpha = \frac{1}{l} \frac{\partial l}{\partial T_{cr}}$ is the linear expansion coefficient of the crystal and $l_a = l_{a_1} + l_{a_2}$ is the length of that part of the OPO resonator which is filled

with air. This coefficients also give an impression of the instability of the OPO output frequencies with respect to two crucial factors: T_{cr} and ν_P.

In the special case of a lithium niobate crystal pumped by a Nd:YAG laser and a signal wavelength around $1.5\,\mu$m, contributions of all last terms of both the numerators and denominators in equations (2.68) and (2.69) are at least one order of magnitude smaller than the values of the other terms. Thus, we can simplify these equations as following:

$$\left(\frac{\partial \nu_S}{\partial T_{cr}}\right)_{\nu_P} \approx \nu_S \frac{\left(\frac{\partial n_P}{\partial T_{cr}} - \frac{\partial n_S}{\partial T_{cr}}\right)}{n_S + \frac{l_a}{l}}, \tag{2.70}$$

$$\left(\frac{\partial \nu_S}{\partial \nu_P}\right)_{T_{cr}} \approx \frac{\nu_S}{\nu_P} \frac{n_P + \frac{l_a}{l}}{n_S + \frac{l_a}{l}}. \tag{2.71}$$

We can see from (2.71) that the relative instability of the signal frequency is approximately equal to that of the pump frequency, provided that the crystal temperature is stable. The stability coefficient of the signal frequency versus the crystal temperature T_{cr} (2.70) mainly depends on the difference between the derivatives of the refraction indices of both the pump and the signal waves over T_{cr}. For a semi-monolithic pump-enhanced SRO with a PPLN crystal of length $l = 20$ mm and ratio $l_a/l \simeq 0.5$, this coefficient is in the order of 300 kHz/mK.

Clearly, it is also an advantage to increase the length l_a of the OPO resonator in order to decrease the sensitivity of the signal frequency with respect to fluctuations of the crystal temperature. This sensitivity can be reduced by one order of magnitude by using a long cavity with $l_a/l \simeq 20$.

Chapter 3

OPO setup with an intracavity etalon

In this chapter, the experimental realization of the extended OPO setup with intracavity etalon is demonstrated. A photograph of the up-to-date OPO setup is shown in Fig. 3.1 and its scheme in Fig. 3.2. This is a continuous wave singly resonant OPO with enhanced pump. It is based on a periodically poled lithium niobate crystal (PPLN) and pumped by a monolithic Nd:YAG laser at 1064 nm. The extended OPO cavity is resonant for both the signal and the pump waves. The cavity length is locked to the pump laser [1, 2] using the Pound-Drever-Hall technique [74]. Thus, the output properties of the OPO closely mirror the properties of the pump laser.

The OPO contains a specially designed intracavity etalon (ICE), which allows controlled access to any desired wavelength in a wide emission range. Coarse selection of the output wavelength can be achieved by choosing the appropriate crystal poling period and changing the PPLN crystal temperature. The OPO can be fine-tuned by tuning the pump frequency. Tilting the ICE or varying its temperature synchronously with sweeping the pump frequency provides continuous tuning over several GHz. The range of mode-hop-free tuning is only limited by the possibility to continuously sweep the frequency of the pump laser.

The OPO exhibits excellent long-term stability with low output frequency drift showing mode-hop-free operation over several days. The idler radiation has a narrow linewidth of about 10 kHz. Idler, signal or even its non-phase-matched combination, which are also present in the OPO output, can be phase locked to any stable external optical reference.

41

3.1   Overview of OPO components

The OPO setup is placed on an air floated optical table (Newport, M-RS-4000-48-12). It occupies a space of 65 cm × 65 cm. To avoid the influence of ambient air flows on the PPLN crystal temperature and the OPO cavity length, the OPO resonator is covered with a plexiglass box. The whole OPO setup is in turn surrounded with a wooden box and covered with a plexiglass top plate. The Nd:YAG pump laser is located outside the wooden box.

The OPO arrangement is schematically shown in Fig. 3.2. To provide intrinsically stable operation of the OPO, insensitive to external perturbations, all optical components building the OPO resonator and the pump bending mirrors are supported by high-performance opto-mechanical mounts. The beam height is chosen to be as low as possible at ~ 78 mm.

The OPO resonator is built from four mirrors M1-M4 and involves an intracavity etalon. The multi-grating PPLN crystal is situated inside a temperature stabilized oven which is located on two crossed translational stages allowing to choose a certain QPM grating period and the optimal resonator beam parameters.

The beam of the pump laser passes $\lambda/4$ and $\lambda/2$ plates which are used for correction of its elliptically polarized radiation. Some details about properties of the pump laser output beam can be found in Ref. [75]. To prevent back-reflections from the OPO cavity into the pump laser, a Faraday-isolator is installed between them. The isolator is equipped with two polarizing beam splitter cubes (PBS). The first PBS is mounted in that way that the (horizontally) P-polarized pump beam is transmitted.

Since the polarization of the pump beam after the Faraday-isolator is 45° rotated with respect to the initial one, a second $\lambda/2$ plate is used to rotate it to S-polarization. Then the pump beam is reflected towards the OPO cavity by a highly reflecting mirror and a dichroic beam splitter. The latter has a high reflectivity for the pump wavelength, a high transmission ($> 99.5\,\%$) for the idler wavelength ($2.9 - 3.4\ \mu$m) and a residual transmission of $60 - 90\,\%$ for the signal wavelength in the range of $1.3 - 1.9\ \mu$m.

The pump beam is focused onto the entrance face of a PPLN crystal using an uncoated CaF_2 lens with a focal length of 119 mm. The lens is mounted in a kinematic XY-mount, itself situated on a Z-translation stage. An additional AR coated 500 mm lens after the second $\lambda/2$ plate serves for
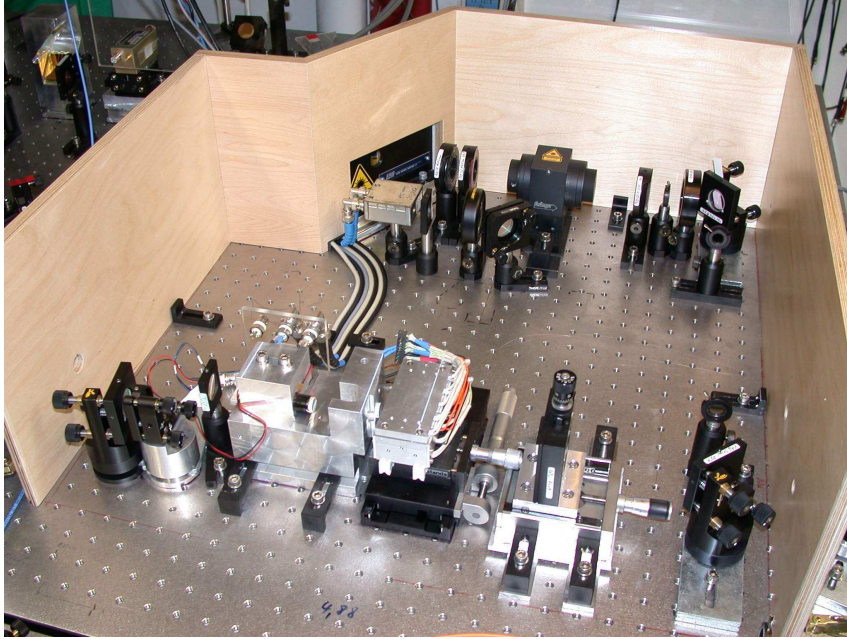
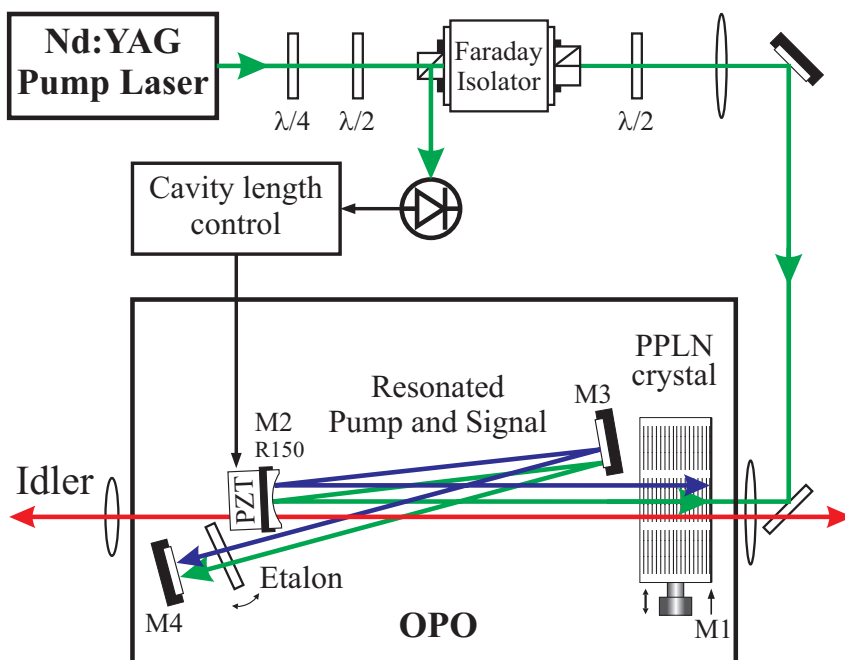**Figure 3.1:** *Photograph of the OPO setup.*

Figure 3.2: *Schematic of the OPO setup (see text for details).*

the optimal mode matching of the focused pump beam with the OPO cavity.

All optical components used for delivering the pump beam insert up to 15 % losses for the pump power before it reaches the PPLN crystal. The first $\lambda/2$ plate in combination with the PBS at the input of the optical isolator is also used for eventual attenuation of the pump beam.

The part of the pump beam which comes back from the OPO cavity passes through the Faraday-isolator and is reflected aside by its first polarized beam splitter cube. After attenuation below 1 mW it is sent to a lock photodetector. The signal of this detector is then used for locking the length of the OPO resonator to the pump frequency by means of the Pound-Drever-Hall method as described later in Section 3.3.1.

3.2   Pump laser

A monolithic diode-pumped Nd:YAG laser (LZH, Laser Zentrum Hannover), based on a non-planar ring oscillator (NPRO) design [76], is used as pump source of the OPO. It emits up to 1 W single-frequency output power at 1064 nm with an intrinsic linewidth of $\sim$ 5 kHz. Narrow linewidth, high reliability, and long-term repeatability of the output characteristics over many years of operation make this laser very suitable for our applications.

The pump laser can be frequency tuned by changing the Nd:YAG crystal temperature. The temperature is stabilized within several millikelvin and can be changed using a slow external input of the crystal temperature controller. The sensitivity of this input is about 1 °C/V and its time constant is $<$ 1 s. The frequency of the pump laser is tunable over 40 GHz by $\sim$ 20 °C crystal temperature variation. The continuous tuning range of the pump frequency was measured to be about 9 GHz with a slope of $\sim$ 4.5 GHz/°C, as shown in Fig. 3.3.

The pump laser is also provided with a fast modulation input. This is connected to a piezoelectric transducer (PZT) which is glued to the Nd:YAG crystal. By applying a voltage to this input the PZT squeezes the crystal, changing the resonator length and hence the laser output frequency. The input has a sensitivity of about 1 MHz/V at low frequencies and a bandwidth of $\sim$ 100 kHz. Using the PZT, the pump laser can precisely be tuned over tens of MHz. We use this input for fast modulation, rapid sweeping and control of the pump laser frequency.
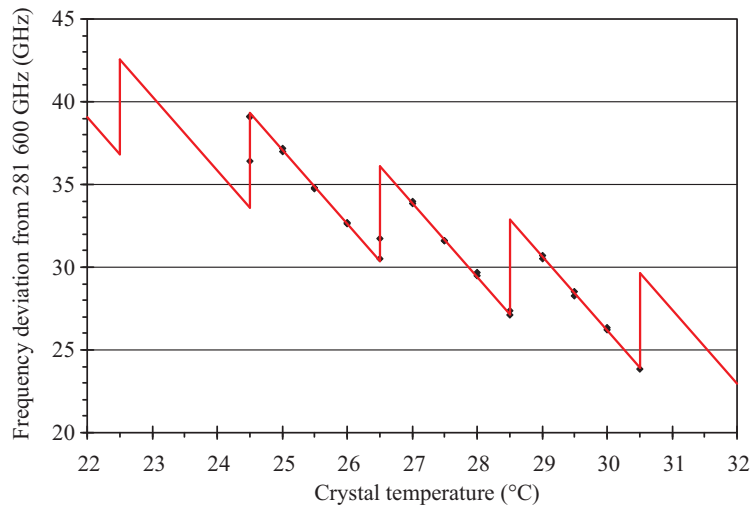
Figure 3.3: *Pump laser tuning versus Nd:YAG crystal temperature. The continuous tuning range is about 9 GHz with a slope of ~ 4.5 GHz/°C.*

The frequency stability of a laser can be determined by a beat measurement with a second similar laser or with respect to some stable optical reference. To characterize the pump laser, we used an iodine stabilized Nd:YAG laser as such a reference. The latter is similar to a system which is reported in [77, 78]. The results of stability measurements of the iodine optical frequency standard are presented in Section 6.6.2. The beat frequency between the pump laser and the iodine standard was recorded using a PC-based frequency counter board (Guide Technology Inc., GT200-10 Time Interval Counter).

The short-term stability of the free-running pump laser was estimated to be better than 10 kHz for an integration time of 1 ms. At timescales up to 1 s, jitter and random walk of the pump frequency with deviations between 20 and 100 kHz are observed. The middle-term frequency drift over the measurement time of 100 s and long-term drift over 10 hours are shown in Fig. 3.4. It can be seen that at different measurement times, the drifts of the pump frequency can range from tens of kHz/min, by averaging over many hours, up to several MHz over minutes.

The temperature of the Nd:YAG crystal seems to be the main factor affecting the pump laser output frequency and is responsible for considerable frequency drifts. Although the crystal temperature is stabilized, we observed very strong correlation between the ambient temperature and the
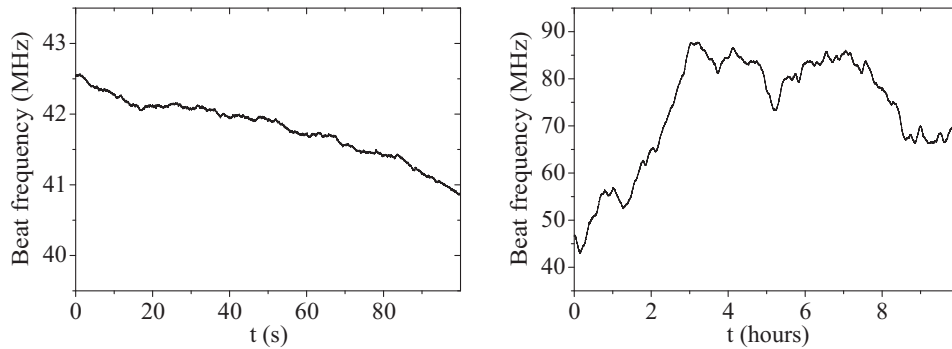
Figure 3.4: *Typical frequency drifts of the free-running Nd:YAG pump laser measured by means of a beat measurement relative to an iodine stabilized Nd:YAG laser. Left: Middle-term drift over a 100-second measurement with a sampling time of 10 ms. Right: Long-term frequency behavior of the pump laser measured over 10 hours; sampling time is 1 s.*

pump laser frequency. This is for example evident from the long-term measurements of the OPO idler frequency that are presented in Section 4.2.2.

In according to Equation (2.69), the frequency excursions of the pump laser are proportionally transferred to the signal and idler frequencies in the case of a singly resonant OPO with resonated pump. The mode-hop-free operation and long-term behavior of the OPO are determined ultimately by the long-term stability and by frequency drifts of the pump laser, provided that the OPO cavity length is tightly locked to the latter.

Rapid changes of the pump frequency also make it difficult to implement free-running OPOs for detection of narrow Doppler-free resonances with widths $\leq$ 100 kHz. In this case, an active control of the pump frequency can be extremely helpful and sometimes unavoidable. Alternatively, the frequency of the idler or signal can slowly be frequency stabilized or phase locked to an available optical reference.

3.3   OPO cavity

The geometry of the OPO resonator is similar to the one usually used for cw dye lasers. Stability characteristics and mode parameters of such kind of cavities were investigated in Ref. [79, 80]. Those results are adapted for the case of a three-mirror OPO cavity in Ref. [75]. The distinguishing feature of

the present cavity is that the resonator modes have one tiny and one broad waist, lying both at the external plain mirrors.

The extended OPO cavity consists of three plane mirrors and one concave mirror (see Figures 3.2 and 3.5). One mirror, M1, is directly coated onto the plane entrance face of the nonlinear crystal and is highly reflecting for the pump ($R_{P_1} \approx 98\,\%$) and the signal ($R_{S_1} > 99\,\%$ for $1.35 - 1.65\,\mu$m, with a maximum of $99.9\,\%$ at $1.5\,\mu$m), but highly transmitting ($> 98\,\%$) for the idler ($3 - 4\,\mu$m). The concave mirror, M2, with a curvature radius of 150-mm and the plane mirrors, M3 and M4, have a reflectivity better than $99.7\,\%$ for the pump and signal, and $\leq 1\,\%$ for the idler.

The backsides of all these mirrors are additionally antireflection (AR) coated for the idler wave with a reflectivity $\leq 0.5\,\%$. They have a rest-reflectivity for the pump and signal waves of up to $30\,\%$. The plane mirror, M3, reflects both the pump and the signal waves by its edge and is installed as near as possible to the axis M1-M2 in order to minimize the angle of incidence at the concave mirror and therefore astigmatic aberrations of the resonator mode.

The concave mirror is located ~ 64 mm away from the AR-coated crystal surface. The optical cavity length is 380 mm, corresponding to a free spectral range (FSR) of ~ 395 MHz. One waist of the fundamental cavity mode with $\omega_0 \approx 35\,\mu$m (for the pump wave) is located at the entrance face of the crystal, another one with $\omega_0 \approx 740\,\mu$m at the end mirror, M4. (In the initial setup, described in [7], the concave mirror, M2, of 100-mm radius of curvature was located 43 mm from the crystal, with the cavity length being about 420 mm and FSR of 360 MHz.)

The internal 1/2-inch plane mirror, M3, of the OPO is glued to a massive aluminum block and placed in the immediate vicinity of an oven containing the PPLN crystal. The 1/2-inch concave mirror, M2, is mounted on a hollow piezoelectric transducer (PZT) which is glued to another small aluminum block. The concave mirror and the PZT are axially aligned with a hole which is marginally drilled through the block. The PZT and the mirrors are correspondingly glued to each other and to the aluminum blocks using a 5-minute two part epoxy. The desired arrangement of both mirrors with respect to the crystal can be adjusted and fixed after an appropriate positioning of the blocks.

To avoid etalon effects, the second plane face of the crystal is polished with a small wedge of $\sim 0.25°$ tilt and then AR-coated for all three wave-
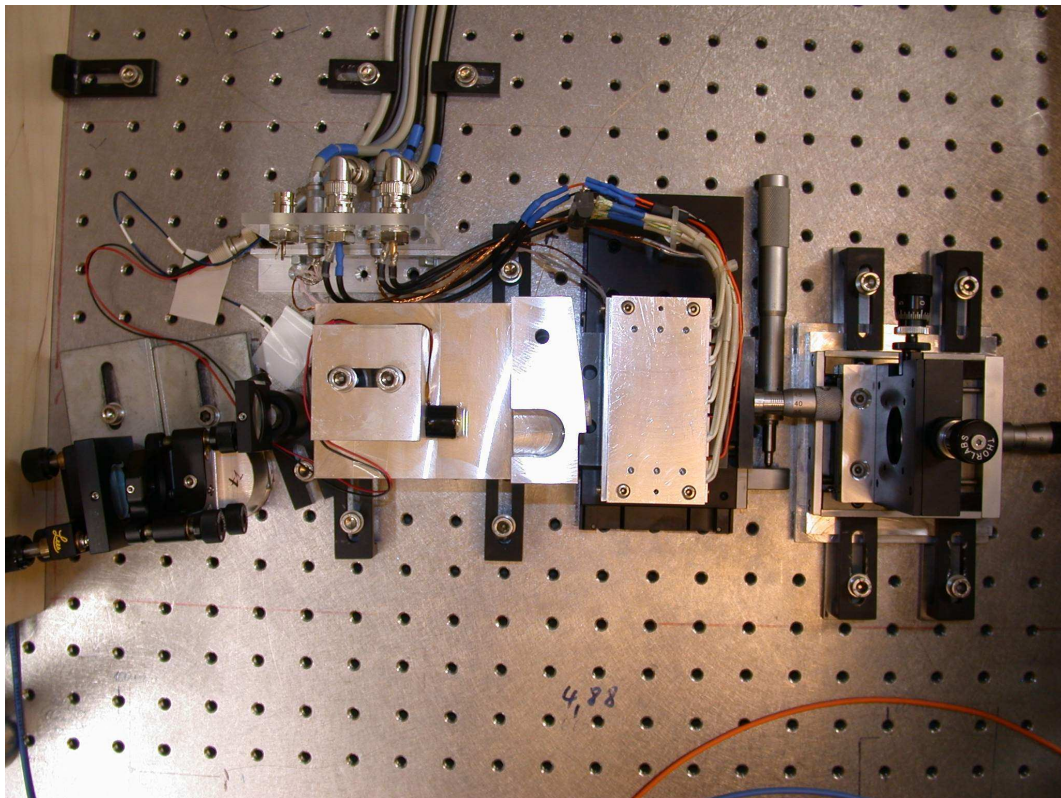
Figure 3.5: *Photograph of the extended OPO cavity setup with an intracavity etalon.*

lengths with residual reflectivities of 0.15 % for the pump, < 1 % for the signal (for wavelength $1.35 - 1.65\,\mu$m, with a minimum 0.1 % at 1.5 μm) and < 2 % for the idler. As we will see later the performance of this antireflection coating is very critical for the condition of low threshold and high efficiency operation of the OPO.

The pump beam is focused into the PPLN crystal with an effective mode matching up to ~ 99 % to the fundamental mode of the OPO cavity. The optimal cavity mode waist can be fixed by changing the distance between the concave mirror and the crystal. The mode matching quality of the pump beam is optimized by minimizing the power in transversal resonator modes. This is usually monitored in the pump wave power which is reflected from the OPO cavity under the OPO oscillation threshold, while the cavity length is scanned over several FSRs.

The pump and signal waves are both resonated in the same folded cavity, which length is locked to the pump laser. The idler wave is not resonated and leaves the cavity through the mirrors M1 and M2. The idler power is emitted approximately equal in both directions. The idler output through the mirror M1 is usually sent to the spectroscopy experiment. The second output through the M2 mirror is first collimated with an uncoated CaF_2 lens with a focal length of 150 mm and used for monitoring the output power and the operating wavelength, and for phase locking the idler frequency to a methane stabilized He–Ne laser.

3.3.1 Cavity length stabilization

The long-term stability and spectral characteristics of an OPO are determined by fluctuations of the optical cavity length. A stable resonator and PPLN crystal temperature both ensure the mode-hop-free operation of the OPO. Since the frequency stability of the pump laser is much better than that of the corresponding mode of the OPO cavity, the active stabilization of the cavity length to the pump frequency is of great importance. The bandwidth and the quality of the cavity lock then determines the linewidth and frequency drifts of the OPO output radiation.

One of the mirrors of the OPO resonator, M2, is mounted on a low voltage PZT (Piezomechnik GmbH, model HPSt 150/14-10/12) with a resonance frequency of 45 kHz. This hollow stack type PZT has a capacity of 2.6 μF and a maximal stroke of 12 μm by applying the voltage between 0 V
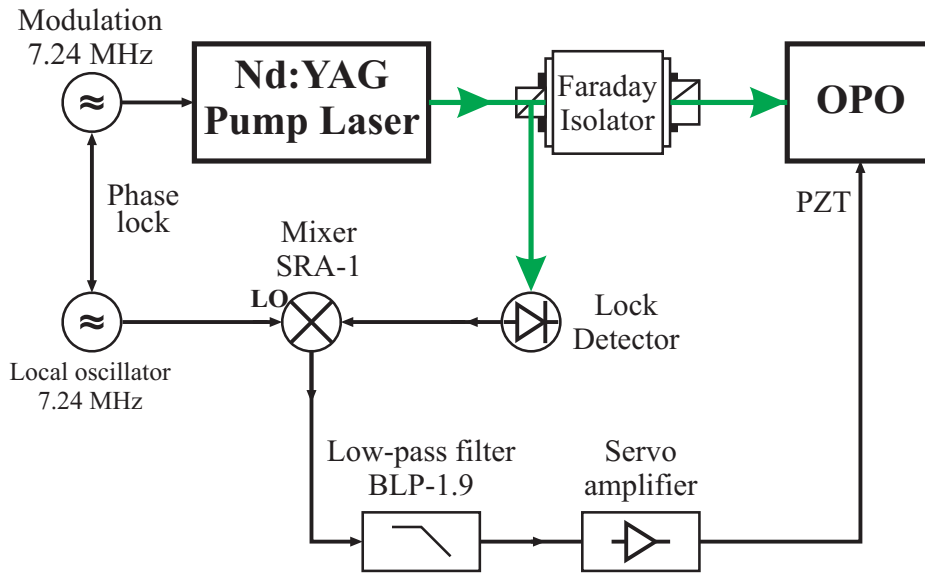
Figure 3.6: *Stabilization scheme of the OPO cavity length.*

and 150 V. To lock the OPO cavity to the narrow-linewidth pump laser, the Pound-Drever-Hall method [74] is used. The typical linewidth of the Fabry-Perot resonances of the extended OPO cavity ranges from 5 to 10 MHz. The stabilization scheme of the OPO cavity length is depicted in Fig. 3.6.

The frequency of the Nd:YAG pump laser is phase-modulated by applying a modulation signal to its PZT input from a radio frequency generator. The chosen modulation frequency of 7.2417 MHz corresponds to a PZT resonance frequency. Using PZT resonances is the simplest approach to achieve frequency deviations corresponding to a modulation index near unity.

A part of the modulated pump beam reflected from the OPO cavity is sent to a lock detector. The latter consists of a fast InGaAs photodiode (Epitaxx, ETX 500T) with a 140 MHz bandwidth followed by a 180 MHz transimpedance amplifier (Philips, NE5211) with a 14 kΩ transimpedance gain. The output of the lock detector contains a phase shifted signal at the modulation frequency, with the shift showing a strong dispersion dependence while sweeping the frequency of the pump laser through resonances of the OPO cavity.

To achieve a phase demodulation signal, a double-balanced mixer (DBM) (Mini-Circuits, SRA-1) is used as a phase detector. The lock detector output is mixed in the DBM with a local oscillator (LO) at the same fre-

quency. The oscillator is phase locked to the modulation generator. The low frequency output of the intermediate-frequency (IF) port of the mixer, which is filtered with a 1.9 MHz low-pass filter (Mini-Circuits, BLP-1.9), then provides the phase demodulated signal.

A frequency discriminator signal occurs by choosing the proper phase relation between the modulation frequency and LO frequency. The zero lock point corresponds to the central frequency of the OPO cavity resonance. The discriminator lock signal is sent to a servo amplifier consisting of a proportional-integral (PI) controller and a PZT-driver. The output of the servo amplifier is then fed back to a piezoelectric transducer controlling the OPO cavity length.

3.3.2 PPLN crystal and emission range

A 19 mm long periodically poled lithium niobate (PPLN) crystal (congruent melt, mole ratio Li/Nb = 0.946) with a 0.5 mm $\times$ 50 mm aperture is the core of the OPO. The crystal contains 33 gratings with QPM periods ranging from 28.98 μm to 30.90 μm in increments of 0.06 μm. Each grating has a width of 1.4 mm. They are separated by 0.1 mm un-poled gaps, as can be seen in the microphotograph in Fig. 3.7 showing a fragment of one of the QPM gratings at the mirror coated face of the PPLN crystal. At crystal temperatures between 140 °C and 190 °C, these QPM gratings can provide quasi-phase-matching for signal waves in the wavelength range 1.50 μm to 1.98 μm, corresponding to 2.30 μm to 3.67 μm for the idler wave. These wavelength ranges are calculated using the Sellmeier equation (2.50).

Originally, the input face of the PPLN crystal, which is perpendicular to the grating vector, was coated with a broadband highly reflecting mirror for the pump ($R_{P_1} \approx 97\,\%$) and the signal ($R_{S_1} > 99\,\%$ for $1.5 - 1.8\ \mu$m) beams, but highly transmitting ($> 95\,\%$) for the idler beam ($2.5 - 3.2\ \mu$m). The $\sim 0.5°$ tilted output face of the crystal was antireflection coated for all three wavelengths with residual reflectivities of $0.2\,\%$ for the pump, $< 1\,\%$ for the signal (for wavelength $1.55 - 1.75\ \mu$m, with a minimum $0.2\,\%$ at $1.65\ \mu$m, according to specifications) and $< 3\,\%$ for the idler.

Unfortunately, this AR coating was not broad enough to allow the OPO to oscillate at all of the 33 QPM periods of the PPLN crystal. Moreover, the minimum of the OPO threshold of ~ 200 mW was displaced in respect to the signal wavelengths around 1.7 μm. As it is shown later in Sec. 4.2.1,

at the wavelength of 1.57 μm the threshold reached the value of as much as 810 mW which is practically the maximum available pump power at the OPO input.

To enable optimal operation of the OPO near the signal wavelength of 1.55 μm, which corresponds to the idler wavelength of interest, 3.39 μm, we have decided to cut the PPLN crystal in two pieces along the 21st QPM grating which has a period of 30.18 μm. The first part with an aperture of 0.5 mm $\times$ 18 mm is preserved with the original coating.

The second part of the crystal with dimensions of 0.5 mm $\times$ 33 mm was again polished and coated as described in subsection 3.3. The optimized input mirror is highly reflecting for the pump ($R_{P_1} \approx 98\%$) and the signal ($R_{S_1} > 99\%$ for 1.35 – 1.65 μm, with a maximum of 99.9% at 1.5 μm), but highly transmitting ($> 98\%$) for the idler (3 – 4 μm). The $\sim 0.25°$ tilted and AR coated crystal face has residual reflectivities of 0.15% for the pump, $< 1\%$ for the signal (for wavelength 1.35 – 1.65 μm, with a minimum 0.1% at 1.5 μm) and $< 2\%$ for the idler.

Both parts of the PPLN crystal are mounted side by side between two gilt copper blocks (60 mm $\times$ 20 mm $\times$ 5 mm), cf. right part of Fig. 3.7. This crystal mounting inside the copper block assembly reduces the temperature gradients along the QPM gratings. This assembly is then located in a temperature stabilized oven (Fig. 3.8) which allows tuning of the OPO output frequencies by the crystal temperature.

The temperature tuning data of the OPO for PPLN crystal temperatures between 140 and 190 °C are presented in Fig. 3.9. The signal wavelengths are measured with a high-resolution wavemeter (Burleigh, model WM–1500). Then, the idler wavelengths are calculated from the signal measurements.

We found that for this temperature span the OPO signal wave is tunable between 1.501 μm and 1.825 μm. This gives a range for the idler tuning between 2.555 μm and 3.660 μm.

These OPO tuning data are truncated at the long-wavelength side of the signal tuning range compared to the expected 1.98 μm. While the OPO still oscillated, its output power levels became insufficient for wavelength measurements with the wavemeter due to the rapidly increasing threshold for the signal wavelengths longer than 1.825 μm.

In this measurement an extended OPO cavity setup without etalon is used. The temperature of the crystal was stable within 0.1 K, with an absolute accuracy of the temperature reading being better than 2 K. During the
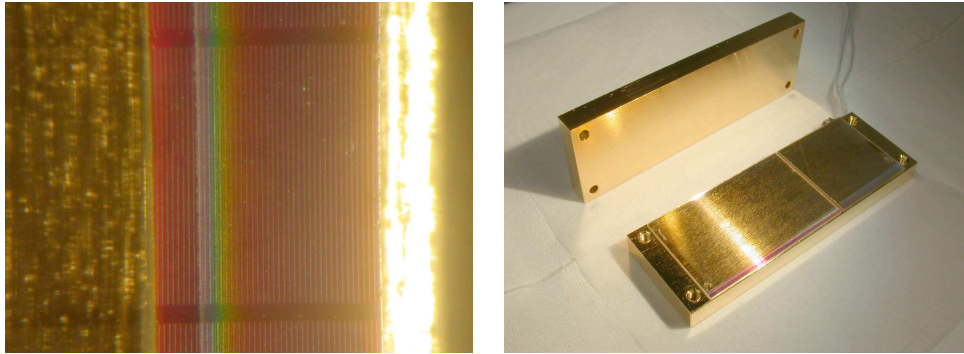
Figure 3.7: *PPLN crystal. Left: microphotograph of one of the QPM gratings near the entrance face of the crystal; here the periodically-poled domains become visible due to a spuriously coated top side of the crystal. Right: arrangement of the two crystal parts before mounting them between two gilt cooper blocks.*
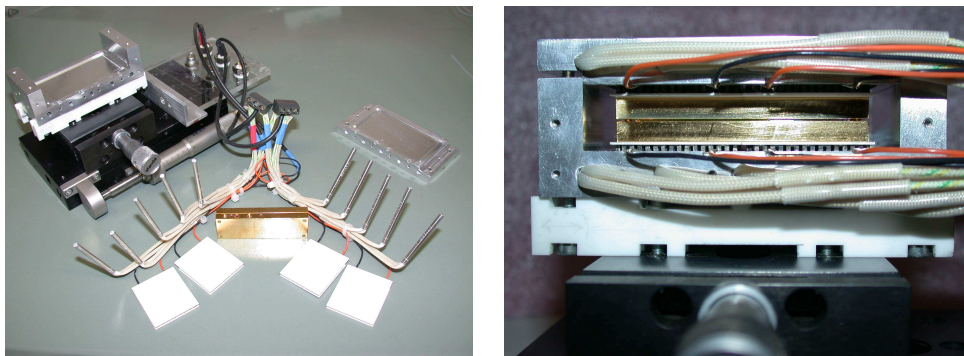

Figure 3.8: *PPLN crystal in a two-stage temperature stabilized oven.*

wavelength measurement the signal output frequencies exhibited mode-hops in the range up to 300 GHz. Every point is obtained as an average value with an accuracy better than 1 nm. One can see from the tuning data that the Sellmeier equation (2.50) is not accurate enough for calculating the quasi-phase-matching wavelengths for long and very short wavelengths of the OPO idler.

3.3.3   Crystal temperature stabilization

To guarantee mode-hop-free operation of the OPO, the temperature of the PPLN crystal has to be stabilized better than several tens of millikelvin. The crystal is placed inside a two-stage temperature controlled oven which is shown in Fig. 3.8. The crystal temperature can be tuned from 20 °C to more than 200 °C.

The temperature of both stages is measured using platinum-resistor-sensors (PT100) and regulated with a temperature stabilization system consisting of two PID-controllers, which have independently adjustable proportional (P), integral (I) and differential (D) gain parameters. To minimize errors of temperature measurements and influence of ambient temperature changes, a 4-point technique has been implemented in the temperature controllers for the precise measurement of the resistance of PT100-sensors.

The first stage of the oven consists of an external aluminum shell (88 mm × 46 mm × 34 mm) which is heated using 10 cartridge heaters (Wattlow, FIRERODE 1/8 in. 60 W 120 V). It consumes about 35 W of electrical power to maintain the internal temperature of 175 °C. Having a time constant of several tens of seconds, this external oven stage can compensate slow ambient temperature drifts controlling the temperature inside the shell at the level of about 5 mK.

The second stage is based on four high-temperature Peltier thermoelectric coolers (Melcor, model HT3-12-30) which support a gilt cooper block assembly (60 mm × 20 mm × 10 mm) containing the PPLN crystal from above and bottom. The block temperature is normally set about 5 °C higher than that of the external stage. It is limited to below 225 °C which is the maximum allowed operation temperature of the Peltier-elements. This stage provides an effective regulation of the fast temperature fluctuations (at the time scale of 1 s). The temperature of the PPLN crystal is controlled within 2 mK, with an absolute accuracy better than 2 K.
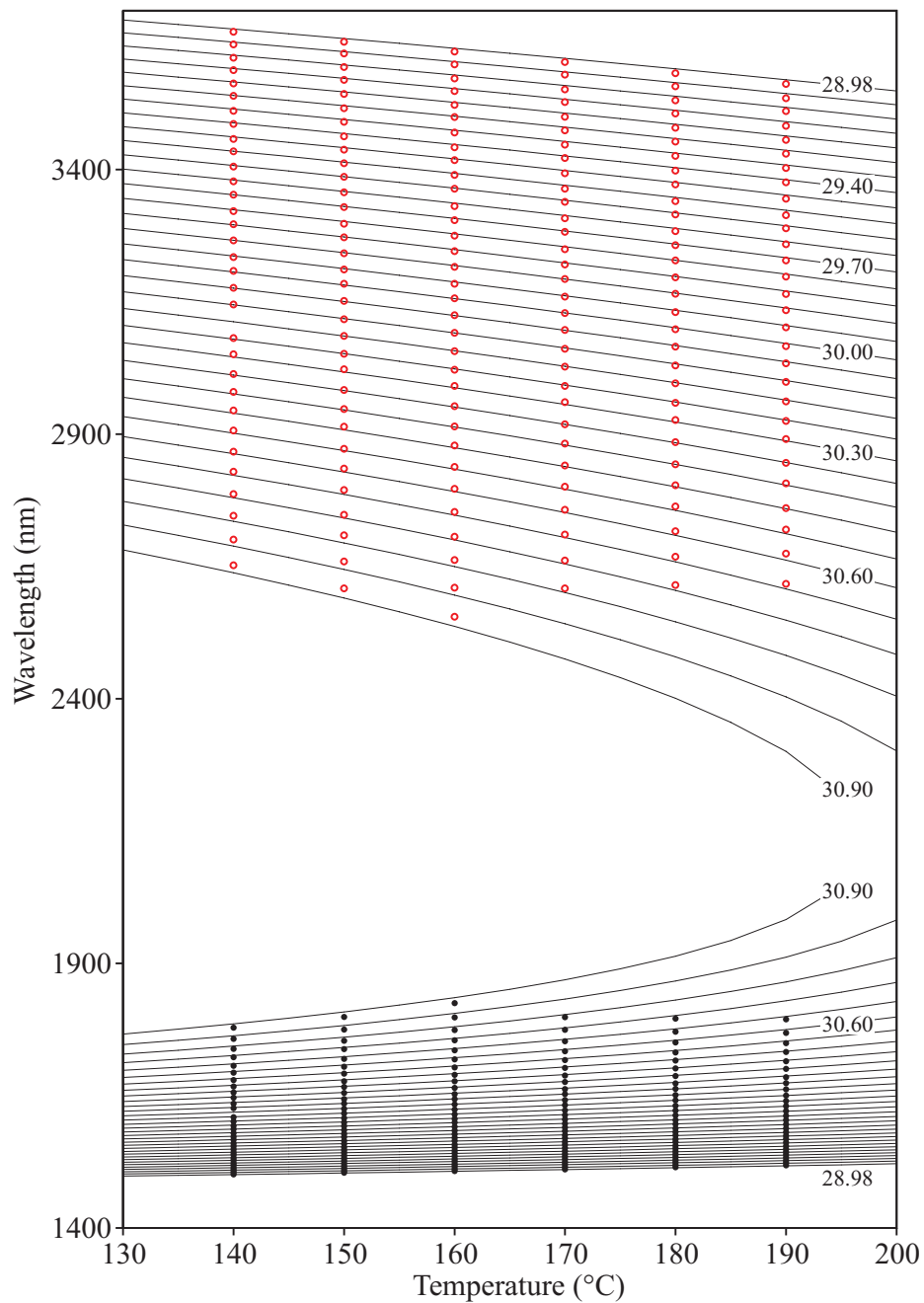
Figure 3.9: *Tuning of the signal and idler wavelengths of the OPO by changing the PPLN crystal temperature. The signal wavelength (black circles) was measured with a high-resolution wavemeter, the idler wavelengths (open red circles) are calculated. Solid lines are calculated from the Sellmeier equations [70], (see also equation (2.50)) for the 33 QPM periods 28.98 μm to 30.90 μm (external to internal lines) with steps of 0.06 μm.*

The oven is held on two perpendicular translation stages. It is thermally isolated from the first of them by mounting on two bars which are made from a machinable glass ceramic (Corning, MACOR) having low thermal conductivity. One translation stage with a 50 mm stroke is used to select one of the QPM grating periods of the PPLN crystal for the coarse tuning of the OPO wavelength. The second stage is needed to set the distance between the PPLN crystal and the internal concave mirror, M2, within the stability range of the OPO resonator and thus to optimize the cavity mode waist at the input face of the crystal.

3.4   Intracavity etalon

The intracavity etalon (ICE) is made of a 1 mm thick undoped YAG plate of 12.7 mm diameter. The free spectral range of the etalon is about 83 GHz. The ICE is specially coated to provide a reflectivity of 15 % per surface for the signal and $< 1\,\%$ for the pump and idler waves. The etalon transmission frequency can be tuned either by tilting or by changing its temperature.

In the first case the tuning between several successive transmission maxima can be done relatively fast, with frequencies up to hundreds of Hertz. For this purpose we used an optical galvanometer scanner (GSI, model G306) allowing a precise angle scan over $\pm\,6°$ with a load-free natural resonant frequency of 300 Hz. The scanner is very useful for the examination of the etalon influence on the pump wave and thus on the threshold and output parameters of the OPO.

In the long-term operation a kinematic mirror mount (Thorlabs, KM100) is more suitable to hold the ICE and adjust its tilt. To stabilize and tune the temperature of the intracavity etalon, a PID-controller is used. It is similar to those which are implemented for the temperature stabilization of the PPLN crystal. The ICE is mounted in a 1 inch adapter which is heated with three 130 Ω resistors connected in series. The temperature of this assembly is measured with a PT100 sensor and stabilized to better than 5 mK. By applying ~ 45 V to the heater (5.2 W) the etalon temperature ~ 60 K above the room temperature can be maintained.

The temperature tuning coefficient of the etalon for the signal wave can be determined as $\Delta\nu_S/\Delta T = -(\Delta l/l)\,\nu_S/\Delta T = -\alpha\,\nu_S$, $\alpha = (1/l)\,\partial l/\partial T$ is the linear expansion coefficient of the ICE substrate. In the special case
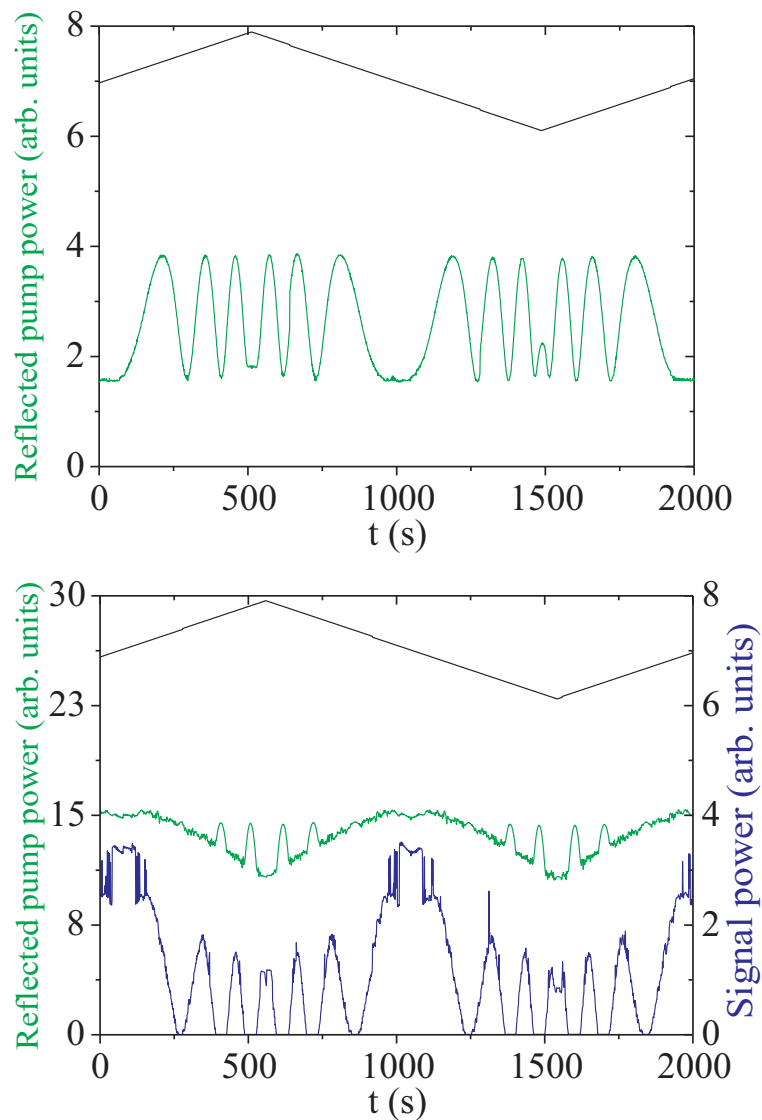
Figure 3.10: *Effect of the etalon tilt tuning on the pump wave and the signal output power. The OPO cavity length is locked to the pump frequency. The tilt of the etalon is linearly swept proportionally to the voltage of the galvanometer driver (upper traces). Top: Power of the pump wave reflected from the OPO cavity below threshold (lower trace). Bottom: Power of the pump wave reflected from the OPO cavity above threshold (middle trace) and output power of the signal wave (lower trace).*

of a YAG etalon with $\alpha = 6.9 \cdot 10^{-6}$ K^{-1} the estimated tuning coefficient is $\Delta \nu_S / \Delta T = -1.33$ GHz/K. Thus, to tune the frequency of the 1 mm thick YAG ICE over one FSR at $\lambda_S = 1.55\,\mu$m, the etalon temperature has to be swept over $\Delta T_{(\lambda_S/2)} = 62.4$ K.

Fig. 3.10 shows the influence of the etalon on the pump wave below and above threshold as well as on the output signal power. The length of the OPO cavity is locked to the pump frequency as described in Section 3.3.1.

To minimize walk-off losses, the intracavity etalon is placed near the cavity end mirror where the beam is almost collimated. The walk-off losses are negligible compared to the spurious etalon effects caused by the residual 0.75 % reflectivity of the ICE surfaces for the pump wave. The latter, while affecting the threshold and tuning behavior of the OPO, did not prevent its stable operation.

Chapter 4

OPO characterization

In this chapter, the tuning behavior of a real singly resonant OPO with resonated pump and the influence of spurious etalon effects on its frequency and tunability are discussed. Here we present the experimental results characterizing the main features of the OPO, as well as direct measurements of the linewidth and long-term behavior of the idler wave with respect to a methane stabilized He–Ne laser. Finally, we demonstrate the phase lock of the OPO idler frequency to the latter.

4.1   Tuning behavior of the OPO

Let us now consider the tuning characteristics of a pump enhanced SRO with resonated signal wave. For simplicity of this analysis, we assume that the crystal temperature is stable, the OPO cavity is non-dispersive for both waves and the OPO oscillates far from the degeneracy wavelength. We suppose that the pump laser provides narrow linewidth, single frequency radiation with a frequency jitter being much smaller than that of the OPO cavity. Moreover, the pump frequency jitter in our case is also smaller than the width of the OPO cavity resonances.

The parametric gain curve for the signal wave is normally much broader than the OPO cavity resonances and even than the cavity free spectral range (FSR). The mechanism of the parametric gain in an SRO is very similar to the laser gain of homogeneously broadened laser lines. The signal wave starts to oscillate on the OPO cavity mode nearest to the maximum of the gain curve, as soon as the pump power reaches the threshold. This oscillating

mode then depletes the pump wave, leaving the pump power circulating in the resonator, and hence the parametric gain at threshold level. Thus, the gain at the other cavity modes remains lower than their losses. The OPO continues to generate signal radiation on that first arising mode while it stays closest to the maximum of the gain curve.

4.1.1 Tuning an ideal pump resonant SRO

Precise tuning of the OPO can be done by changing the frequency of the pump laser. With the OPO cavity length being locked to the pump laser, a linear sweep of the pump laser frequency results in a linear tuning of the cavity, so that $\Delta L_{\mathrm{res}}/L_{\mathrm{res}} = \Delta\lambda_{\mathrm{P}}/\lambda_{\mathrm{P}} = -\Delta\nu_{\mathrm{P}}/\nu_{\mathrm{P}}$. Since the signal and pump waves are both resonated in the same cavity, we also have $\Delta L_{\mathrm{res}}/L_{\mathrm{res}} = -\Delta\nu_{\mathrm{S}}/\nu_{\mathrm{S}}$. Thus, the signal frequency follows the pump laser according to the relation $\Delta\nu_{\mathrm{S}} = (\nu_{\mathrm{S}}/\nu_{\mathrm{P}})\Delta\nu_{\mathrm{P}}$. This however, is confined to one free spectral range (FSR) of the OPO cavity equal to $c/2L_{\mathrm{res}}$ around the maximum of the parametric gain curve.

This situation is illustrated in Fig. 4.1. For simplicity, the relation between the interacting frequencies is chosen to be $\nu_{\mathrm{S}}/\nu_{\mathrm{P}} = 2/3$. Frequency hops of the signal wave to the next neighboring cavity mode occur when the signal frequency approaches the $\pm 1/2$ FSR points with respect to the maximum of the parametric gain curve. Between two successive signal frequency hops, the OPO cavity length changes by one half of the signal wavelength, i. e. $\lambda_{\mathrm{S}}/2$.

The tuning behavior of the idler wave can be determined by subtracting the changes of the signal frequency from those of the pump laser. As it can be seen, the idler frequency exhibits spectral gaps, when the OPO is tuned by varying the pump frequency. However, all these uncovered idler frequencies can easily be reached by locking another cavity mode to the pump laser.

4.1.2 Tuning behavior of a real OPO

The above consideration assumes the ideal case of a symmetric smooth gain curve with a single maximum (Fig. 4.2 a). But in reality, this ideal situation is usually disturbed by parasitic etalon effects and frequency dependent losses inside the OPO resonator and nonlinear crystal. These cause the appearance
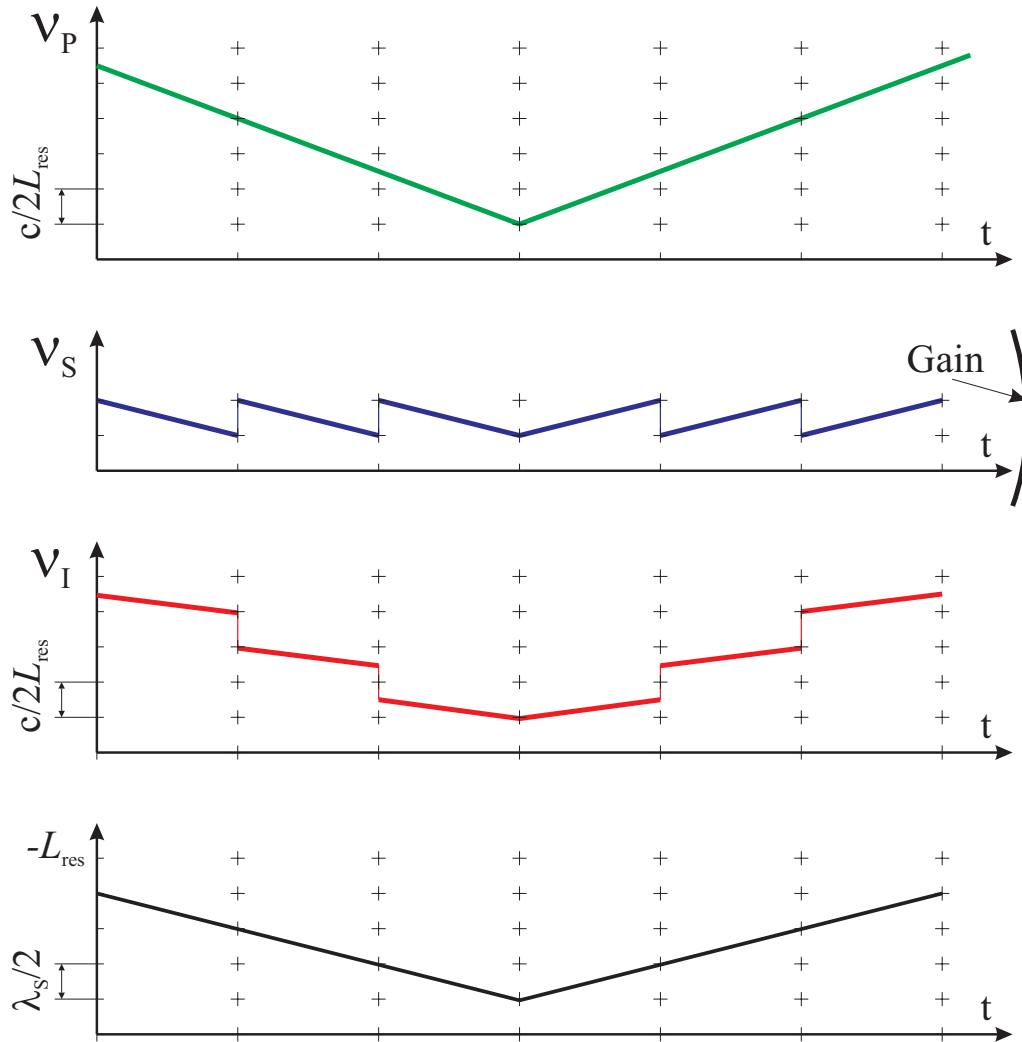
Figure 4.1: *Tuning behavior of an ideal pump + signal resonant OPO by sweeping the pump frequency. Since the OPO cavity length is stabilized to the pump frequency, it changes proportionally ($\Delta L_{\mathrm{res}}/L_{\mathrm{res}} = -\Delta \nu_{\mathrm{P}}/\nu_{\mathrm{P}}$) as well. The signal frequency is localized near the maximum of the gain curve and hops to the next cavity mode after the cavity length varies by $\lambda_{\mathrm{S}}/2$. The frequency of the idler, which is the difference between the pump and signal frequencies, exhibits spectral gaps equal to $c/2L_{\mathrm{res}}$.*

of sporadic local maxima in the effective parametric gain. The relative location of these maxima with respect to the very broad gain line fluctuates with variations of the ambient and crystal temperatures, as well as with the resonator length. They can be found at a distance of many free spectral ranges of the cavity apart from the center of the parametric gain curve (Fig. 4.2 b).

In this case, the tuning of the signal frequency, and hence that of the idler frequency are subjected to hops between the widely separated cavity modes. The tuning continuity and localization of the signal frequency around the parametric gain center are completely destroyed, with many frequency regions becoming unreachable.

To overcome the influence of this spurious effects on the OPO output frequency and come back to a situation similar to that for an ideal unperturbed gain curve, one has to provide additional mode selection (Fig. 4.2 c). One of some possible solutions is to insert a Fabry-Perot etalon into the OPO cavity.

4.1.3 Action of an intracavity etalon

The intracavity etalon (ICE) has to provide considerable additional losses for those cavity modes to which the signal frequency prefers to hop without etalon. To do this in a predictable way, it should only affect the signal wave and not the pump. Therefore, a dichroic optical coating of the etalon has to be specially designed in order to have minimal residual reflectivity at the pump wavelength.

The influence of the intracavity etalon on the OPO performance is shown in Figures 4.3 and 4.4. The first figure shows a typical tuning behavior of a singly resonant OPO without etalon, whereas the second one gives impressions how the same OPO behaves by inserting an ICE into the OPO resonator. In this case, a 1 mm thick YAG etalon with a FSR of ≈ 83 GHz (see Section 3.4) is placed into the extended OPO resonator of length 320 mm (FSR ≈ 470 MHz).

Here we see the results of the idler frequency tuning by varying the pump laser frequency over ~ 7 GHz. The pump laser is continuously tuned by linearly sweeping the temperature of the Nd:YAG crystal with a period of 150 s. The upper pictures of both figures show the range of idler wavelengths around 2.74 μm within a frequency window of 150 GHz. In each case, the lower picture presents a 10 GHz zoom of the corresponding upper one.
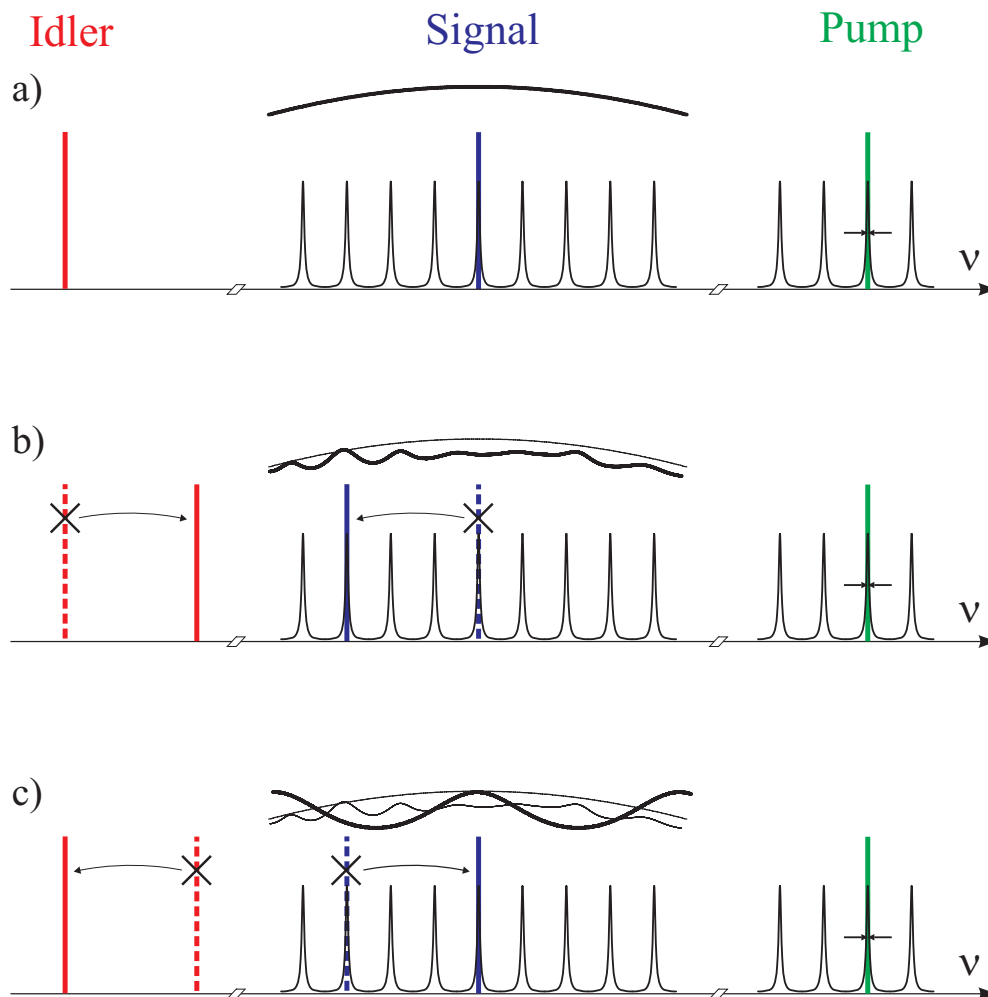
Figure 4.2: *Influence of spurious etalon effects on the output frequency of a pump enhances SRO. Cavity length is locked to the pump frequency. a) An ideal case of the smooth parametric gain curve: the signal is generated near the gain maximum. b) Parasitic etalon effects and frequency dependent losses cause the hops of the signal frequency between local maxima of the effective gain. c) An intracavity etalon (ICE) provides additional mode selection and helps to avoid these hops. The signal frequency now occurs near one of the transmission maxima of the etalon.*
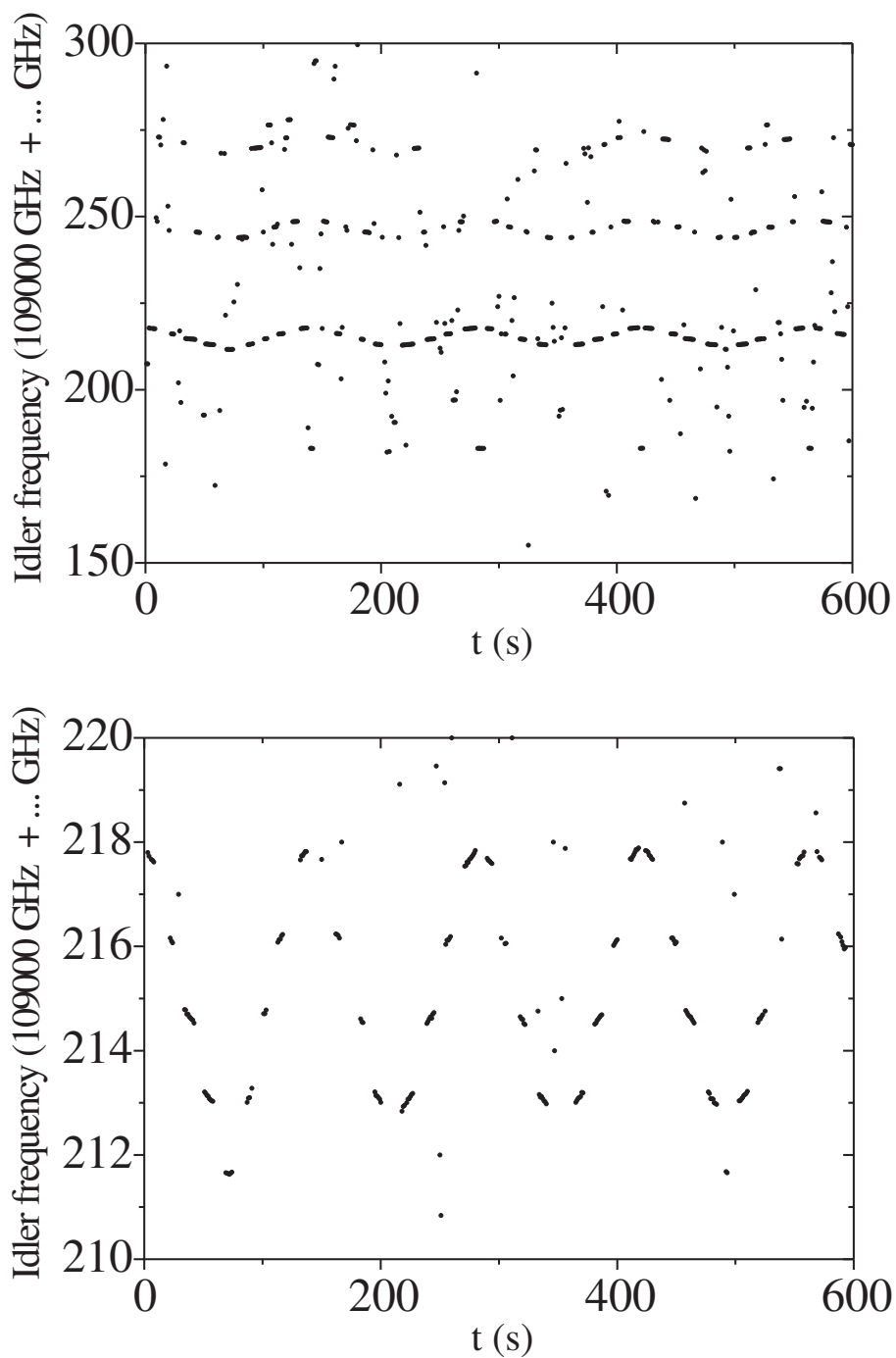
Figure 4.3: *Typical tuning behavior of the OPO idler frequency without intracavity etalon. The OPO is tuned by varying the pump frequency. The lower figure is a 10 GHz zoom part of the upper one.*
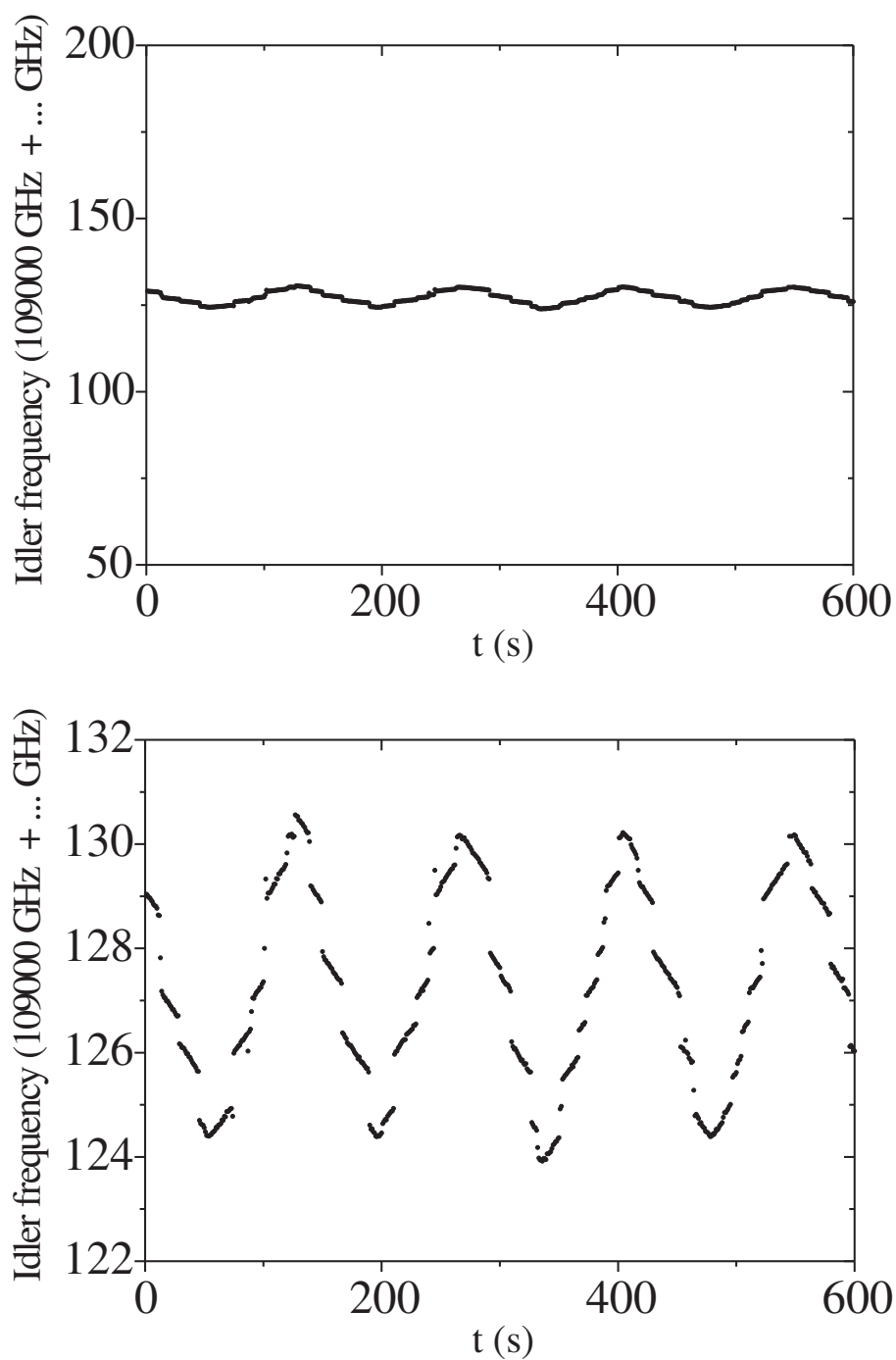
Figure 4.4: *Tuning behavior of the OPO idler frequency with an intracavity etalon. The OPO is tuned by varying the pump frequency. The lower figure is a 10 GHz zoom part of the upper one.*

By tuning the OPO without ICE, its signal frequency hops between the cavity modes separated by several tens to hundred free spectral ranges, (up to 55 GHz), with these hops being transferred directly to the idler frequency (Fig. 4.3).

The same behavior is usually observable in semi-monolithic OPOs. Typically, attempts to tune the OPO to a certain frequency of interest fail. This unreliable tuning behavior restricts the practical use of such kind of OPOs for spectroscopy, because of unpredictable gaps in the spectral coverage.

The situation is completely different if an intracavity etalon is used. The etalon suppresses the far mode hops allowing the OPO to generate the signal wave close to the etalon maximum, which is the nearest one to the center of the unperturbed gain curve. If the pump frequency is tuned, the idler frequency is confined within a frequency range of the order of the pump frequency sweep as shown in Fig. 4.4.

Some divergency from the ideal behavior (cf. with Fig. 4.1) can result from the etalon influence on the pump wave, as mentioned in previous chapter. Furthermore, the hysteresis-like dependence of the idler frequency on the tuning direction can be seen, probably due to the thermal effects in the PPLN crystal.

4.1.4 Closing gaps in the idler frequency tuning spectrum

The position of frequency gaps presented in the idler tuning spectrum depends on the frequencies of the resonated pump and signal waves. By locking the OPO cavity length to the nearby pump resonances these gaps can be covered as shown in Fig. 4.5.

Here, a 4 mm thick YAG etalon with a FSR of ≈ 21 GHz, which is slowly heated up, is placed into the same 320 mm long extended OPO cavity (FSR ≈ 470 MHz). Initially the idler frequency is scanned with the span a bit smaller than the OPO cavity FSR.

As the etalon transmission maximum moves with the increasing of the etalon temperature, the signal hops to the next cavity mode which results in the appearance of the frequency gap of one FSR in the idler wave. In the middle third of the measurement run between 700 s and 1500 s the cavity length of the OPO was several times relocked to different nearby cavity resonances of the pump wave.

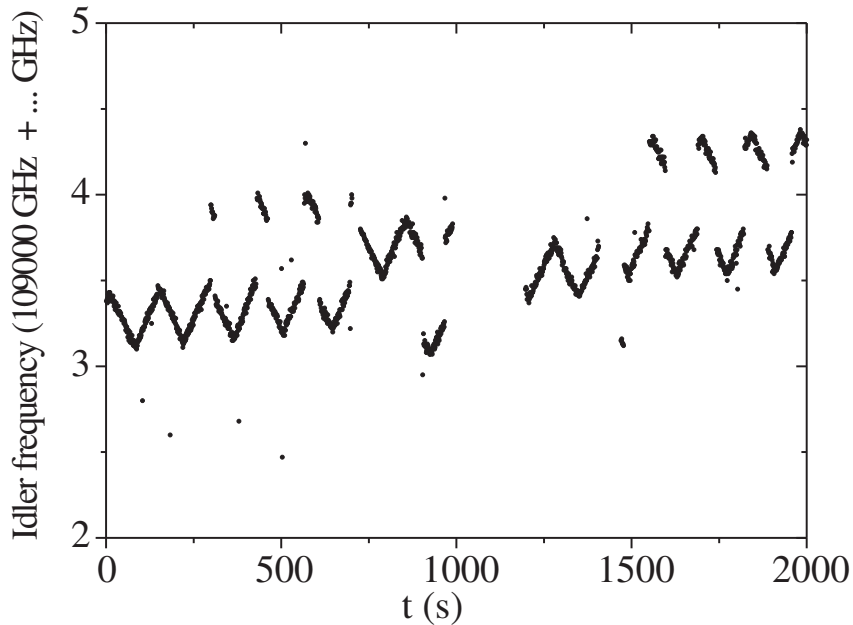The synchronous tuning of the pump frequency and the etalon transmis-

Figure 4.5: *Influence of the ICE tuning on the idler output frequency. Locking the OPO cavity length to nearby pump resonances results in closing gaps in the idler frequency spectrum (for details see text).*

sion frequency results in extended continuous mode-hop-free tuning operation.

4.1.5 Continuous tuning

Fig. 4.6 presents results of the OPO continuous tuning obtained by synchronously sweeping the pump frequency and tilting the ICE using a galvanometer scanner. The pump frequency is swept linearly with a period of ~ 200 s by changing the pump crystal temperature. The galvanometer scanner is then driven using a feed-forward signal of the same period and appropriately chosen amplitude and phase with respect to the signal controlling the pump frequency.

The wavelengths of the both signal and idler waves were measured with a high-resolution wavemeter (Burleigh, model WM–1500) in series. The signal and the idler wavelengths wer centered at ≈ 1.68 μm and ≈ 2.89 μm, respectively.

Continuous tuning ranges of ≈ 1 GHz for the idler wave and ≈ 1.8 GHz for the signal wave are achieved. The continuous tuning range of the signal

corresponds to ~ 5 free spectral ranges of the 420 mm long OPO resonator (FSR $\approx$ 360 MHz). In this case the tuning range was limited by the PZT servo-amplifier and could be easily extended. In theory it should only be limited by the continuous tuning range of the pump laser.

4.2   OPO features

We have seen that the introduction of the intracavity etalon provides well-defined tuning behavior and access to any desired wavelength, whereas without etalon no reliable tuning could be achieved. To characterize the OPO output radiation, we performed power measurement of the signal and idler waves as well as determined its frequency properties.

4.2.1   Threshold, efficiency and output power

According to the theoretical considerations in Section 2.3, the threshold power of a PR-SRO depends on the mirror transmissions and total losses for the signal and pump waves as well as the effective nonlinearity provided with the nonlinear crystal. The total passive losses of the resonator for the pump can be determined by measuring the OPO cavity finesse and coupling efficiency of the pump wave under threshold. The total signal wave losses can then be found from the signal output power characteristics.

The results of the OPO threshold measurements for two different antireflection coatings of PPLN crystals and two OPO setups are shown in Fig. 4.7. All power measurements were performed using a thermopile sensor (Molectron, PM3) connected to a power meter (Molectron Detector Inc., model MAX5200).

Measurements 1 and 2 were done for setups with an originally coated PPLN crystal as described in Sec 3.3.2. The Curve 1 corresponds to a semi-monolithic cavity with a concave mirror of 25 mm of curvature. Curve 2 was measured with an extended cavity setup with a concave mirror, M2, of 100 mm radius. The AR coating has in this case residual reflectivity of ~ 0.2 % at 1.7 μm resulting in an OPO threshold of ~ 200 mW for the semi-monolithic cavity. For the wavelengths shorter then 1.6 μm the OPO threshold exceeded the maximum available pump power.

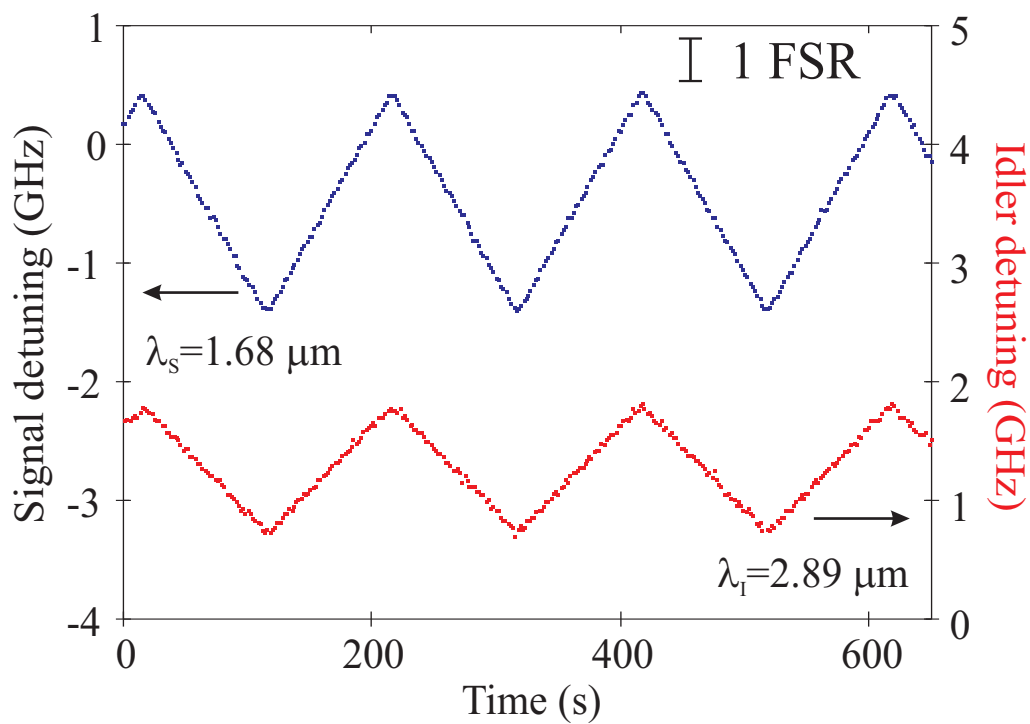With a new AR coating, optimized for signal wavelength around 1.55 μm

Figure 4.6: *Continuous tuning of the OPO over 1.8 GHz for the signal and 1 GHz for the idler, achieved by synchronously sweeping the pump frequency and tilting the ICE. For comparison, the FSR ≈ 360 MHz of the cavity is also displayed. Both frequencies were measured with a high resolution wavemeter.*
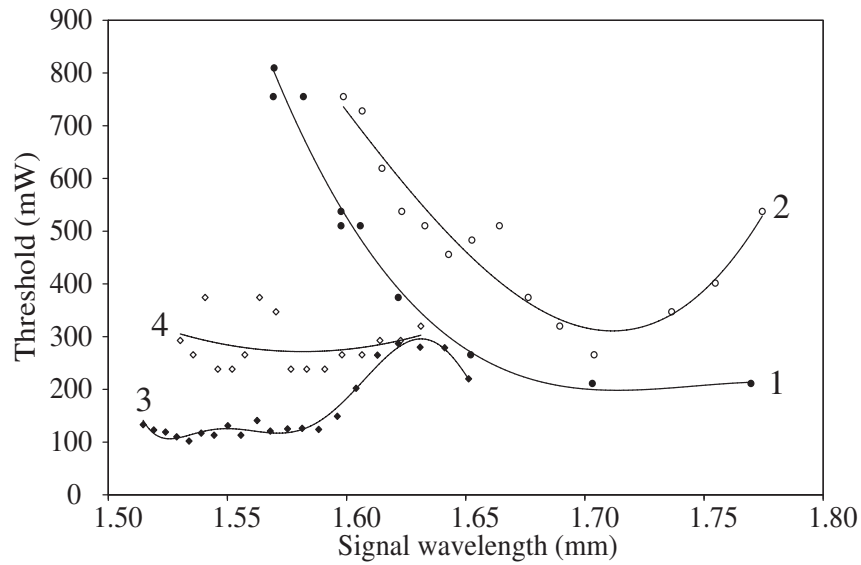
Figure 4.7: *Measurements of the OPO threshold for different AR coatings of the PPLN crystal and with or without an intracavity etalon. See text for details.*
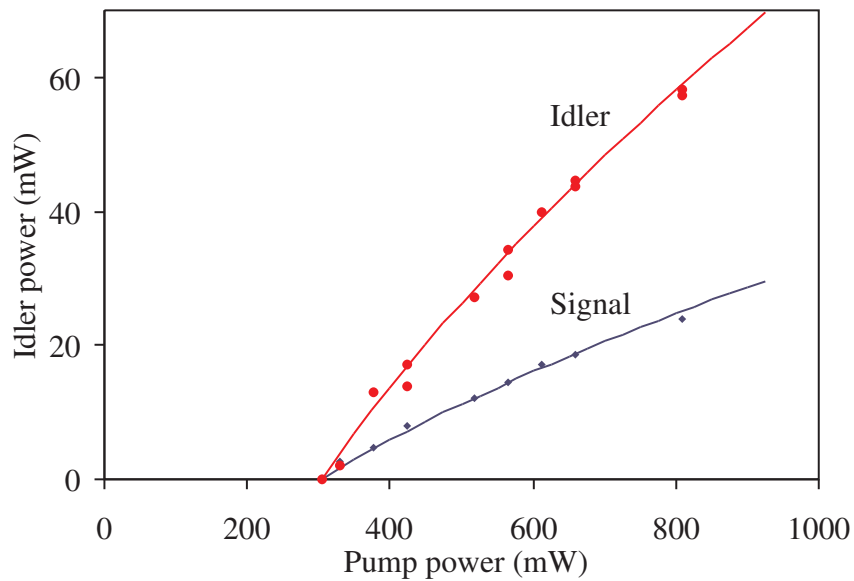

Figure 4.8: *Total measured power of idler (red circles) and signal (blue diamonds), which is emitted from both outputs of the OPO with an intracavity etalon, versus power of the pump beam. Solid lines show theoretical fits according to Eqs. (2.64) and (2.65)*
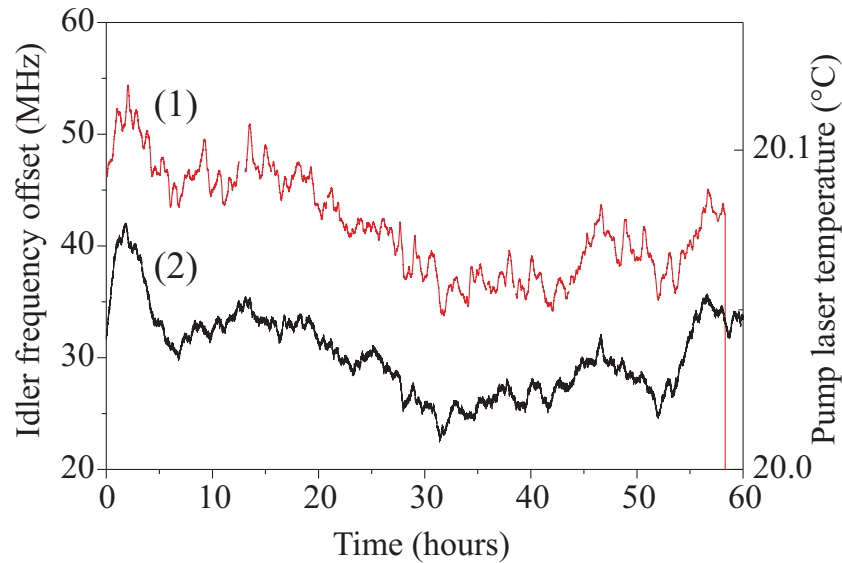
Figure 4.9: *Long term idler frequency behavior of the free-running OPO measured with respect to the methane stabilized He–Ne laser at 3.39 μm. The idler frequency (1) is strongly correlated with the ambient temperature of the pump laser (2) and shows more than two days mode-hop-free operation with a mean long term drift of about 200 kHz/hour.*

(residual reflectivity $\sim$ 0.1 %), the minimum OPO threshold without intra-cavity etalon reached as low as $\sim$ 100 mW (curve 3). Curves 3 and 4 were both measured using the same extended cavity setup as for the curve 2, without and with the intracavity etalon, respectively.

The minimum threshold pump power of the OPO with the ICE was 305 mW at a signal wavelength of 1.55 μm as shown in Fig. 4.8. A finesse of 85 and a measured input mirror transmission of 1.8 % for the pump wave-length yield round-trip cavity losses of $\sim$ 5.5 %, of which $\sim$ 1 % can be attributed to the etalon. At a pump input power of 808 mW the total idler output power through the mirrors M1 and M2 at 3.39 μm was $\sim$ 58 mW and the signal power was $\sim$ 24 mW, both mainly limited by the nonoptimal transmission of the mirror M1 for the pump wave (see Sec. 2.3.1).

4.2.2 Long-term frequency stability

Fig. 4.9 shows the data of a long-term idler frequency measurements of the free-running OPO with respect to a transportable methane stabilized

He–Ne laser [23, 24, 25]. The beat frequency between the OPO idler and the He–Ne laser was measured with averaging time of 10 s each point using a PC-based counter board (Guide Technology Inc., GT200-10 Time Interval Counter).

We observed mode-hop free operation of the OPO over 58 hours with a long term idler frequency drift of ~ 200 kHz/hour. One can see very good correlation of the idler frequency with the ambient temperature, with coefficient of proportionality of ~ 300 MHz/K. As it was mentioned previously in Sec. 3.2 for this behavior of the idler frequency is mainly responsible the Nd:YAG pump laser.

4.2.3   Linewidth measurements

To determine the spectral characteristics of the OPO we performed a beat measurement between the idler wave and the narrow linewidth (~ 50 Hz) radiation of the transportable He–Ne/CH$_4$ stabilized laser [24, 25, 26] at 3.39 μm.

The signal of the beat frequency was tuned to $\sim 2,5$ MHz and then 1 ms long data series were recorded using a 200 MHz digital oscilloscope (LeCroy, WaveRunner LT224) with sampling rate of 10 MS/s. Thereafter the data were Fast Fourier transformed.

For an integration time of ~ 1 ms we found a linewidth of the idler radiation of the free-running OPO at the order of 10 kHz (Fig. 4.10). For integration times longer than 10 ms the output linewidth becomes dominated by frequency jitter of the pump laser and can reach up to several hundreds of kHz.

We have compared our OPO with a commercial version (LINOS Photonics, OS 4000), which is also based on our design and the result of the beat measurement is shown in the inset.

4.3   Phase locking the OPO to an optical reference

Narrow linewidth and capability of a fast frequency modulation means that we are also able to phase lock the OPO to any optical reference, be it an optical resonator, an optical frequency standard or a fs frequency comb. For the first time we have demonstrated the phase locking of the idler wave
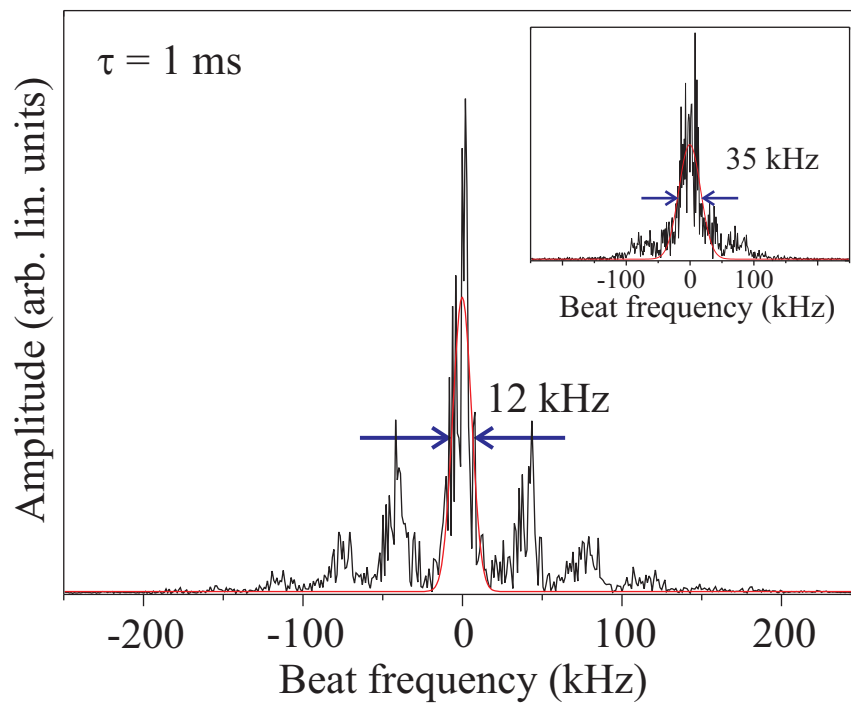
Figure 4.10: *The OPO idler output linewidth. Beat frequency measurements with a methane stabilized He–Ne laser at 3.39 µm give an idler linewidth of about 12 kHz. Inset: Beat frequency of our OPO with a commercial OPO (LINOS Photonics).*
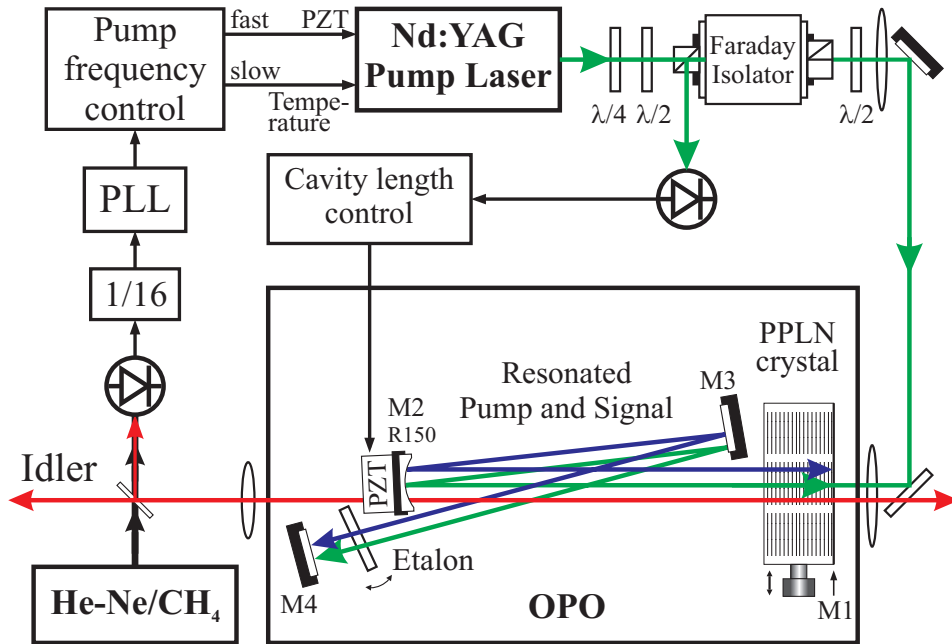
Figure 4.11: *Phase locking scheme of the OPO to a methane stabilized He–Ne laser.*

frequency to a methane stabilized He–Ne laser.

The setup of the idler frequency phase lock is shown schematically in Fig. 4.11. The OPO cavity length is locked to the frequency of the pump laser as described in Sec. 3.3.1. The beat signal of the idler wave with the He–Ne laser at 16 MHz is initially prescaled dividing by 16. Then it is sent to a phase detector based on fast phase/frequency discriminator chip (AD9901, Analog Devices) which is supplied with a 1 MHz local oscillator referenced to a rubidium microwave clock.

The phase error signal of the Phase Lock Loop (PLL) is processed using a servo amplifier with separate fast and slow outputs. The fast control signal is then sent to the PZT of the Nd:YAG pump laser, the slow signal to the temperature controller of the pump laser crystal.

Fig. 4.12 shows the beat signal of the idler, phase locked to a methane stabilized laser. Above a certain gain level in the PLL essentially more and more optical power goes into the carrier.

Another example of the OPO idler frequency phase locking is presented in Fig. 4.13 in logarithmic scale. Integration of the beat signal spectrum indicates that the carrier contains about 82% of the idler wave optical power.
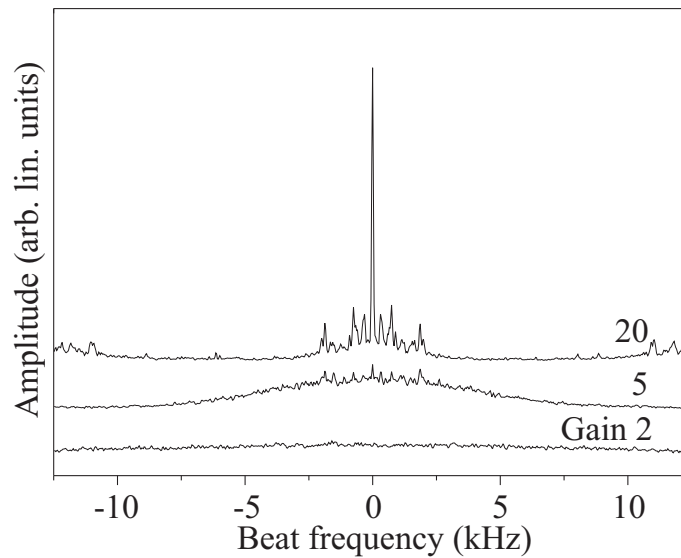
Figure 4.12: *Beat signal by phase locking the OPO to the He–Ne/CH$_4$ laser using three different relative gains of a phase lock loop (PLL). The curves are plotted with offsets and labelled by the PLL gain. In the case of the maximum gain, the PLL bandwidth is $\sim$ 15 kHz.*
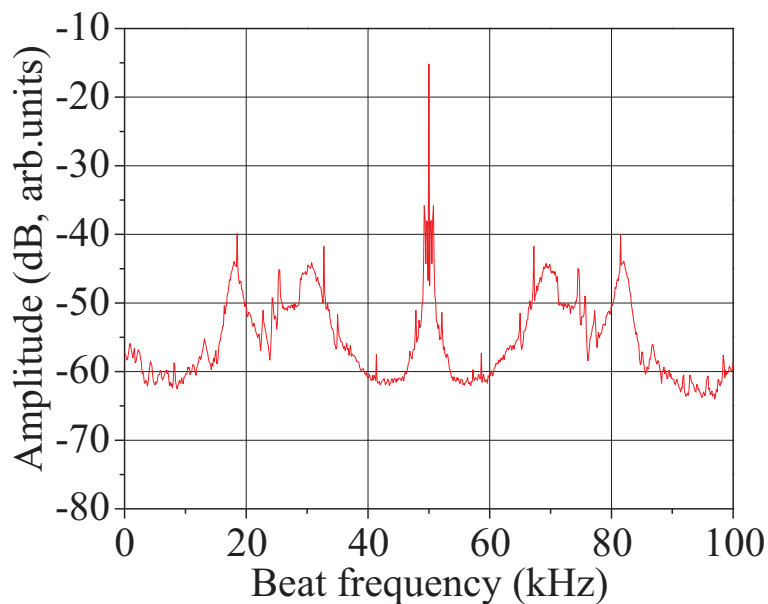

Figure 4.13: *Phase lock of the OPO idler frequency to the He–Ne/CH$_4$ laser.*

Chapter 5

Demonstration of Doppler-free spectroscopy of CH$_4$ using OPO

To demonstrate the capabilities of the new OPO design with intracavity etalon, we performed Doppler-free spectroscopy on the F$_2$ $^{(2)}$ component of the P7 rotation-vibrational transition of the methane molecule at 3.39 μm. This line is traditionally used as a high-stability reference line in He–Ne optical frequency standards.

Due to the availability of the transportable He–Ne/CH$_4$ optical frequency standard [23, 24, 25] we could find and record the nonlinear resonances of this methane line much more easily. Additionally, we had the possibility to slowly frequency lock or even to phase lock the OPO to the methane stabilized laser in order to eliminate the idler frequency drift and diminish its jitter.

5.1 Optical setup

Doppler-free measurements were performed using the frequency modulation spectroscopy (FMS) technique [81] in a 2 m long methane cell, as shown in Fig. 5.1. First, the vertically polarized idler beam, emitted from one output of the OPO, passes a Rochon prism polarizer, RP1, (Karl Lambrecht Corp., model MFRV-9). Then it is split into saturating and probe beams in proportion 5 to 1 and sent through the methane cell.

The probe beam is phase modulated by an electro-optic modulator (EOM) (Gsänger, model LM 3 LN) at the frequency of 1.24 MHz (modula-
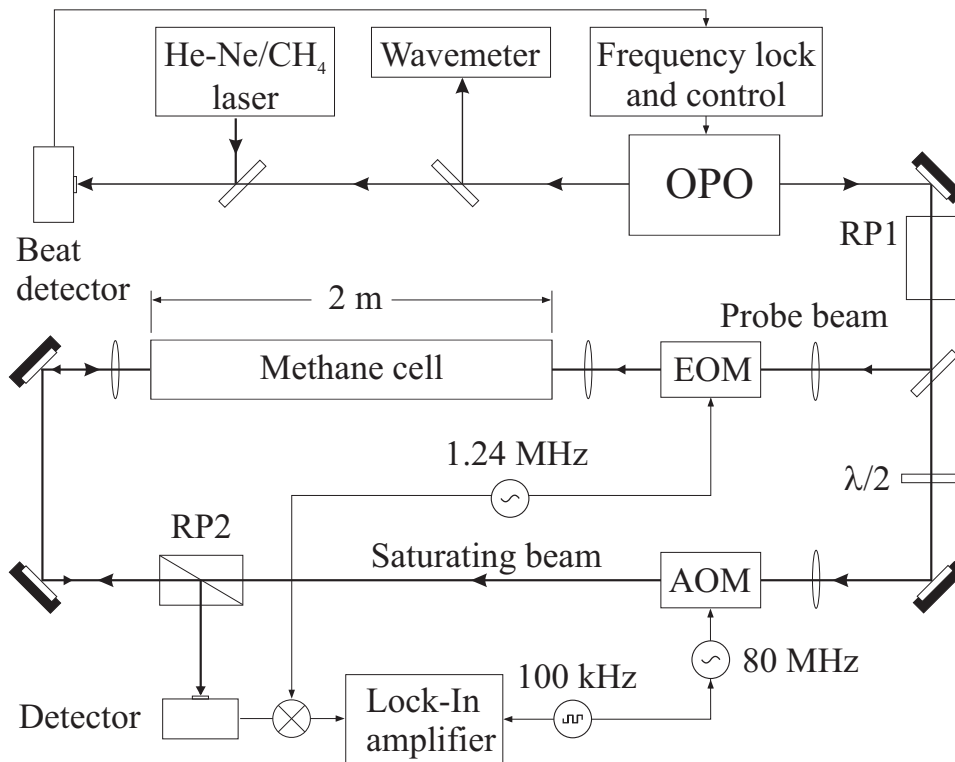
Figure 5.1: *Doppler-free spectroscopy setup. One OPO idler output is split into saturating and probe beams and sent through the methane cell. The probe beam is phase modulated by an electro-optic modulator (EOM). The saturating beam is chopped by the acousto-optic modulator (AOM). After the spectroscopy cell the probe beam is sent to a fast photodetector which output is analyzed by a phase sensitive detection circuit and a lock-in amplifier to extract the spectroscopic signal. The second OPO idler output is used for frequency monitoring by a wavemeter and frequency-locking to a He–Ne/CH$_4$ laser. RP1, RP2 - Rochon prism polarizers.*
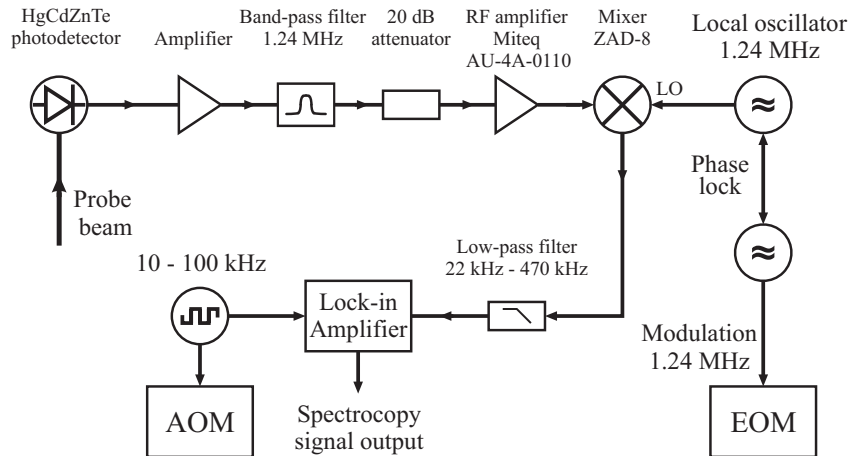
Figure 5.2: *Electronic scheme of the FM spectroscopy setup.*

tion index ~ 1). The saturating beam is chopped by an acousto-optic modulator (IntraAction Corp., model AGM-802A9) at the frequency which can range between 10 kHz and 100 kHz. The polarization of the saturating beam becomes additionally rotated by passing a specially built periscope lift [21]. The both beams are expanded with telescopes built each from two uncoated CaF_2 lenses.

The diameter of the collimated counter-propagating probe (2 mW) and saturating (10 mW) beams inside the cell is about 8 mm, resulting in a transit-time broadening of approximately 30 kHz and a saturation parameter of ~ 0.1 at a methane pressure of 6 mTorr. Passing the methane cell, the probe beam is reflected by the second Rochon prism polarizer, RP2, and sent to a 10 MHz fast HgCdZnTe thermoelectrically cooled photovoltaic detector (Vigo System, model PDI-2T-4) (in Fig. 5.2).

The detected probe beam includes a modulated signal depending on the detuning from the absorption line center. After bandpass filtering and amplification of the signal at the modulation frequency, it is then mixed with the local oscillator frequency using a double-balanced mixer (DBM) (Mini-Circuits, ZAD-8), in order to provide the phase sensitive measurement. By selecting an appropriate phase of the local oscillator frequency one can achieve Doppler-free resonances with dispersion profiles.

Chopping of the saturating beam with an acousto-optic modulator (AOM) in combination with lock-in detection is used to eliminate the Dopp-

ler broadened background and spurious amplitude modulation. Using orthogonal polarizations for the pump and probe beams, together with the 80 MHz frequency shift provided by the AOM , helps very effectively to avoid perturbations of the OPO due to back reflections from the spectroscopy experiment.

5.2   Recording of Doppler-free resonances

The FM spectroscopy signals, obtained after the lock-in amplifier (SRS, SR830 DSP), were recorded using a digital oscilloscope (LeCroy, WaveRunner LT224) or a PC-based 14 Bit data acquisition card (Decision Int., Super 14 Bit AD/DA Card).

Using the OPO, first Doppler-free dispersion resonances of the P7 $F_2^{(2)}$ line of methane at 3.39 μm were detected for methane pressures from 6 mTorr to 99 mTorr. To suppress slow frequency drifts of the OPO, the idler frequency was slowly frequency-locked, with a bandwidth <100 Hz, to the He–Ne stabilized laser with an offset frequency of 40 MHz. It was then linearly scanned through the saturated resonance by changing the offset frequency. Thereafter, the resonances were recorded by sweeping idler frequency in 50 s with 5 MHz span and using lock-in time constant of 30 ms.

Fig. 5.3 shows Doppler-free resonances of the P7 $F_2^{(2)}$ line for different pressures between 6 and 99 mTorr. The results of calculated linewidths obtained from the theoretical fits shown in Fig. 5.3 are presented in Ref. [75]. The observed pressure broadening coefficient of 16.2 kHz/mTorr is in good agreement with the previously published data in Ref. [82].

The narrowest resonance is here obtained at methane pressure of 6 mTorr. The observed linewidth of 500 kHz can be attributed to a combination of pressure broadening $\sim$ 200 kHz ([82]) and medium-term jitter $\sim$ 200 kHz to 400 kHz of the OPO frequency. At higher pressures the linewidth was dominated by pressure broadening.

To observe more narrower resonances we had to eliminate the idler frequency jitter. For this, to detect Doppler-free resonances at low pressures, $\leq$1 mTorr, the idler frequency was phase locked to the methane stabilized He–Ne laser. Tuning the idler over a 2 MHz wide range, we obtained the Doppler-free dispersive signal shown in Fig. 5.4. The observed linewidth of 150 kHz can be mainly attributed to the saturation broadening.
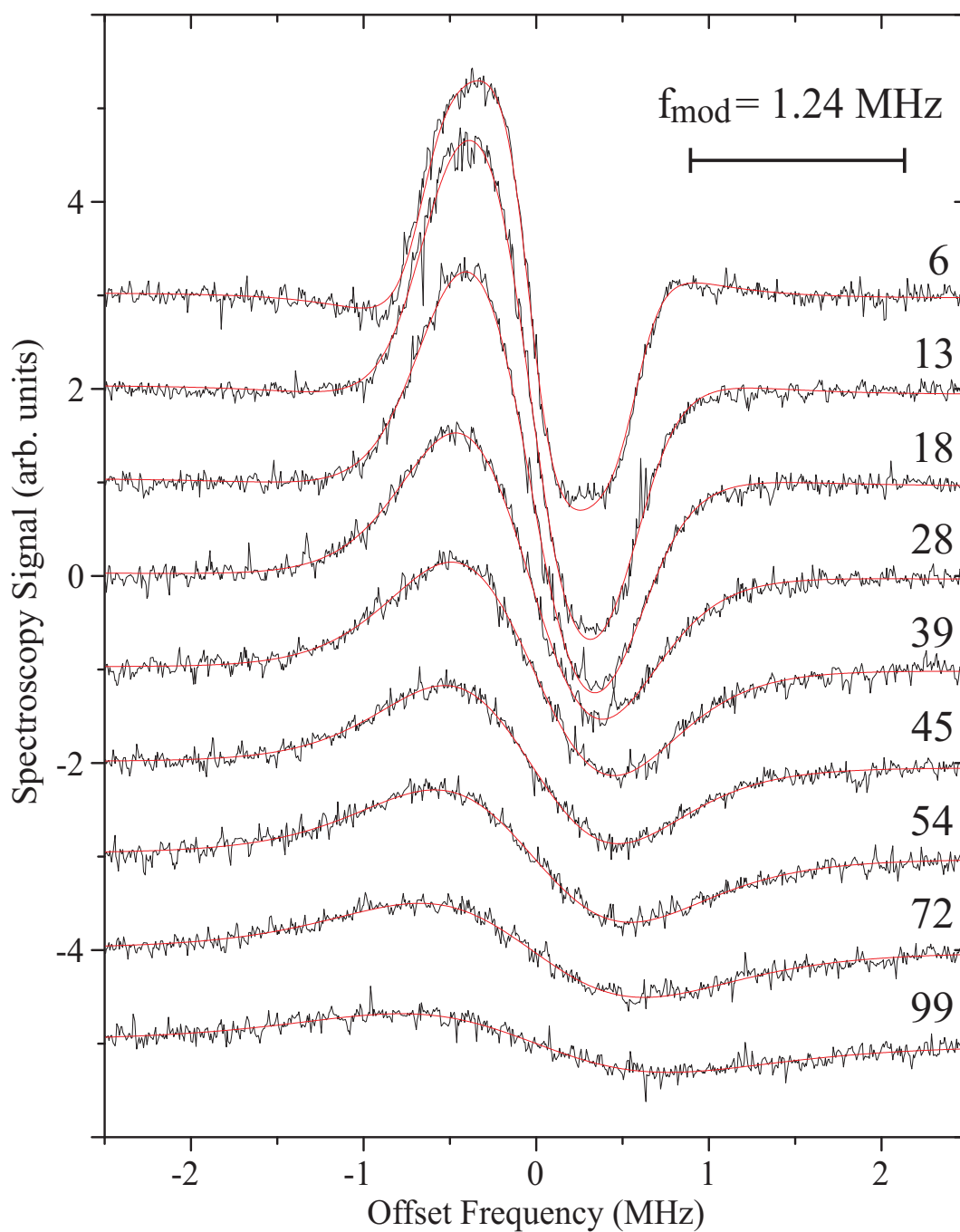
Figure 5.3: *Doppler-free resonances of the methane P7 $F_2^{(2)}$ line at 3.39 µm for different pressures. The curves are plotted with offsets and labelled by the CH_4 pressure in mTorr. Lines: fit according to the theoretical model [81].*
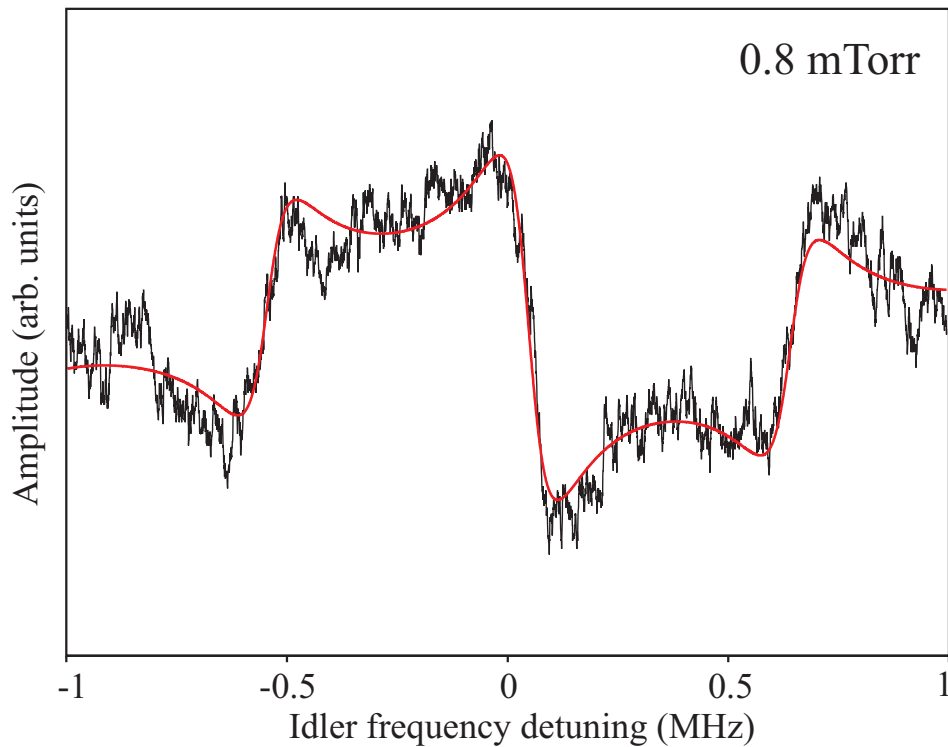
Figure 5.4: *Doppler-free resonance of the methane P7 $F_2^{(2)}$ line (3.39 μm) at the methane pressure of 0.8 mTorr. 150 kHz FWHM obtained by scanning the OPO idler frequency, phase locked to He–Ne/CH_4, over 2 MHz frequency range. Line is fited according to the theoretical model [81].*

Chapter 6

Combining OPO and Ti:Sapphire femtosecond frequency comb

In the previous two chapters it was shown that cw OPOs are well suited for purposes of high-resolution molecular spectroscopy. Pump enhanced cw singly resonant OPOs with an intracavity etalon are quite reliable tools and have excellent long-term stability. They not only offer a wide tuning range and high output power levels, but also a narrow linewidth and the possibility of phase locking to stable optical references.

Recent developments of femtosecond laser frequency combs have marked a breakthrough in optical metrology [30, 31], which also opens new perspectives for cw OPOs as multipurpose spectroscopic and metrological tools. In combination with a Ti:Sapphire optical frequency comb, a cw OPO can phase coherently link the infrared and the visible spectral ranges [34, 35].

In this chapter, after a brief review of methods of femtosecond optical frequency metrology, it is shown how to establish such a connection. A new concept of optical frequency measurements using a Ti:Sapphire femtosecond laser comb and an OPO, both referenced to a methane infrared optical frequency standard, is presented. First, our femtosecond laser frequency comb is introduced. Then the phase locking of the comb and the OPO to a methane stabilized laser is demonstrated.

Finally, we present absolute frequency comparisons between methane and iodine stabilized lasers as a first implementation of this new technique. The possibility to employ an OPO–comb tandem for high-resolution infrared spectroscopy and metrology is also discussed.

6.1   Methods of femtosecond metrology

The idea to make use of a frequency "ruler" emitted by pulsed lasers for measuring large separations between atomic lines was conceived about 30 years ago [83, 84]. It was independently suggested by the US group of Prof. T. W. Hänsch and the Russian group of Prof. V. P. Chebotayev. The realization of this idea was then demonstrated by the group of T. W. Hänsch at Stanford University [85]. In this first experiment a train of picosecond pulses from a synchronously pumped mode-locked cw dye laser was used for Doppler-free two-photon spectroscopy of sodium at 579 nm. Accurate measurements of optical frequency differences of up to 1000 GHz with kHz-precision were shown to be feasible.

Only two decades later, after dramatic developments in the field of solid-state lasers (e.g. see review [86]), and especially the inventions of the Ti:Sapphire laser and the Kerr-lens mode locking [87], Prof. T. W. Hänsch and his team at the Max-Plank-Institute für Quantenoptik in Garching have re-opened common and wide-spreading interest to this method and showed its manyfold improvement. A frequency difference measurement covering a 45 THz frequency gap using an optical comb generated by a femtosecond mode-locked laser was demonstrated [88, 89, 90, 91]. The separation between the comb modes was shown to be equal to the pulse repetition rate of the laser within an experimental uncertainty of 6×10^{-16}. The uniformity of the comb spectrum spacing has been verified with an accuracy of at least 3×10^{-17}. This achievement marked the beginning of the rapidly growing now femtosecond optical frequency metrology.

Owing to the progress in another research field, namely the investigation of photonic crystal materials, and specially the fabrication of highly nonlinear photonic crystal fibers (PCF) [92, 93], the generation of a comb spectrum spanning over one optical octave became possible [33]. This enabled the next significant step, solving in a simple way the main metrological problem, how to phase coherently connect an optical frequency with a primary cesium microwave standard.

The cumbersome and very complex setups of harmonic frequency multiplication chains used before for measuring only some certain optical frequencies [26] has given way to the universal and compact femtosecond frequency combs suitable for precise measurements in the entire optical spectral range.

Frequency combs based on femtosecond lasers consist of a multitude of optical frequencies f_n according to the expression $f_n = n f_{\text{rep}} + f_0$, where f_{rep} is the repetition rate of the femtosecond laser (typical values for f_{rep} are 0.1–1 GHz) and $f_0 < f_{\text{rep}}$ is the offset frequency due to pulse-to-pulse carrier-envelope phase shift, and $n \sim 10^5 - 10^6$ is an integer. These two microwave frequencies represent the two degrees of freedom of such a frequency comb. Measuring and controlling them is essential in implementing an optical clockwork capable of phase-coherent frequency comparisons.

Methods of femtosecond optical frequency metrology are based on establishing a phase-coherent relation between an optical frequency within a femtosecond comb spectrum and that of a primary microwave clock or of an optical frequency standard. An optical frequency ν_n can be determined by measuring the beat signal δ_n with a corresponding line of the femtosecond comb f_n, so that $\nu_n = f_n + \delta_n = n f_{\text{rep}} + f_0 + \delta_n$. All three involved radio-frequencies have to be measured and/or controlled with respect to the microwave standard. The value of n can be determined by a preliminary measurement of the optical wavelength using a high-performance wavemeter with a resolution better than f_{rep}. While the comb spacing f_{rep} is straightforward to measure, the control of the offset frequency f_0 is a non-trivial task requiring ingenious schemes, including the self-referencing of octave spanning combs and offset-eliminating configurations [88, 32, 30, 33].

Let us consider now some techniques of measuring optical frequencies with femtosecond laser combs, as well as the methods allowing to extract and control the carrier-envelope offset frequency. The application of one or another scheme is dictated by the specific accuracy requirements of the measurement.

6.1.1 Measurement of optical frequency differences

The first and easiest task which can be solved with an optical comb is to measure the optical frequency differences between two widely separated cw narrow-linewidth lasers with frequencies ν_1 and ν_2.

If we detect the beat frequency δ_1 between the first laser and a nearby to the left comb line, the laser frequency ν_1 can be expressed as $\nu_1 = n_1 f_{\text{rep}} + f_0 + \delta_1$. Analogous for the second laser we can write $\nu_2 = n_2 f_{\text{rep}} + f_0 + \delta_2$. It is easy to see, that the difference between both laser frequencies $\nu_{21} = \nu_2 - \nu_1 = (n_2 - n_1) f_{\text{rep}} + (\delta_2 - \delta_1) = n_{21} f_{\text{rep}} + \delta_{21}$ does not depend on

the carrier-envelope offset frequency. The repetition rate frequency of the comb can be phase locked or measured with respect to an atomic microwave clock.

If only the comb spacing is referenced to the microwave frequency standard but the comb offset frequency remains free-running, we obtain a floating ruler suitable for precise measurements of optical frequency differences. In this case, the measurement accuracy is determined by the microwave reference.

The difference of two widely separated optical frequencies can itself be an optical frequency. Thus, if a femtosecond laser frequency comb spreads over one optical octave and its f_{rep} is stabilized, absolute optical frequencies can be measured [33, 94, 95]. The realization of octave spanning combs has extremely simplified the problems of optical frequency metrology. Now, optical frequencies can be measured directly with respect to the primary Cs microwave frequency standard.

6.1.2 $2f - f$ technique

Fig. 6.1 demonstrates the principle of the $2f - f$ technique. A measurement of the difference between the frequency $\nu_1 = f$ of a laser (e.g. Nd:YAG laser, $\lambda = 1064$ nm) and its second harmonic $\nu_2 = 2f$ (at 532 nm), which are both located within the spectrum of a femtosecond laser frequency comb, gives in result the absolute optical frequency of the laser itself: $\nu_1 = 2f - f = \nu_{21} = n_{21} f_{\text{rep}} + (\delta_2 - \delta_1) = n_{21} f_{\text{rep}} + \delta_{21}$.

The comb offset frequency f_0 does not influence the measurement and in principle can be free running. The comb spacing f_{rep} can be either phase locked to a microwave frequency standard or also be free-running. In the last case, f_{rep} has to be measured simultaneously with two frequency beats δ_1 and δ_2 followed by processing of the recorded signals in order to obtain the absolute value of the measured laser frequency.

The $2f - f$ technique can also be used for the implementation of an optical clock. The stability of the measured laser frequency $\nu_1 = f$ can be comparable or better than that of a microwave frequency standard. For example, this is the case for an iodine stabilized Nd:YAG laser as compared to a hydrogen maser [96]. Thus, if the comb spacing is locked to the maser, the measurement accuracy of the optical frequency will be limited by the last one. Nevertheless, phase locking of the comb repetition rate to
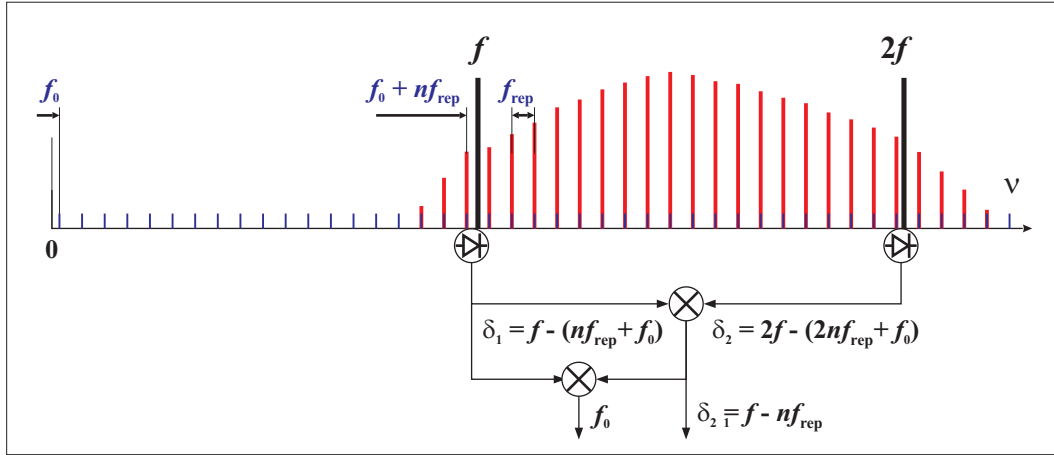
Figure 6.1: *Measurement of an absolute optical frequency with an octave spanning femtosecond comb using the $2f - f$ technique.*

the optical frequency f using the difference between two beat frequencies $\delta_2 - \delta_1 = f - n_{21} f_{rep}$ provides a stable microwave signal at the frequency f_{rep} with the performance of the optical frequency standard. Such an optical clock can be much more precise than the best current microwave clocks.

On the other hand, using this method, one can also determine the comb offset frequency f_0. Measuring the beat signal δ_1 of a laser of frequency f with the n-th line of the comb $\delta_1 = f - (n f_{rep} + f_0)$ simultaneously with the beat signal δ_2 of its second harmonic $2f$ with the $2n$–th line of the comb $\delta_2 = 2f - (2n f_{rep} + f_0)$, and then processing the difference $\delta_2 - 2\delta_1 = 2f - (2n f_{rep} + f_0) - 2(f - (n f_{rep} + f_0)) = f_0$ gives the absolute value of the comb offset frequency. Thus, f_0 can be stabilized, and hence, the pulse-to-pulse carrier-envelope phase shift can be controlled.

6.1.3 Self-referencing technique

Sometimes it is very desirable to have an absolutely stabilized optical comb with well-defined parameters of spacing and offset. In this case the self-referencing technique is usually applied [30]. The comb offset frequency can be easily determined also without need to use an additional laser (Fig. 6.2). To do this one has to take a red part of an octave spanning femtosecond comb around the n-th line of the comb with frequencies $f_n = n f_{rep} + f_0$ and double its frequency in a nonlinear crystal. The resulting beam has to be overlapped at a fast photodetector with another one of the corre-
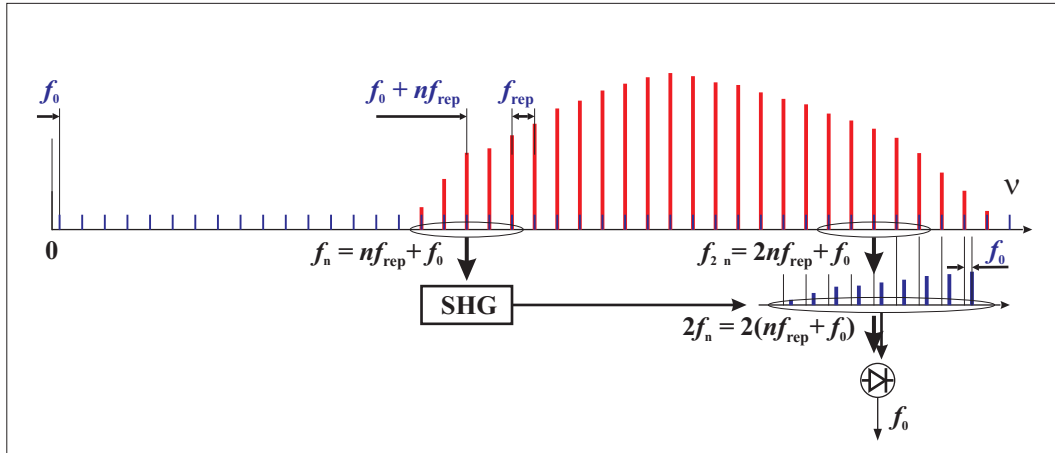
Figure 6.2: *Controlling an octave spanning femtosecond comb using the self-referencing technique.*

sponding blue part of the comb around the $2n$-th line $f_{2n} = 2n f_{\text{rep}} + f_0$ in order to obtain a heterodyne beat equal to the comb offset frequency: $2f_n - f_{2n} = 2(n f_{\text{rep}} + f_0) - (2n f_{\text{rep}} + f_0) = f_0$. One only has to take care of temporal overlapping of the interacting pulses in these two beams using an adjustable delay line. Practically a large number of comb lines ($\sim 10^4 - 10^5$) can contribute to the f_0 beat signal thus highly enhancing the signal-to-noise ratio.

Self-referenced femtosecond combs can properly be considered as synthesizers of optical frequencies [30, 97, 98], coherently connecting microwave and optical frequency ranges. They are also used in all-optical clocks transferring the highest stability of optical frequency standards based on single trapped ions [99, 100, 101, 102] to the microwave output frequency.

6.1.4   SFG and DFG combs

Another approach eliminating the influence of the comb offset frequency is based on generation of secondary combs using the processes of sum- or difference-frequency generation (SFG and DFG). The accuracy of these processes was verified by M. Zimmermann *et al.* [103] down to the level $< 10^{-20}$. SFG and DFG combs allow to perform absolute frequency measurements in the infrared spectral region, which is far from available for nowadays combs. Moreover, this method can be implemented without relying on photonic crystal fibers (PCF) [92, 93] and local laser oscillators phase
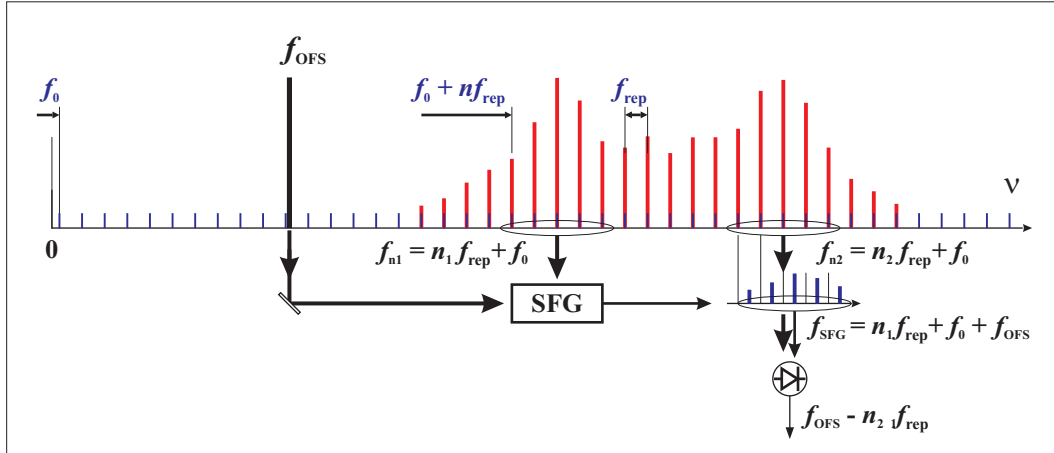
Figure 6.3: *SFG comb.*

locked to the femtosecond comb [104, 105].

Employment of a SFG comb can be considered as an extension of the techniques described above. For example, such a comb can be generated in a SFG crystal by combining some part from the red-side of an original comb $f_{n_1} = n_1 f_{\text{rep}} + f_0$ with radiation of an infrared or a visible optical frequency standard f_{OFS} (see Fig. 6.3). Performing the heterodyne beat frequency measurement between the SFG comb $f_{\text{SFG}} = n_1 f_{\text{rep}} + f_0 + f_{\text{OFS}}$ and the original one $f_{n_2} = n_2 f_{\text{rep}} + f_0$, gives the offset-insensitive signal $f_{\text{SFG}} - f_{n_2} = f_{\text{OFS}} - n_{21} f_{\text{rep}}$. This signal can be used for phase locking the comb spacing to the frequency of the optical standard, and thus for realizing an optical clock. For their realization SFG clockworks usually need additional transfer oscillators such as diode lasers or a commercial cw OPO [106, 104]. On the other hand, if instead of the optical standard some narrow-linewidth infrared cw laser is used and f_{rep} is phase locked to a primary microwave standard, this scheme will be useful for high-resolution spectroscopy.

Based on this method, an optical clockwork without control of the carrier-envelope frequency was experimentally implemented by O. Mücke *et al.* [104]. Here the IR idler radiation of a commercial OPO at 3.39 μm was mixed in an SFG crystal with one part of a custom-tailored mode-locked Ti:Sapphire emitting two strong peaks at 670 and 834 nm. The repetition rate of the femtosecond laser was phase locked to a local microwave cesium clock and in doing so a direct link between microwave and infrared
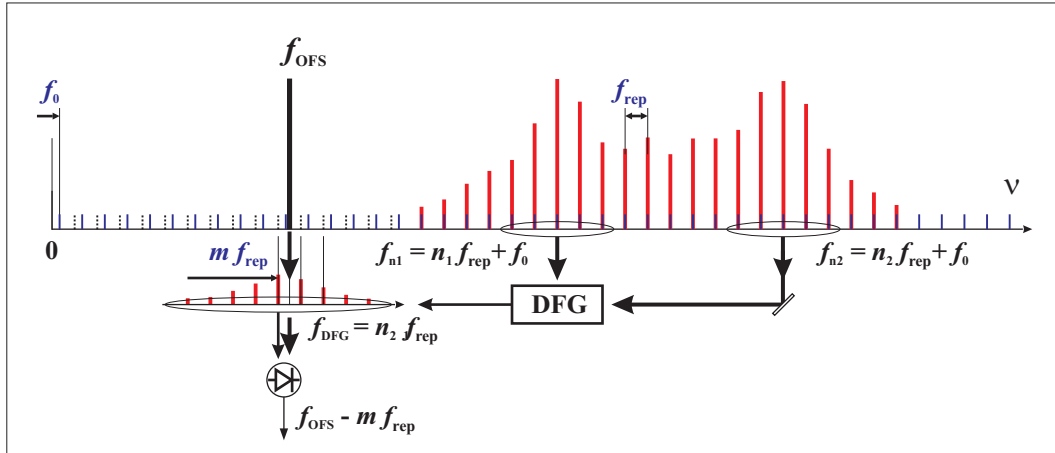
Figure 6.4: *DFG comb.*

frequencies was established.

Similarly, an absolute frequency measurement of 10 μm infrared radiation was performed by phase-locking the comb spacing to the frequency difference of two laser diodes, phase locked in turn to a CO_2/OsO_4 standard [106].

In contrast to SFG combs, the generation of DFG combs occurs without an additional cw laser. They are independent from carrier-envelope offset frequency, with an offset being equal to zero. Fig. 6.4 describes the principle of this method, sometimes also called as self-differencing technique. Some red and blue parts of a femtosecond laser comb are mixed in a DFG crystal. It is clear that the offset frequency present in the original comb disappears in the generated secondary DFG comb [103].

In some experiments offset-free DFG combs were produced in the IR spectral region between 7.5 and 12.5 μm with average power in the range of tens of μW using two independent synchronized femtosecond Ti:Sapphire lasers [107]. In other experiments this was done by using the self-differencing technique [103, 108, 105].

Following this method S. Foreman *et al.* [105] demonstrated the implementation of a simple IR methane-based optical molecular clock. The setup is similar to the one mentioned above regarding the SFG-clockwork [104]. It is based on a femtosecond Ti:Sapphire laser with a specially designed cavity and emitting spectral peaks at 670 and 834 nm. The frequency difference between them corresponds to the wavelength range around 3.39 μm where

a methane optical frequency standard [23, 24, 25] is available. An infrared DFG comb originates by focusing two spectral components of the original comb spectrum into a PPLN crystal after their optimal spatial and temporal overlapping. The observed IR comb spreads over $\sim 270\,\text{nm}$, with an average power of tens of μW and with $< 1\,\text{nW}$ per comb mode. One component of this offset-free comb and hence the comb repetition rate was phase locked to the methane standard. f_{rep} serving as the optical clock output was compared with both a hydrogen maser and an iodine-based optical clock. The instability of the CH_4 clock, measured with respect to the iodine, was limited by the photodetection excess noise. The single-sideband phase noise of this clock scaled up to 1 GHz carrier frequency at offsets less than 10 Hz from the carrier is lower than that of the best available low-noise microwave oscillators.

Another interesting application of DFG combs was reported by T. Fuji *et al.* [108]. They achieved self-stabilization of the carrier-envelope phase using a DFG comb produced from a spectrum of a mode-locked Ti:Sapphire laser broadened in a PCF. This secondary offset-free comb can then be tuned in order to be overlapped with an original femtosecond laser spectrum. In doing so, injection seeding can be obtained and therefore a self-stabilized generation of the femtosecond pulses without carrier-envelope phase shift.

6.1.5 Transfer oscillator technique

There are also many other schemes combining some of those mentioned above and several of them are described in Ref. [32]. An especially interesting one is a concept of an optical frequency measurement proposed and realized by H. Telle *et al.* [109], employing a femtosecond mode-locked laser as a free-running transfer oscillator without any stabilization.

In this scheme the femtosecond laser is slowly frequency stabilized while all heterodyne frequency beats are pre-filtered with fast PLL tracking oscillators and processed using fast harmonic PLLs and analog electronics. The advantage of this transfer concept is that the servo bandwidths can be several MHz broad because they are are no longer limited by mechanical resonances of the mirror transducers. In this case the result of optical frequency measurements is not affected by the additive noise of the measurement process itself and does not depend on noise properties of such a transfer oscillator.

6.2   Mutual phase locking of an OPO and a femtosecond laser comb

In the following, we will present our method of absolute frequency measurements ensuring a phase coherent connection between the infrared and the visible optical ranges. It is based on combining a continuous wave OPO and a Ti:Sapphire femtosecond optical frequency comb and has several advantages compared to the generation of the secondary combs.

It is clear that SFG and DFG combs are well suitable for metrology and high-resolution spectroscopy. The drawback of these schemes is the low output power (tens of μW total, with $< 1\,$nW per comb mode), which for spectroscopic applications generally necessitates the use of an additional IR local oscillator laser. All these approaches phase-coherently connect IR frequencies and primary microwave clocks via f_{rep} but not the optical frequencies. They are either tailored to very specific goals or quite complex, and generally they require a number of non-linear crystals and supplementary lasers to make them useful for spectroscopic applications.

Thus, a specific benefit of the new method presented here is that it consolidates all these subsystems into a single cw OPO, and provides a direct phase-coherent link between two optical frequencies, the visible and the infrared.

The scheme itself is based on the fact that a cw pump enhanced singly resonant OPO emits not only strong signal (S) and idler (I) waves, but also a set of weak (a few μW) components resulting from non-phase-matched mixing processes of the resonated pump (P=S+I) and signal waves [34]. Some of these (2S, P+S, 2P) are located within the emission range of a Ti:Sapphire femtosecond laser comb.

Forming suitable differences of the heterodyne beat frequencies with adjacent comb lines then allows mutual phase locking of OPO optical frequencies and the microwave frequencies f_{rep} and f_0 characterizing the femtosecond comb. This can be implemented following a variety of schemes, e.g. the basic four-step locking scheme as illustrated in Fig. 6.5:

1. *Phase lock the OPO idler frequency* I *to a* He–Ne/CH$_4$ *standard.*

2. *Phase lock the comb spacing* f_{rep} *to the frequency difference between the lines* P+S *and* 2S, *which is equal to the already stabilized idler frequency* I, [(P+S)-2S=I].
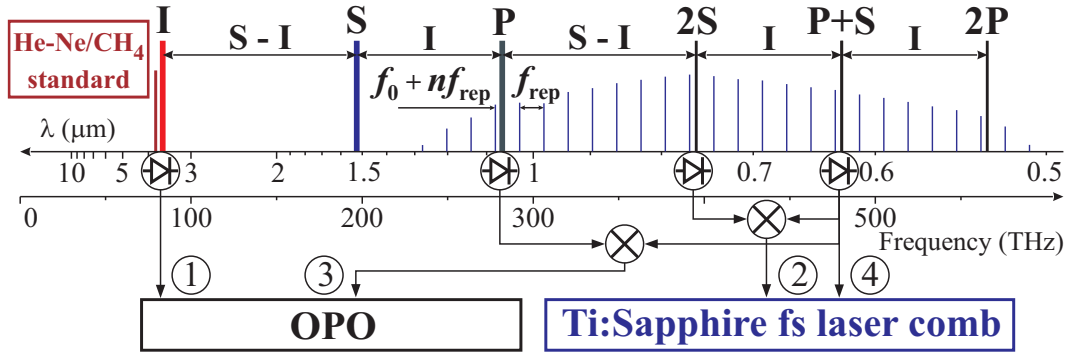
Figure 6.5: *Scheme of phase locking of the OPO output frequencies and a femtosecond laser frequency comb to a He–Ne/CH$_4$ frequency standard. The circled numbers refer to the four-step scheme described in the text.*

3. Measure and stabilize the difference between frequencies (P+S) and P, and therefore the signal frequency S using the comb, [(P+S)-P=S]. As a result, the stability of the methane standard is transferred to the signal and pump frequencies, and thus the entire OPO spectrum.

4. Measure and stabilize the comb offset frequency f_0 relative to one of the OPO lines, e.g. P.

The first two steps alone are already sufficient for implementing a methane-based infrared optical molecular clock analogous to that reported by Foreman *et al.* [105]. Thus, a phase coherent link between optical and microwave frequencies can be created. The last two steps then phase lock the whole femtosecond frequency comb and all OPO output lines to the He–Ne/CH$_4$ standard.

This scheme can mathematically easily be represented as follows. Since the OPO idler frequency I is phase locked to the frequency of the methane standard ν_{CH_4} with a constant offset frequency Δ_I, we can write I $= \nu_{CH_4} + \Delta_I$. The frequencies of the P, 2S, and P+S OPO lines can each be expressed via the frequency of the n_i-th comb line nearby to the left ($\nu_i = n_i f_{rep} + f_0$) and the heterodyne beat frequency δ_i:

$$
\begin{aligned}
\text{P} &= n_1 f_{rep} + f_0 + \delta_1 , \\
2\text{S} &= n_2 f_{rep} + f_0 + \delta_2 , \\
\text{P} + \text{S} &= n_3 f_{rep} + f_0 + \delta_3 .
\end{aligned}
\tag{6.1}
$$

Subtracting the last two equations we find:

$$
\begin{aligned}
n_{32}\, f_{\text{rep}} + \delta_{32} &\equiv (n_3 - n_2)\, f_{\text{rep}} + (\delta_3 - \delta_2) = (P + S) - 2S \\
&\equiv I = \nu_{\text{CH}_4} + \Delta_I \, .
\end{aligned}
\tag{6.2}
$$

If we phase lock the frequency difference $\delta_{32} = \delta_3 - \delta_2$ to a synthesized radio-frequency Δ_{32}, we obtain a simple relation between the comb repetition rate and the methane standard frequencies:

$$
f_{\text{rep}} = \frac{(\nu_{\text{CH}_4} + \Delta_I - \Delta_{32})}{n_{32}} \, .
\tag{6.3}
$$

The infrared optical frequency ν_{CH_4} of the methane standard is at least 10^5 to 10^7 times higher than the frequencies Δ_I and Δ_{32}, which are phase locked to a microwave standard. The relative stability of the methane frequency is 2 to 3 orders of magnitude better than that of the microwave reference. Thus, the instability of the comb repetition rate is mainly determined by the performance of the methane optical frequency standard.

By measuring the heterodyne beats δ_3 and δ_1 of the P+S and P lines of the OPO with the comb in the third step and then by forming the frequency difference $\delta_{31} = \delta_3 - \delta_1$, we find the absolute OPO signal frequency S in terms of the stabilized f_{rep}, and hence in terms of the methane optical frequency ν_{CH_4}:

$$
\begin{aligned}
S &\equiv (P + S) - P = (n_3 - n_1) f_{\text{rep}} + (\delta_3 - \delta_1) \\
&= \frac{n_{31}\left(\nu_{\text{CH}_4} + \Delta_I - \Delta_{32}\right)}{n_{32}} + \delta_{31} \, .
\end{aligned}
\tag{6.4}
$$

It is easy to see, that the 2P line of the OPO can also be used instead of the 2S or P+S OPO lines to form the frequency beat with the comb. Finally, we are able to determine the comb offset frequency from one of the equations (6.1), since we now absolutely know all OPO output frequencies and the comb repetition rate in terms of ν_{CH_4}.

It should also be noted that for the realization of the presented scheme it is actually not necessary to ultimately stabilize the signal and pump frequencies of the OPO as well as the comb offset frequency f_0. Simultaneous measurement of them already provides the full information about OPO and comb frequencies.

Even in the second step one does not need to phase lock the comb repetition rate frequency f_{rep} to the methane standard but only measure it with respect to the last one. Together with signal and pump frequencies measured in turn and then the comb offset f_0 in terms of f_{rep} or—what is the same—in terms of the methane frequency, it will be easy to determine the absolute frequencies of all comb lines and any unknown laser frequency of interest. In this case the comb runs absolutely free and is used as transfer oscillator [109]. In our experiments presented here only f_{rep} and the OPO idler frequency were phase locked to the methane standard while the comb offset f_0 and OPO signal and pump frequencies remained free-running.

The scheme shown in Fig. 6.5 transfers stability and information about the absolute frequency of the infrared frequency standard to all lines of the Ti:Sapphire femtosecond laser comb. Such an optical comb referenced to the methane molecular transition can be used for absolute frequency measurements in the near-infrared and visible spectral ranges.

It is also evident that this scheme is reversible and can take advantage of the new developments in visible optical frequency standards [99, 100, 101, 102, 110]. Our method is suitable for the synthesis of highly-stable infrared radiation with tens of milliwatts power levels and absolutely known frequencies within the tuning ranges of the OPO signal and idler. Just to remember, our OPO presented in Section 3 is tunable between 1.50 μm to 1.98 μm (signal) and 2.30 μm to 3.67 μm (idler).

In this case, the femtosecond laser comb has initially to be stabilized to an atomic [111] or a single ion optical frequency standard [112, 101]. One can also use a high-performance fountain microwave clock [113]. Thereafter, we have to measure the P, 2S, and P+S heterodyne beats (δ_1, δ_2, and δ_3, respectively) of the OPO output radiation with neighboring comb lines followed by processing the corresponding beat frequency differences.

The signals $\delta_{32} = \delta_3 - \delta_2 = I - n_{32} f_{rep}$ and $\delta_{31} = \delta_3 - \delta_1 = S - n_{31} f_{rep}$ exactly track the changes of the idler and signal frequencies (see (6.1)). Phase locking of these beat requency differences to the comb repetition rate frequency transfers the stability of the used optical reference from the visible spectral range to the OPO signal and idler. Finally, it is enough that only the comb spacing f_{rep} is phase locked to the optical frequency standard, but the comb offset frequency remains free-running, as long as we are interested in the beat differences.

In the next sections we will present the experimental setup of our fem-

tosecond laser frequency comb and describe the scheme of its referencing to the methane optical frequency standard.

6.3   Setup of the Ti:Sapphire femtosecond laser frequency comb

The optical setup of the Ti:Sapphire femtosecond laser frequency comb consists of the following subsystems:

- the mode-locked Ti:Sapphire laser pumped by a 5 Watt laser at 532 nm (Coherent, Verdi);

- the photonic crystal fiber (PCF) generating a comb spectrum between 0.5 μm and 1.1 μm;

- the optical system for providing heterodyne frequency beats, where the beams coming from the methane and iodine stabilized lasers are combined with the comb beam and thereafter spectrally separated and filtered.

Here we describe the arrangement of the Ti:Sapphire femtosecond laser and the generation of the comb spectra. The optical and electronic schemes concerned with the combination of the laser frequency comb and the OPO will be described later in the next two sections.

The optical setup is built on a 900 mm $\times$ 900 mm $\times$ 112 mm optical breadboard (Newport, model M-RG-36$\times$36-4) placed on an air floated optical table (Newport, model M-RS4000-48-12), which is separated from the OPO spectroscopy table. A wooden box around the setup to suppress acoustical perturbations on the femtosecond laser cavity is provided. The breadboard is located under an air-conditioning flow box and surrounded by plexiglass window plates. The long term temperature fluctuations at the top of the breadboard are kept at a level below 0.2 °C.

6.3.1   Ti:Sapphire femtosecond mode-locked laser

Our frequency comb is based on a femtosecond mode-locked Ti:Sapphire laser (GigaOptics, GigaJet-20), which is shown in Fig. 6.6. It is a ring laser with a repetition rate $f_{\rm rep}$ ~750 MHz. The laser resonator is assembled on a 32 cm $\times$ 27 cm stainless steel baseplate, put on the main breadboard and
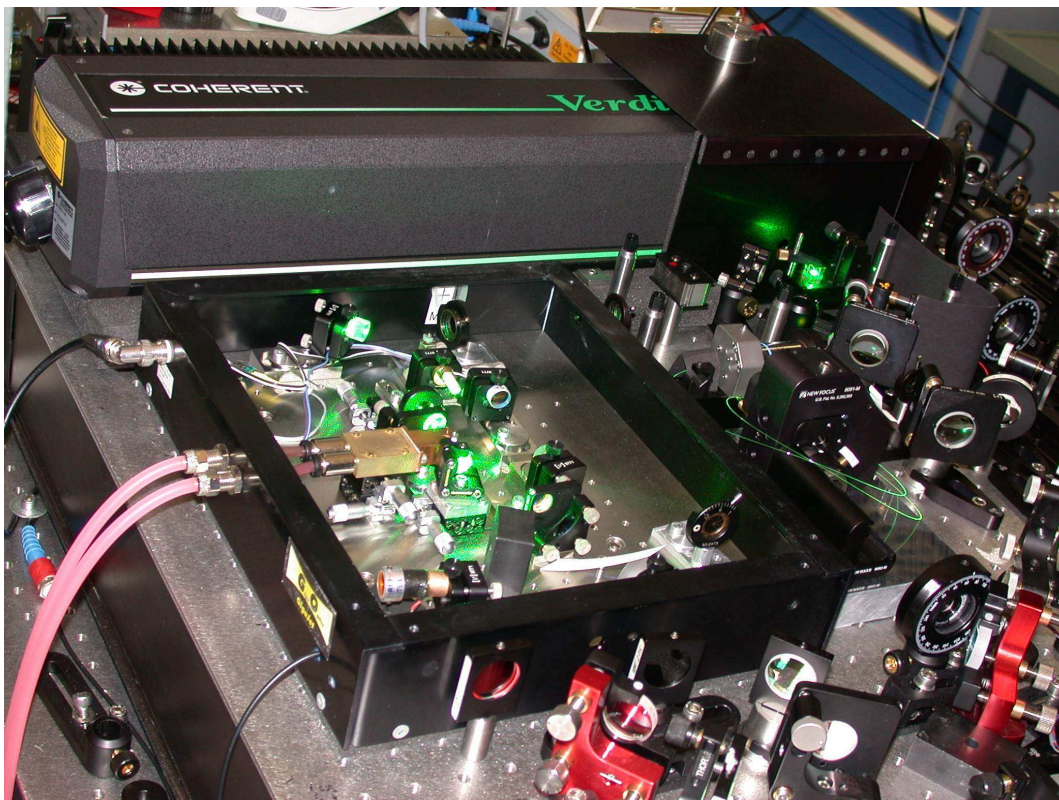
Figure 6.6: *Femtosecond Ti:Sapphire laser GigaJet-20.*

fixed by screws at the four 10 mm thick feet, with the intermediate space filled with a polyethylene foam.

The compact 40 cm long prism-less resonator consists of six mirrors arranged in a double bow-tie geometry. Three of them are specially designed flat mirrors with negative group-velocity dispersion (NGVD). They effectively compensate the dispersion of the laser crystal allowing to build a very short cavity. One of these mirrors is glued to the piston-mode PZT with a capacity of ≈ 15 nF. This allows for a fast modulation of the laser cavity length and phase locking the repetition rate frequency to a microwave reference.

The Ti:Sapphire crystal is placed between two concave mirrors with a radius of curvature of 30 mm which are highly reflecting (R> 99.9%) at wavelengths 750 nm to 850 nm. The output femtosecond beam leaves the cavity through the output coupler mirror with a reflection of R=98% at 750 nm to 850 nm. The crystal is pumped through the input concave mirror using a f=30 mm focusing lens. The backside of the mirror and the lens are both antireflection coated for the pump wavelength at 532 nm. Another concave mirror is placed on a translation stage in order to be able to set the cavity length within the stability range. The crystal is mounted on a water cooled copper block situated on an X-Y translation stage allowing the optimal positioning of the active crystal with respect to the resonator mode waist. To cool the crystal, a water chiller is used which is normally intended for the cooling of CPUs in personal computers.

Pump laser

The femtosecond laser is pumped in a single pass by a 5 W frequency-doubled single-frequency Nd:YVO$_4$ laser (Coherent, Verdi 5W). The pump laser is mounted on a pedestal copper plate (430 mm × 250 mm × 15 mm) to allow very efficient removal of the excess heat. For the heat dissipation from the Verdi pump laser, a 400 mm × 150 mm × 40 mm heatsink (Fischer Elektronik, model SK 479) with a thermal resistance of 0.3 K/W is applied, which is fixed to the edge of the copper plate and placed outside of the breadboard and the wooden box. Having low thermal resistance, this heatsink maintains the temperature of the pump laser baseplate ~ 10 K above the ambient temperature. Such passive cooling is very good alternative to the original heat sink plate.

To avoid thermal load of the pump laser on the femtosecond laser and

the optical setup of the frequency comb, and to minimize the temperature gradients, the copper plate is thermally separated from the main breadboard. It stands on four plastic feet (Ø 30 mm × 10 mm) made from a special polyamide doped with 30 % glass fibres (Ensinger, Tecamid 6 GF 30) having low thermal conductivity, high hardness and about the same linear expansion coefficient as stainless steel. The plate is bolted to the main board with plastic screws. The intermediate space between them is filled with a polyethylene foam.

The output beam of the pump laser is vertically polarized, but for the pumping of the Ti:Sapphire femtosecond laser the horizontal polarization is needed. Besides that, the height of the pump beam output is 75 mm but the height of the beam plane of the femtosecond laser is 50 mm. The output beam from the Verdi first passes a zero order air-spaced $\lambda/2$–plate (Special Optics, model 8-8008-1/2-0532) remaining still vertically polarized. Then it is descended and reflected by 90° with respect to the original beam with a periscope and the polarization of the reflected beam becomes horizontal. After that, the beam passes a polarization beam splitter (PBS) cube and is reflected to the pump input of the femtosecond laser.

The PBS together with the $\lambda/2$–plate at the output of the Verdi works as an adjustable attenuator. Each of them introduce about 3.5% losses. The maximum power of the pump laser was measured to be 5.5 W. Just before the femtosecond laser input we have ~ 5.1 W of pump power.

Mode-locked operation of the Ti:Sapphire laser

The cavity of the femtosecond laser initially has to be adjusted for maximal power of the continuous wave output radiation. This is typically 550 mW to 600 mW after the output coupler in both directions corresponding to counterpropagating cavity roundtrips. Thereafter the resonator has to be set to the inner edge of the cavity stability range by decreasing the distance between the two concave mirrors. This is done by moving the second concave mirror placed on the translation stage. The mode-locked operation is usually started by moving this mirror in the direction of the stability range center and slightly knocking its mount.

There is principally no preference for a certain direction of the round trip pulse propagation. Thus, the train of pulses comes from one of the two outputs with equal probability. Nevertheless, the femtosecond laser

cavity can be adjusted so that the pulses propagate in the direction of the pump beam. In this case, the femtosecond laser output usually appears after passing three negative group-velocity dispersion (NGVD) mirrors.

At the maximum available pump power and the optimal adjustment of the laser cavity, it is possible to get up to 590 mW average power in the pulsed regime. According to the Ti:Sapphire laser specifications, the duration of pulses should be less than 30 fs. The output spectrum of the femtosecond laser depends on the distance between the concave mirrors and the position of the focusing lens. We observed nearly Gaussian form spectra centered between 780 nm and 800 nm with a full width at half maximum of about 30 nm to 50 nm.

6.3.2   Photonic crystal fiber

To realize our method introduced in Section 6.2, we need a laser frequency comb spanning the range between 600 nm and 1100 nm. For this purpose we broaden the spectrum of the femtosecond Ti:Sapphire laser in a photonic crystal fiber (PCF) [92, 93].

Such fibers have a very small silica core (1.5 μm to 2 μm) at the center, symmetrically suspended on a thin cobweb silica microstructure filled with air (see Fig. 6.7). Due to the presence of the air holes, the refractive index of the cladding is effectively much lower than that of bulk material. In this environment the fiber core works as a waveguide with distinctly modified dispersive properties. Most importantly, the zero-crossing point of the group velocity dispersion (GVD) is shifted into the visible wavelengths, depending on the silica core diameter and cobweb structure of the cladding.

Intense optical pulses propagating in a PCF which have the carrier wavelengths near the zero-GVD-point cause the generation of red-shifted solitons and blue-shifted nonsolitonic radiation [114, 115, 116]. The output spectrum can be broadened over a spectral range of more than one octave showing the typical infrared solitonic peaks. The broadening of this spectrum, its form, and the spectral power distribution depend on the parameters of the photonic crystal fiber and that of the propagating femtosecond pulses.

The properties of the PCF output can also be changed by the input beam characteristics, such as mode matching and polarization. Usually, the output spectrum slowly degrades, with the lifetime reaching tens of hours by illuminating the fiber at the maximum available average power of the fem-

tosecond input.

The most critical point of the femtosecond laser comb setup is the generation of a more or less uniform continuum, having no dips at the wavelengths of interest, where the OPO lines are emitted. In our specific applications, namely for referencing the comb to the methane standard, the wavelengths around 631 nm, 775 nm and 1064 nm are especially important.

We tested different photonic crystal fibers. Two samples of them were kindly provided by Prof. Jonathan Knight from the University of Bath, UK. Some others have now become commercially available from "Blaze Photonics", established by the same people. We found that not all of the tested PCFs are optimal for the implementation of our method introduced in Section 6.2, as it was not always possible to use the generated comb spectra to perform the heterodyne beat measurements with the three corresponding OPO output lines simultaneously. We were only able to reproduce comb spectra suitable for these purposes using two fiber samples with core diameters of about 2 μm (see Fig. 6.7).

Photonic crystal fibers with smaller cores give broader spectra reaching the near ultraviolet spectral region down two 400 nm and show an infrared solitonic peak around 1.3 μm. Nevertheless, they exhibit relatively low power per comb mode and many narrow highs and lows at the red wavelengths. Using shorter pieces of these fibers or low input power levels typically does not help. When the infrared peak of the comb is moved to the OPO pump wavelength (1064 nm) by optimizing the input beam parameters, these PCFs still do not produce enough power at 631 nm. Furthermore, if one of the local spectral peaks accidentally coincides with the desired red wavelength its position is strongly affected by the power and polarization of the femtosecond laser as well as the coupling efficiency and the beam pointing.

Preparation and installation of a PCF

In our experiments we have used bare photonic crystal fibers of lengths ranging from 15 cm to 80 cm. Before installing we had to make some preparations. The procedure is the following. First of all both ends of a PCF have to be stripped and cleaved. Then, the input end is mounted into a fiber chuck adapter (Newport, model FPH-J), which is in turn set onto a five-axis single-mode-fiber positioner (New Focus, model 9091-M). The po-
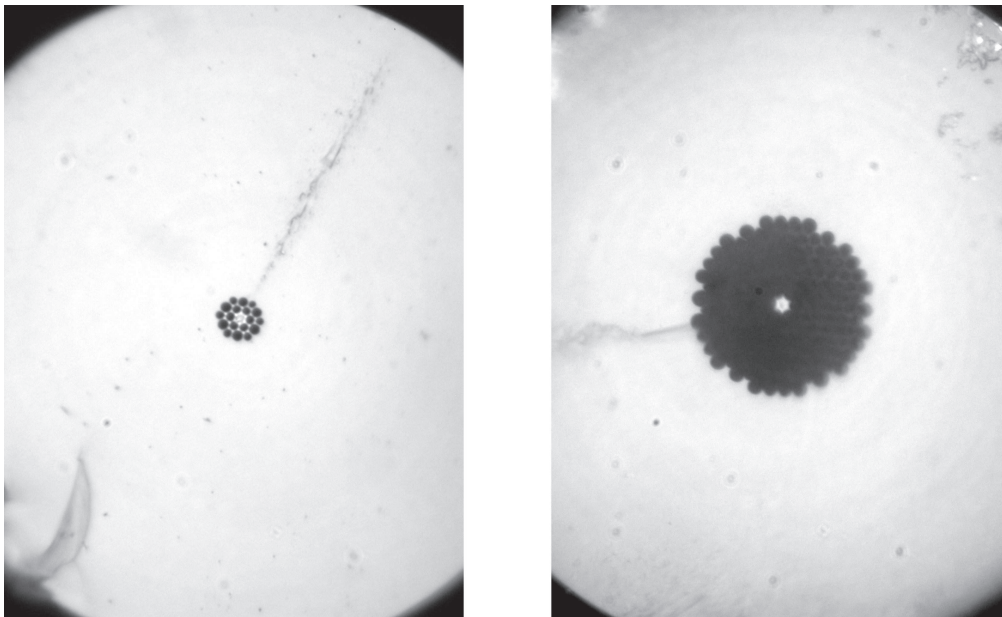
Figure 6.7: *Photographs of cleaves of two PCF samples with core diameters of 2 μm obtained with a microscope (Leica, DMRX). The first PCF, "2 μm cobweb" (left), was provided by Prof. J. Knight, the second sample (right) is a commercial PCF (Blaze Photonics, NL-2.0-735). One can resolve the silica core and a hexagonal silica-air photonic microstructure.*

sitioner allows to adjust all three translations and the two tilt motions independently. It provides a fine translational resolution of 0.02 μm for X, Y directions, 4.4 μm along the focused laser beam, and a tilt resolution of 231 μrad per 5° knob turn.

A focusing lens is mounted onto an adjustable objective holder (New Focus, model 9123) which is placed on a coupler body (New Focus, model 9092-M). The last one is directly attached to the fiber positioner. This fiber coupler system has excellent mechanical long-term stability which is very important for our applications.

The output end of the photonic crystal fiber is glued inside a 3 cm piece of a glass pipe with an outer diameter of 2 mm and an inner one a little bit larger than the thickness of the fiber coating. This pipe is then mounted using a home-made adapter and placed onto a five-axis tiny fiber positioner (New Focus, model 9016-M). By rotating the adapter around its axis one can adjust the polarization of the output comb beam.

Since a diffraction grating, which is later used for separating the different spectral components of the femtosecond comb, needs a P-polarized beam, the output end of the PCF has to be aligned properly. To do this, the comb beam is collimated with a microobjective and sent through a PBS cube before it reaches the grating, with the S-polarized component reflected from the cube being minimized.

Comb spectra

The output beam of the femtosecond Ti:Sapphire laser is bent by two broadband dielectric mirrors which are highly reflective at 750 nm to 820 nm. Passing an achromatic $\lambda/2$-plate (Special Optics, model 8-9012-1/2-600-900) it is focused by an antireflection coated aspheric lens into the photonic crystal fiber in order to produce a femtosecond continuum. For the PCFs with a 2 μm core we have used aspheric lenses with two different focal lengths of 1.45 mm and 2.75 mm (Thorlabs, C140TM-B and C390TM-B).

Usually, at the output of the photonic crystal fiber we obtain between 40 % and 70 % of the power of the femtosecond laser which is coupled into the PCF (depending on the PCF and the focusing lens). As a rule, the 1.45 mm focusing lens gives a better result, although it has smaller clear aperture and inserts more diffraction losses.

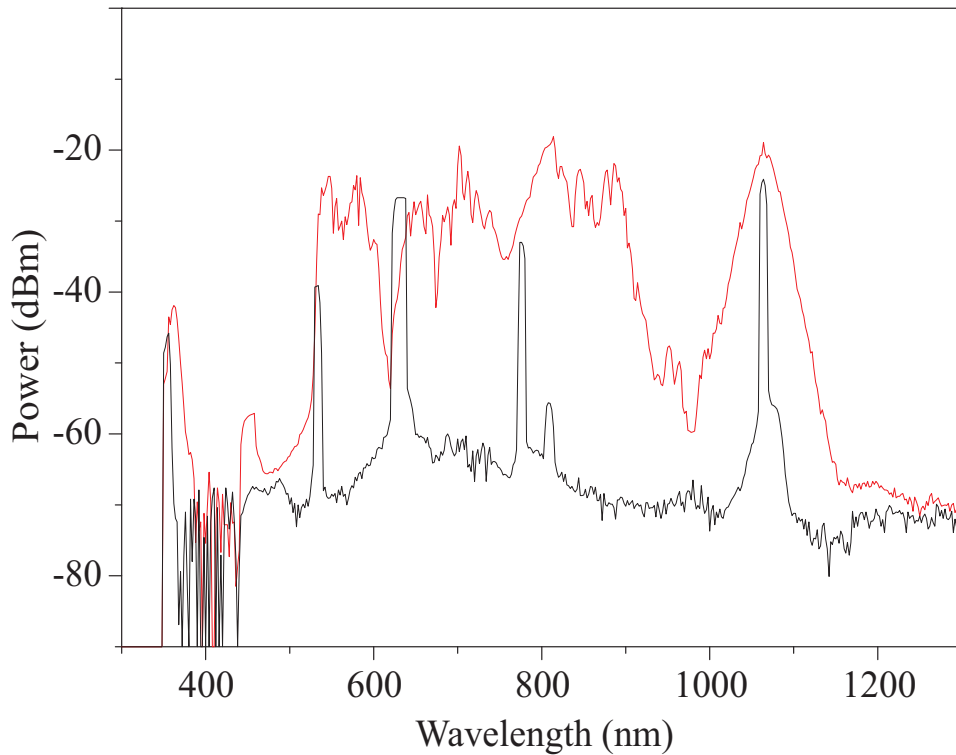To collimate the beam after the PCF, we use an achromatic microscope

Figure 6.8: *Typical Ti:Sapphire femtosecond laser comb spectrum alongside the OPO output spectrum.*

objective (Olympus, Ach 40x/0.65). Despite of the fact that the performance of this objective is not specified for infrared wavelengths and is not optimal for our applications, we have obtained approximately equal beam diameters for the visible and infrared comb components in the far field. The micro-objective transmits about 67 % of the power of the octave spanning comb, the losses for the different spectral comb parts ranging from 20 % to 60 %. In the best case, the collimated comb beam has about one half of the average power from that of the femtosecond laser which is coupled into the PCF.

For observing and recording the comb spectra, an optical spectrum analyzer (Anritsu, model MS9030A with an optical unit MS9701B) has been used. The collimated comb beam is reflected by two mirrors with a protected silver coating, and after attenuation with a neutral density filter sent to the analyzer through a multi-mode optical fiber.

A typical comb spectrum that we observed using 2 μm core PCFs is shown in Fig. 6.8 alongside the OPO output spectrum. The spectrum here is
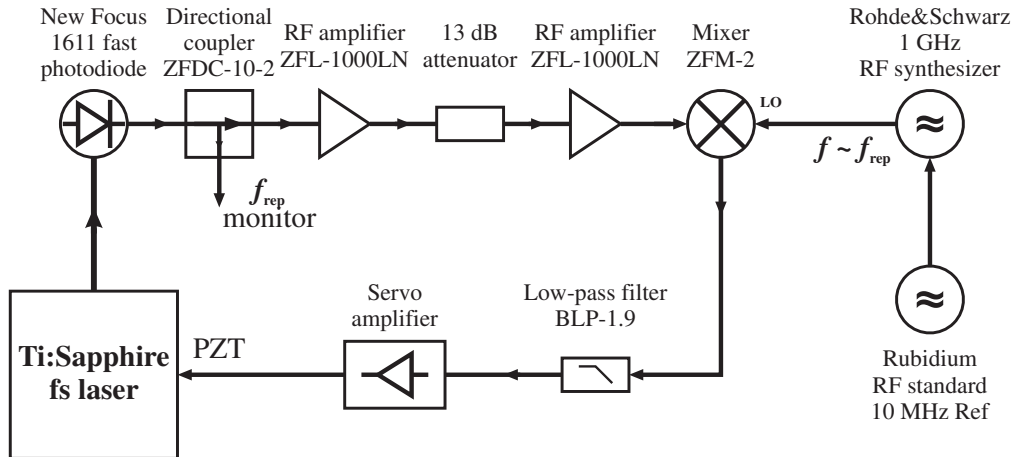
Figure 6.9: *Schematics of the electronic setup for phase locking the comb spacing to a rubidium microwave frequency standard.*

optimized for the mutual phase locking of the comb and the OPO. The optimization of the comb spectrum, which is generated in the PCF, can be done by attenuating the power and adjusting the polarization of the input beam. In this case, the maximum of the infrared solitonic peak [114, 115, 116] is around the wavelength of the OPO pump laser at 1064 nm and the red part of the comb has maximal power near the OPO output at 631 nm.

6.3.3   Stabilization of the comb spacing

It is straightforward to determine the repetition rate of the femtosecond laser comb by measuring the beatnotes between adjacent comb lines with a high-speed photodetector. For this we sent $\sim$ 0.5 mW of the femtosecond radiation, leaking through the first, bending mirror directly after the Ti:Sapphire laser, to a photodetector (New Focus, model NF1611) with a bandwidth of 1 GHz.

The resulting electronic signal at the comb repetition rate frequency of $f_{rep} \sim$ 750 MHz has a level of -35 dBm with a signal-to-noise ratio of more than 70 dB in a resolution bandwidth of 100 kHz. This signal is then amplified up to the level of 0 dBm using low noise amplifiers (Mini-Circuits, ZFL-1000LN) (see Fig. 6.9). For monitoring the beatnote of the repetition rate frequency, a tap output of a directional coupler (Mini-Circuits, ZFDC-10-2) is sent to a spectrum analyzer.

To phase lock f_{rep} to a microwave frequency reference, we have to perform a phase sensitive comparison of the obtained signal with a local oscillator (LO) referenced to this microwave standard. As a phase detector we used a double-balanced mixer (Mini-Circuits, ZFM-2).

The LO signal is provided by a 1 GHz synthesizer (Rohde&Schwarz, model SMG), phase locked to one of our microwave references. For this purpose we use a microwave Rubidium Standard (Efratom) or a GPS-receiver (Arbiter Systems, Model 1083A, Satellite-controlled Frequency Standard). The output of the phase detector is filtered with a low pass filter (Mini-Circuits, BLP-1.9) and sent to a servo amplifier. The resulting signal is sent to the PZT of the femtosecond laser to control the resonator length.

By phase locking the comb spacing to a microwave reference the following should be taking into account. Usually the short-term stability of the repetition rate frequency of the femtosecond laser is better than that of the microwave reference itself. They become comparable at averaging times around 1 ms to 10 ms. This means, that the bandwidth of the phase locked loop has to be chosen smaller than the intersection frequency. In this case, the transfer of the excessive noise at the higher frequencies to the comb f_{rep} frequency and the degradation of its short-term characteristics can be avoided.

6.4   Difference frequency measurements

As mentioned in Section 6.1 femtosecond laser combs with stabilized repetition rate frequency are already suitable for the measurement of optical frequency differences. If a laser under investigation is spectrally separated from an optical frequency standard by several hundreds of GHz, it is not easy to perform a direct heterodyne beat measurement between them. But, if their frequencies are covered by the comb spectrum, it is straightforward to determine the unknown laser frequency relative to the optical reference.

One has to simultaneously measure the heterodyne beats of these two lasers with the neighboring comb lines and synchronously process or subsequently calculate the beat difference. The number of the comb modes over the frequency interval between the two lasers can be determined by a preliminary measurement of their frequencies with a high-resolution wavemeter.

If the frequency gap to be bridged is much smaller than a measured laser frequency, the stability of the used microwave reference can be sufficient without limiting he measurement. Examples of this kind of measurements would be the investigation of new laser sources or high resolution spectroscopy in the vicinity of a secondary optical frequency standard [110].

Using our comb setup we perform an absolute frequency comparison between a Nd:YAG "cryolaser", working at cryogenic temperatures, and an iodine stabilized Nd:YAG laser [77, 78]. The principal transition ($^4F_{3/2} \rightarrow$ $^4I_{11/2}$) in Nd:YAG corresponds to a wavelength of 1064 nm ($R2 \rightarrow Y3$, A–line) at room temperature. Caused by population shifts according to Maxwell's distribution, its emission wavelength jumps to 1061 nm ($R1 \rightarrow$ $Y1$, B–line) when the laser crystal is cooled below 225 K. This means that all frequency measurements at LN_2 or LHe temperature have to deal with a relatively large frequency gap to an available Nd:YAG/I_2 optical reference. The results of these measurements are reported elsewhere in Ref. [117].

To summarize, we bridged a frequency gap of ~ 861 GHz using our femtosecond Ti:Sapphire laser frequency comb. The repetition rate frequency of the comb was referenced to a microwave Rubidium Standard (Efratom). We simultaneously measured two beats of both lasers at 1064 nm and 1061 nm with the comb. Thereafter, we performed a frequency difference measurement of these two beats using a double-balanced mixer. Since the comb just bridged the gap of ~ 3 nm between the "cryolaser" frequency and the frequency of the stabilized Nd:YAG/I_2 laser, the effect of instability of the Rubidium Standard on the result of the measurement was thus 350-fold reduced.

In this measurement we succeed to demonstrate that the middle- and long-term frequency stability of the free-running cryogenic laser, operating at temperatures down to 6.5 K, is more than two orders of magnitude better than that of any existing free-running solid-state laser.

6.5   Referencing a fs comb to a methane IR optical frequency standard

As a rule, optical frequency standards, such as He–Ne/CH_4 or CO_2/OsO_4 infrared systems have much better short term stability than high performance microwave standards up to averaging times of tens of seconds. If we

are going to phase lock the comb to an optical frequency reference we have to use a PLL with much higher bandwidth, i.e. tens of kilohertz.

The comb repetition rate can be phase locked to an infrared frequency standard using the sum– and difference–frequency generation technique as described in Section 6.1. Recently, several IR molecular optical clockworks have been demonstrated [106, 104, 105]. For stabilizing the repetition rate frequency of a femtosecond comb one can also perform frequency difference measurements between heterodyne beats of two optical frequency standards with the comb.

By introducing the method of mutual phase locking of an OPO and a femtosecond laser comb in Section 6.2 we mentioned how to implement a simple IR optical clock based on the methane molecule using the first two steps of the four-step locking scheme shown in Fig. 6.5. In the next section we will present a setup of a direct frequency comparison between I_2 and CH_4 stabilized lasers, in one part of which such a methane clock was also realized.

The optical setup and electronics of a He–Ne/CH_4-based IR optical clock is similar to that shown in Figures 6.12–6.17. In this case only two heterodyne beat measurements between the 2S and P+S lines of the OPO output spectrum and the adjacent lines of a femtosecond Ti:Sapphire laser frequency comb have to be carried out. The frequencies of these beats are $\delta_2 = 2S - (n_2 f_{\text{rep}} + f_0)$ and $\delta_3 = (P + S) - (n_3 f_{\text{rep}} + f_0)$ respectively. This is schematically presented in Fig. 6.10.

First, we phase locked the OPO idler frequency to a methane stabilized He-Ne laser with offset frequency Δ_I as described in Section 4.3, i.e. $I = \nu_{CH_4} + \Delta_I$.

Then, the corresponding parts of the comb spectrum at 755 nm and 631 nm were spectrally separated with a holographic diffraction grating (Edmund Optics, 43775, 1800 Grooves/mm) and optically filtered with Fabry-Perot fused silica etalons (Layertec, d1-d4, Finesse $\sim$ 100). Thereafter we overlapped these two beams with that of the 2S and P+S OPO spectral lines, separated with a dichroic beam splitter.

The generation of both beat signals δ_2 and δ_3, and the electronic processing of their frequency difference signal $\delta_{32} = \delta_3 - \delta_2 = I - n_{32} f_{\text{rep}}$ are similar to that depicted in the right parts of Figures 6.14–6.17. To achieve heterodyne beat signals, silicon avalanche photodiodes (PerkinElmer, C30902E) directly connected to transimpedance amplifiers (MAXIM, models MAX
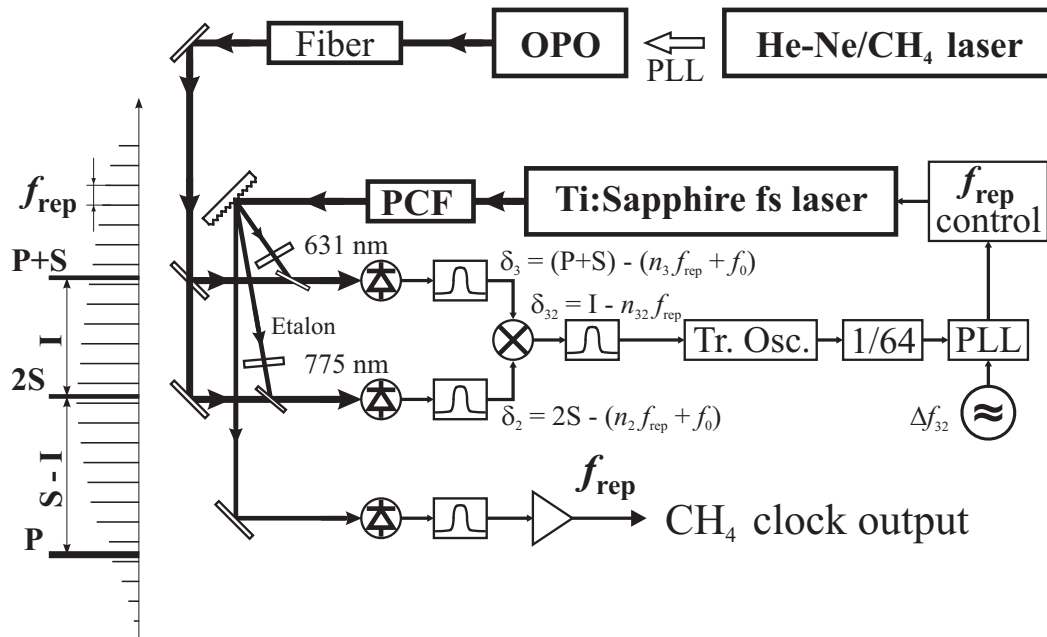
Figure 6.10: *Scheme of a He–Ne/CH$_4$-based IR optical clock. PCF, photonic crystal fiber; Tr. Osc., tracking oscillator.*

3266 or MAX 3267) are used. Typical signal-to-noise ratios of these beats are at the order of (25 to 40) dB in a resolution bandwidth of 100 kHz.

After appropriate amplification and filtering with bandpass filters, these signals are mixed using a double-balanced mixer (DBM) (Mini-Circuits, ZAD-1-1). The obtained frequency difference signal usually has a signal-to-noise ratio of at least 20 dB in a resolution bandwidth of 100 kHz. It is then hard filtered with a bandpass filter, consisting of low pass and high pass filters (Mini-Circuits) connected in series, and sent to a tracking oscillator in order to further improve the signal-to-noise ratio. The tracking oscillator is based on a phase-locked loop (PLL) utilizing a 200 MHz phase/frequency discriminator chip (Analog Devices, AD9901) and a voltage controlled oscillator (Mini-Circuits, model POS-100 or POS-50).

The output frequency of the tracking oscillator is divided by 64 using a 2 GHz prescaler (Motorola, MC12034) and sent to a phase/frequency detector based on a PLL chip (Analog Devices, AD9901). A local oscillator (LO) signal of frequency Δf_{32} for the phase/frequency detector is supplied with a synthesized function generator (SRS, model DS345, Opt 01), phase locked

to the microwave Rubidium Standard.

According to Eq. 6.2, the fluctuations of the frequency difference $\delta_{32} = I - n_{32} f_{\mathrm{rep}}$ after the DBM, and thus that of the phase/frequency detector output signal, exactly correspond to the fluctuations of f_{rep}. If the additionally prescaled to $\delta_{32}/64$ frequency at the input of the phase/frequency detector comes near to the LO frequency, Δf_{32}, a low frequency signal occurs with zero crossings by $\delta_{32}/64 = \Delta f_{32}$.

A DC voltage near the crossings is proportional to the phase fluctuations of f_{rep}. This DC error signal is then controlled to zero by closing a feedback loop, which includes a servo amplifier driving the PZT, and thus changing the length of the femtosecond Ti:Sapphire laser. In doing so, the repetition rate frequency of the comb, f_{rep} becomes phase locked to the He–Ne/CH$_4$ stabilized laser. According to Eq. 6.3 it can be expressed in terms of $\nu_{\mathrm{CH_4}}$. Now the stabilized f_{rep} possess the same stability as the methane standard and can be used as the reference for further frequency measurements. It finally serves as the output of the methane IR molecular clock.

6.6   Frequency comparison between I$_2$ and CH$_4$ stabilized lasers

Here we present the experimental implementation of the method combining an OPO with a Ti:Sapphire femtosecond optical frequency comb for metrology which was described in Section 6.2.

As a first realization of this technique we have performed direct absolute frequency comparisons between a Nd:YAG laser (1064 nm) stabilized on the a$_{10}$ line of the R(56) 32–0 iodine transition near 532 nm [78] and a He–Ne laser stabilized on the ∼300 kHz wide $P(7)$ F$_2^{(2)}$ line of the methane molecule at 3.39 μm. The latter is integrated in a transportable He–Ne/CH$_4$ optical frequency standard and serves as a highly stable (over hundreds of seconds) IR reference laser [23]. The methane standard and reference laser were both previously characterized during several absolute frequency comparisons [25, 26].

Before a detailed consideration of the optical and electronic parts of the experiment, let us summarize again some important information and outline the complete setup. The experimental arrangement of the frequency comparison is shown in Fig. 6.11.
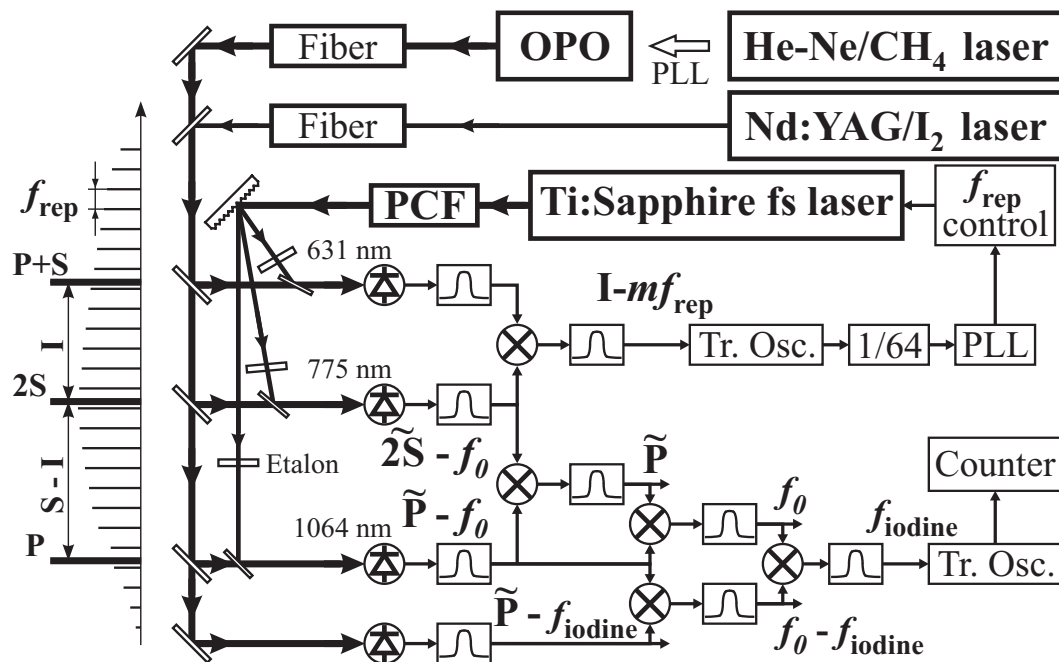
Figure 6.11: *Diagram of the frequency comparison I_2 versus CH_4. PCF, photonic crystal fiber; Tr. Osc.'s, tracking oscillators; m, an integer. $\widetilde{P}$ and $\widetilde{2S}$ are radio frequencies that exactly mirror changes in P and 2S.*

Our frequency comb is based on a femtosecond Ti:Sapphire ring laser with a repetition rate f_{rep} ~750 MHz (see Section 6.3.1). A continuum between 0.5 μm and 1.1 μm with a total power of ~300 mW is generated in a photonic crystal fiber and then split with a diffraction grating into three spectral parts, centered around 1064 nm, 775 nm and 631 nm — corresponding to the OPO lines P, 2S and P+S. After additional filtering with Fabry-Perot etalons these beams are overlapped with the related OPO components and sent to avalanche photodiodes.

Typical power levels here are 10, 0.3 and 1 μW for P, 2S and P+S, respectively. The three resulting OPO beat signals with adjacent comb lines typically have signal-to-noise ratios of (25 to 40) dB in a resolution bandwidth of 100 kHz. In a slight modification of the more general scheme presented above in Section 6.2 we measured the iodine frequency relative to the OPO pump laser.

During the comparisons only f_{rep} was phase locked to the methane standard while the comb offset f_0 remained free-running, similarly to the approach of Telle *et al.* [109]. Frequency differences between the relevant filtered and amplified beats were processed using double-balanced mixers. Frequency generators and counters involved were referenced to a rubidium microwave standard.

The signal used for phase locking of the comb spacing to the stabilized idler frequency and the final signal corresponding to the iodine-stabilized laser frequency were both refined using tracking oscillators. The iodine frequency signal then was recorded using a PC-based counter board (Guide Technology Inc., GT200-10 Time Interval Counter).

6.6.1   Complete setup of I_2 vs CH_4 frequency comparisons

Let us consider the setup of the frequency comparisons between the iodine and methane stabilized lasers. Partially it was presented previously. In Section 6.3 we described those parts of the setup related to the generation of the femtosecond comb spectrum in a photonic crystal fiber (PCF). Then in Section 6.5 we have shown how we phase lock the repetition rate frequency of the comb to the methane optical frequency standard.

First we will describe the optical setup and thereafter outline two modifications of the electronic setup implemented during frequency comparisons between the I_2 and CH_4 stabilized lasers.

Figure 6.12: *Photograph of the Ti:Sapphire femtosecond laser frequency comb setup.*

Optics

A photograph of the Ti:Sapphire femtosecond laser frequency comb is presented in Fig. 6.12. A drawing of the complete optical setup on the 90 cm × 90 cm breadboard is shown to scale in Fig. 6.13.

In Section 6.3.2, we have mentioned the difficulties associated with the simultaneous generation and optimization of the three beats of the OPO output lines with the femtosecond comb. For example, to solve this problem, one can split the output beam of the femtosecond laser and pump two different PCFs. If the mode-locked laser produces enough power this is generally the better choice for this purpose, since one frequency beat can be optimized independently from the other two.

In our specific application, i. e. referencing the femtosecond laser comb to the methane standard and performing a comparison with an iodine stabilized laser we make use of the following fact. The point is that the OPO output P+S line at 775 nm is covered by the spectrum of the Ti:Sapphire femtosecond laser itself. In this case we can directly do the beat frequency measurement of this OPO line with the original femtosecond output. The other two beats at 631 nm 1064 nm can then be easily optimized at the same time.

Therefore, we split the output radiation of the femtosecond laser and send some part bypassing the photonic crystal fiber to immediately form a heterodyne beat at 775 nm. To do this we reflect about 6 % of its power from a bandpass beam splitter (specified as HT@700-900 nm, 0°) and recombine it with the comb beam after the PCF using high-reflecting mirror (HR@750-850 nm, 45°). Both mirrors were not specially designed for these purposes, so we had to choose an optimal angle of incidence of the beams.

The beam splitter is installed so that the reflection from the secondary surfaces is minimized (∼1 % of the residual reflection). We typically have 520 mW to 550 mW just before the photonic crystal fiber and about 32 mW to 35 mW of total average power in the bypass.

The recombining mirror transmits both short and long wavelength parts of the comb spectrum working as an optical notch filter around 800 nm. Although this mirror is not specified for 631 nm and 1064 nm, we found that it has to be set up at an angle of about 25° to insert minimal losses (less than 10 %) for both wavelengths. To install the recombining mirror, we sent the OPO beam in opposite direction to the comb beam. Then, we observed
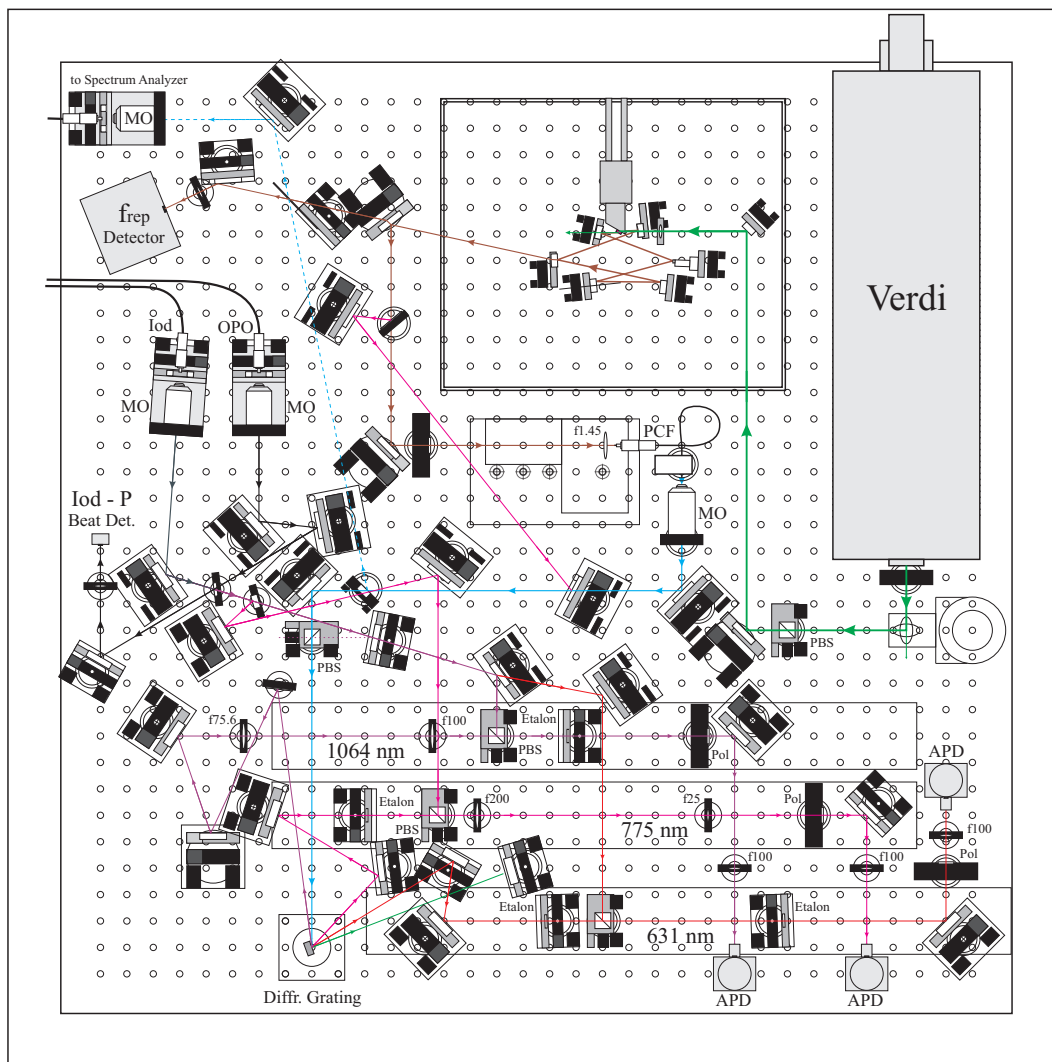
Figure 6.13: *Scheme of the comb optical setup for the frequency comparison between the iodine and methane stabilized lasers.*
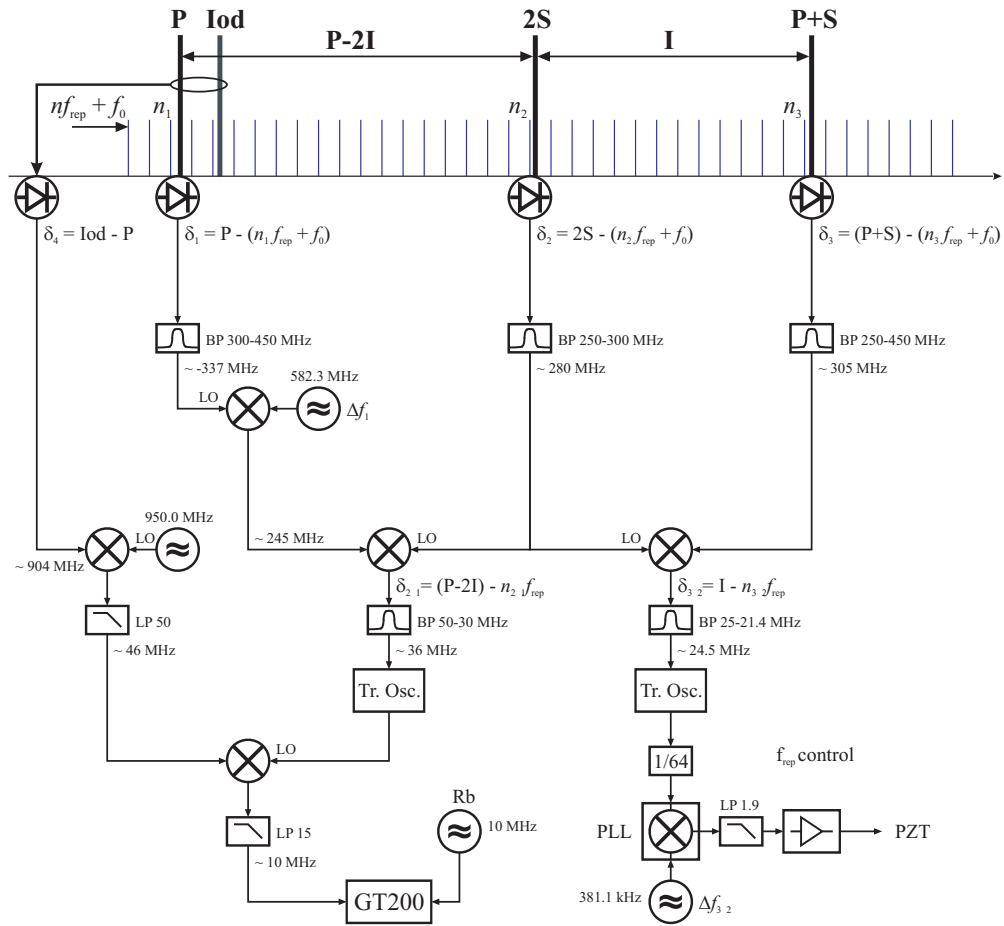
Figure 6.14: *Electronic block scheme 1 of the frequency comparison I_2 vs CH_4.*
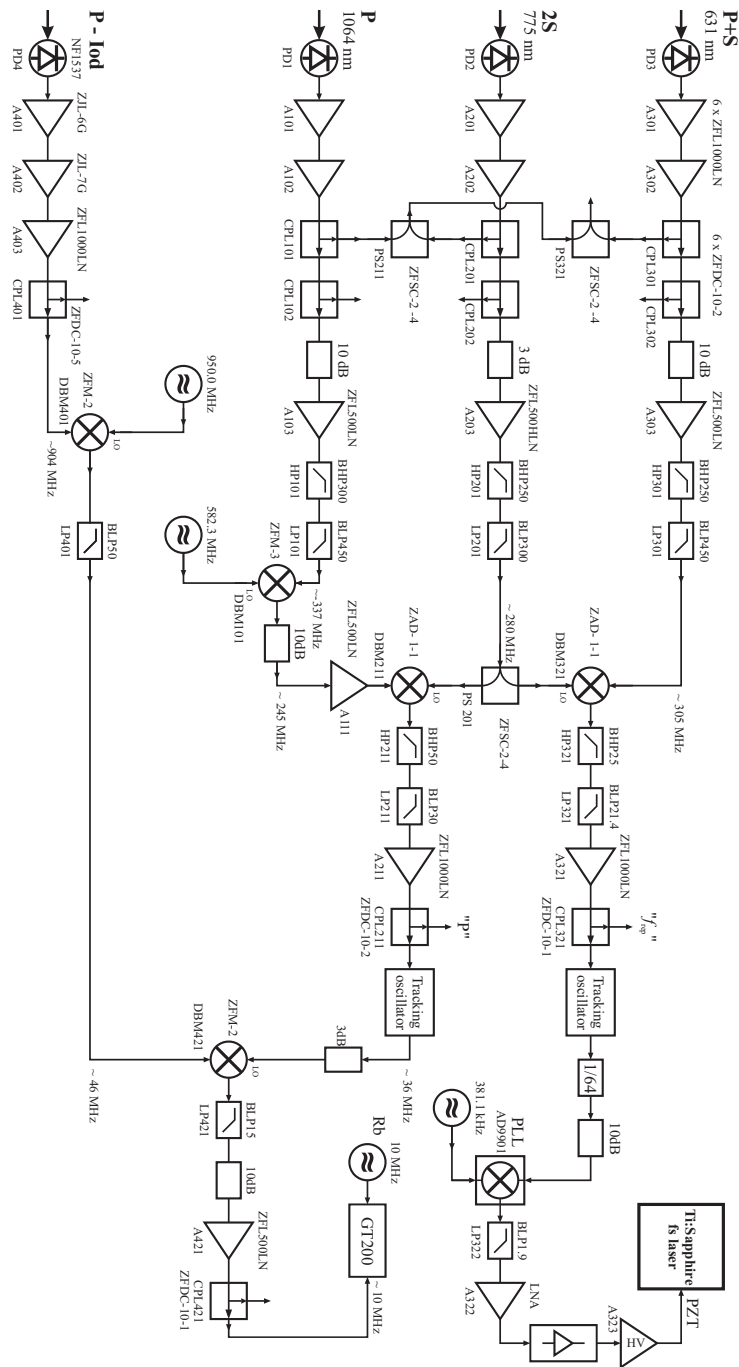
Figure 6.15: *Electronic scheme 1 of the frequency comparison I$_2$ vs CH$_4$.*
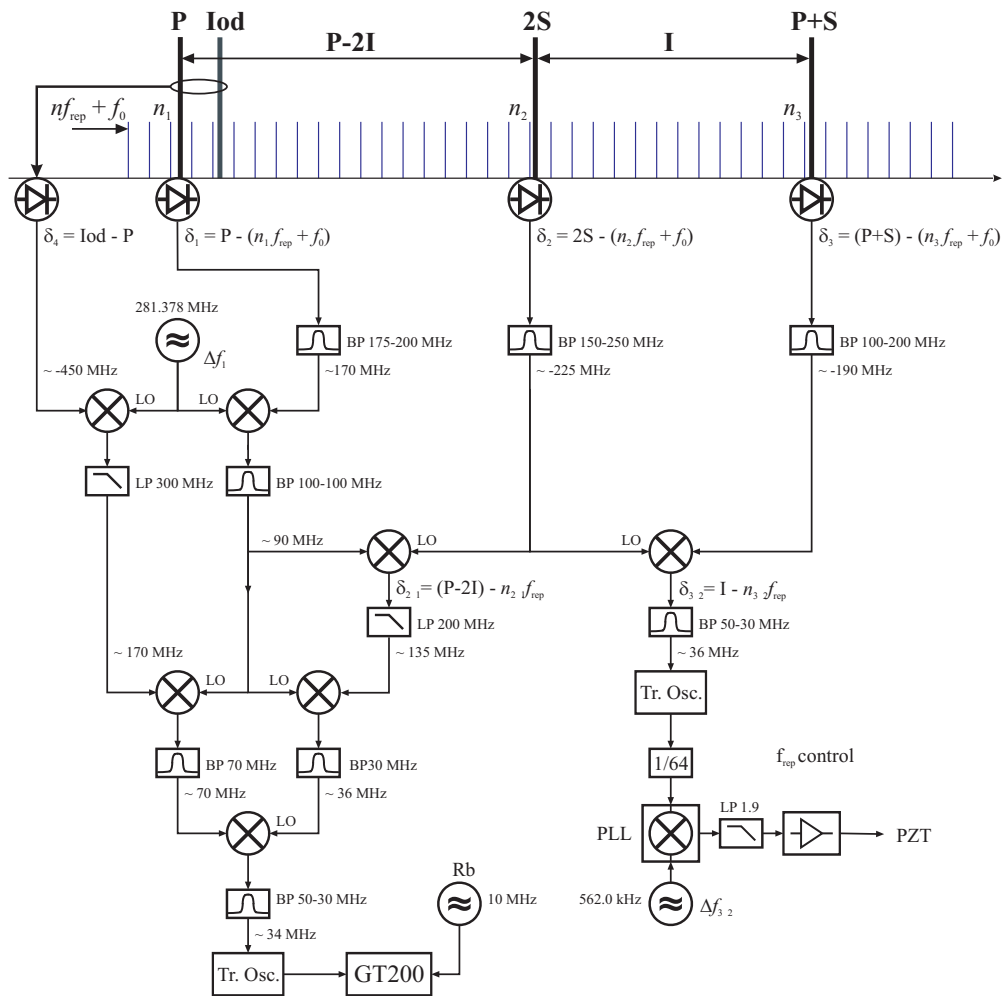
Figure 6.16: *Electronic block scheme 2 of the frequency comparison I_2 vs CH_4.*
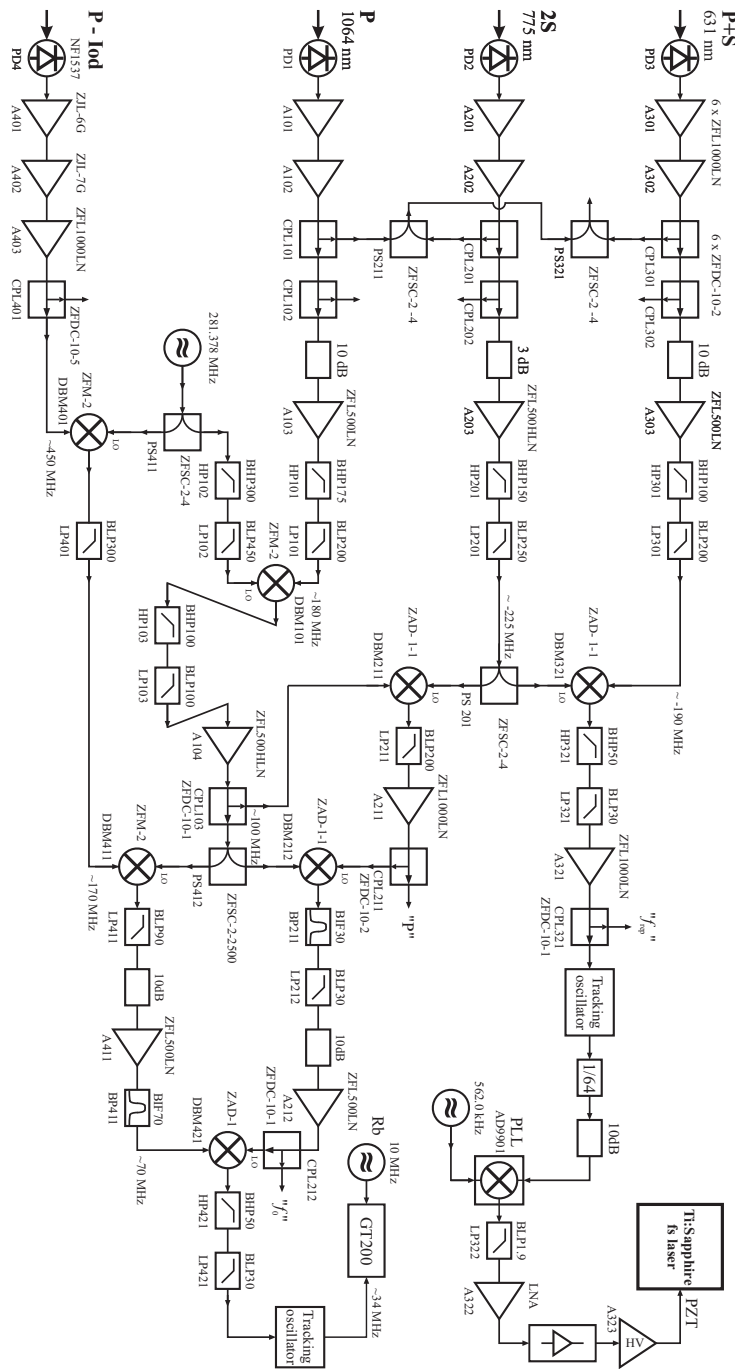
Figure 6.17: *Electronic scheme 2 of the frequency comparison I_2 vs CH_4.*

the reflections of both 631 nm and 1064 nm OPO spectral components and optimized them simultaneously. In this case, the recombining mirror reflects about 90 % of the bypassed femtosecond laser beam, collinearly with the transmitted comb beam coming from the PCF.

The comb beam, prepared in this way, is then sent to a holographic diffraction grating (Edmund Optics, 43775, 1800 Grooves/mm). The grating spatially separates the parts of the comb spectrum around 1064 nm, 755 nm and 631 nm. Thereafter, they are additionally filtered with Fabry-Perot fused silica etalons (Layertec, d1-d4, Finesse $\sim$ 100) and overlapped with the preliminary separated corresponding spectral components of the OPO using polarization beam splitter (PBS) cubes. Passing an adjustable polarizer (CODIXX, colorPol), each pair of the overlapped beams reaches a silicon avalanche photodiode (PerkinElmer, C30902E) directly connected to transimpedance amplifiers (MAXIM, MAX 3266 or 3267) in order to generate three heterodyne beats.

Using the optical bypass for producing the heterodyne beat of the OPO and the comb at 775 nm provides us with a stable beat signal. This beat has a high signal-to-noise ratio (SNR) of about 35 dB in a resolution bandwidth (BW) of 100 kHz, even without any special optimization of the mode matching of the both OPO and comb beams. The other two heterodyne beats at 631 nm and 1064 nm are then easily optimized up to SNR of (25 to 40) dB (in 100 kHz BW)

The electronic filtering and mixing of these beat signals are similar to that, described in Section 6.5. Components used for this are depicted later in electronic schemes.

Electronics

Using the optical setup described above, we performed two different measurement sessions of the frequency comparison between the iodine and methane stabilized lasers. We describe here two modifications of the electronic schemes used for the processing of the heterodyne beats and recovering of the iodine absolute frequency signal.

A simplified electronic block scheme of the first setup is sketched in Fig. 6.14, and its concrete accomplishment is shown in Fig. 6.15. The second setup is presented in Figures 6.16 and 6.17 respectively.

These both schemes are very similar in the part that serves for phase

locking the comb f_{rep} to the methane stabilized He–Ne laser. This part is in detail described in Section 6.5. The main modification consists in the processing of the optical beat differences and extracting of the absolute iodine laser frequency.

The first electronic scheme (Fig. 6.15) has in this last beat processing part only two radio frequency outputs mirroring fluctuations of the OPO pump frequency and the frequency of the iodine stabilized laser to be measured. By comparison, the second setup (Fig. 6.17) additionally provides the signal which resembles the fluctuations of the comb offset frequency f_0, and thus the full information about all individual comb components.

The signal used for phase locking of the f_{rep} to the methane stabilized laser and the final signal corresponding to the frequency of iodine stabilized laser were both refined using tracking oscillators. The iodine frequency signal was then recorded using a PC-based counter board (Guide Technology Inc., GT200-10 Time Interval Counter).

6.6.2 Results of I_2 vs CH_4 frequency comparisons

A number of beat frequency measurements with counter gate times between 1 ms to 10 s were performed during the both comparison sessions. The resulting relative Allan deviation averaged over different measurement runs is shown in Fig. 6.18. The result of the comparison is limited by the iodine stabilized laser performance, which is known from independent measurements relative to a cryogenic optical resonator (CORE) [78]. The accuracy limitation of the new comparison method itself is expected to be much lower than 10^{-13}.

We also succeeded in reversing the scheme and phase locking f_{rep} and the idler frequency to the iodine stabilized laser. Comparisons of the idler frequency with the methane standard will serve as the additional check of the presented measurement method.

The continuous measurement time was restricted by the slow degradation of the photonic crystal fiber, which led to non-uniformities in the comb spectrum and insufficient power levels. The OPO showed very reliable operation and remained phase locked to the methane stabilized laser over several days.
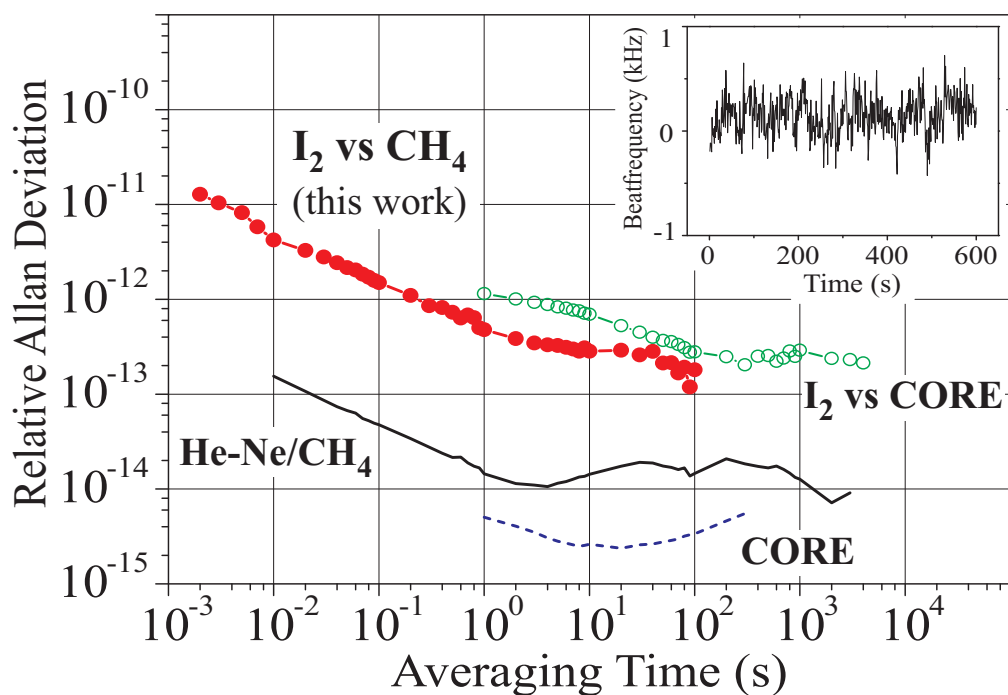
Figure 6.18: *Result of the frequency comparison between the iodine and methane stabilized lasers. Also shown are independent measurements of a similar iodine system [78] with respect to a cryogenic optical resonator (CORE) (open circles) and known performances of the methane standard [25] (solid line) and the CORE [118] (dashed line). Inset: typical beat signal of the I_2 vs CH_4 comparison, counted with a 1 s gate time.*

Chapter 7

Conclusion and Outlook

This dissertation has presented a continuous wave optical parametric oscillator specially developed for high-resolution Doppler-free molecular spectroscopy and metrology. The basic objective was to solve the long-standing problem of controlled access to any desired wavelength in the wide emission range of OPOs, and then to precisely tune the output frequency over the molecular and atomic transitions of interest. To accomplish this goal, a new design for the cw-OPO cavity with an intracavity etalon has been implemented. Based on the concept of the singly resonant cw OPO with resonated pump wave, patented previously by our group, the developed device demonstrates excellent spectral features and long-term stability. These were determined in the direct frequency beat measurements with a methane IR optical frequency standard. An idler radiation linewidth of ~ 12 kHz and mode-hop-free operation of the OPO over more than two days were observed. For the first time, it was shown that an OPO can be phase locked to a highly stable optical reference and thus much more precisely controlled and tuned.

Due to reliable tuning characteristics and narrow linewidth of the built up OPO system, we succeed in the first application of OPOs in Doppler-free spectroscopy. To observe and study nonlinear Doppler-free resonances in methane, a frequency modulation spectroscopy setup has been implemented. The resonances of the $F_2{}^{(2)}$ component of the P7 rotation-vibrational transition of the methane molecule at 3.39 μm were recorded in a wide range of methane pressures and the pressure broadening was investigated.

To gain the most benefit from the special OPO features for optical frequency metrology, the idea to combine the OPO with a femtosecond Ti:Sap-

phire laser frequency comb was proposed. In this concept, the OPO serves as a bidirectional coherent bridge between the infrared and visible spectral ranges. The OPO and femtosecond laser comb referenced to an infrared methane optical frequency standard can be used for precise frequency measurements in the visible. One can also take advantage of the new developments in visible optical frequency standards and synthesize highly-stable infrared radiation with absolutely known frequency within the OPO signal and idler tuning ranges. Consequently, it becomes much easier to compare optical frequency standards of different nature.

As a first demonstration of this new technique the direct absolute frequency comparison between methane and iodine stabilized lasers was performed. For this purpose, a setup of the femtosecond Ti:Sapphire laser frequency comb has been created.

As the current comparisons do not yet challenge the accuracy performance of the system, upcoming measurements will use better optical frequency references (e.g. CH_4 vs CORE) to explore the actual limitations. The ease-of-use of the setup could be improved by using specially designed PPLN crystals in order to enhance the power of the non-phase-matched OPO components 2S and P+S. Another line of development is to use the opposite direction of stability transfer in order to provide stable emission for the purposes of high-resolution Doppler-free molecular spectroscopy in the infrared with output power levels up to several Watts using a modified design [119, 5, 120]. Specifically, this should lead to applications in precision IR spectroscopy, such as metrology of the strong transitions of cold CH_4 molecules [34] and the study of rotation-vibrational transitions in decelerated and trapped OH-radicals [121].

Bibliography

[1] K. Schneider, P. Kramper, S. Schiller, and J. Mlynek. Toward an optical synthesizer: a single-frequency parametric oscillator using periodically poled LiNbO$_3$. *Opt. Lett.*, 22(17):1293–1295, 1997.

[2] K. Schneider and S. Schiller. Narrow-linewidth, pump-enhanced singly-resonant parametric oscillator pumped at 532 nm. *Appl. Phys. B*, 65:775–777, 1997.

[3] K. Schneider, S. Schiller, J. Mlynek, and P. Kramper. Tunable optical parametric oscillator. US Patent No. US5,999,547, December 1999. Applied by University Constance, Germany.

[4] T. J. Kulp, S. E. Bisson, R. P. Bambha, T. A. Reichardt, U. B. Goers, K. W. Aniolek, D. A. V. Kliner, B. A. Richman, K. M. Armstrong, R. Sommers, R. Schmitt, P. E. Powers, O. Levi, T. Pinguet, M. Fejer, J. P. Koplow, L. Goldberg, and T. G. Mcrae. The application of quasi-phase-matched parametric light sources to practical infrared chemical sensing systems. *Appl. Phys. B*, 75:317–327, 2002.

[5] M. M. J. W. van Herpen, S. Li, S. E. Bisson, S. Te Lintel Hekkert, and F. J. M. Harren. Tuning and stability of a continuous-wave mid-infrared high-power single resonant optical parametric oscillator. *Appl. Phys. B*, 75:329–333, 2002.

[6] Frank Müller, Alexander Popp, Frank Kühnemann, and Stephan Schiller. Transportable, highly sensitive photoacoustic spectrometer based on a continuous-wave dual-cavity optical parametric oscillator. *Opt. Express*, 11(22):2820–2825, 2003.

[7] E. V. Kovalchuk, D. Dekorsy, A. I. Lvovsky, C. Braxmaier, J. Mlynek, A. Peters, and S. Schiller. High-resolution doppler-free molecular

spectroscopy with a continuous-wave optical parametric oscillator. *Opt. Lett.*, 26(18):1430–1432, 2001.

[8] A. Hecker, M. Havenith, C. Braxmaier, U. Strößner, and A. Peters. High resolution doppler-free spectroscopy of molecular iodine using a continuous wave optical parametric oscillator. *Opt. Commun.*, 218: 131–134, 2003.

[9] U. Strößner, A. Peters, J. Mlynek, S. Schiller, J.-P. Meyn, and R. Wallenstein. Single-frequency continuous-wave radiation from 0.77 to 1.73 μm generated by a green-pumped optical parametric oscillator with periodically poled LiTaO$_3$. *Opt. Lett.*, 24(22):1602–1604, 1999.

[10] D. R. Weise, U. Strößner, A. Peters, J. Mlynek, S. Schiller, A. Arie, A. Skliar, and G. Rosenman. Continuous-wave 532-nm-pumped singly resonant optical parametric oscillator with periodically poled KTiOPO$_4$. *Opt. Commun.*, 184:329–333, 2000.

[11] K. Schneider, P. Kramper, O. Mor, S. Schiller, and J. Mlynek. Continuous-wave, single-frequency parametric oscillator for the $1.45 - 4\,\mu$m spectral range using PPLN. In W. R. Bosenberg and M. M. Fejer, editors, *Advanced Solid State Lasers*, volume 19 of *OSA Trends in Optics and Photonics Series*, page 256. Optical Society of America, Washington D.C., 1998.

[12] C. D. Nabors, S. T. Yang, T. Day, and R. L. Byer. Coherence properties of a doubly resonant monolithic optical parametric oscillator. *J. Opt. Soc. Am. B*, 7(5):815–820, 1990.

[13] S. Slyusarev, T. Ikegami, and S. Ohshima. Phase-coherent optical frequency division by 3 of 532-nm laser light with a continuous-wave optical parametric oscillator. *Opt. Lett.*, 24(24):1856–1858, 1999.

[14] P. E. Powers, T. J. Kulp, and S. E. Bisson. Continuous tuning of a continuous-wave periodically poled lithium niobate optical parametric oscillator by use of a fan-out grating design. *Opt. Lett.*, 23(3):159–161, 1998.

[15] M. E. Klein, C. K. Laue, D.-H. Lee, K.-J. Boller, and R. Wallenstein. Diode-pumped singly resonant continuous-wave optical paramet-

ric oscillator with wide continuous tuning of the near-infrared idler wave. *Opt. Lett.*, 25(7):490–492, 2000.

[16] F. Kühnemann, K. Schneider, A. Hecker, A. A. E. Martis, W. Urban, S. Schiller, and J. Mlynek. Photoacoustic trace-gas detection using a cw single-frequency parametric oscillator. *Appl. Phys. B*, 66:741–745, 1998.

[17] G. M. Gibson, M. H. Dunn, and M. J. Padgett. Application of a continuously tunable, cw optical parametric oscillator for high-resolution spectroscopy. *Opt. Lett.*, 23(1):40–42, 1998.

[18] G. M. Gibson, M. Ebrahimzadeh, M. J. Padgett, and M. H. Dunn. Continuous-wave optical parametric oscillator based on periodically poled $KTiOPO_4$ and its application to spectroscopy. *Opt. Lett.*, 24(6): 397–399, 1999.

[19] P. Kramper. Entwicklung eines optischen Synthesizers auf der Basis parametrischer Oszillation. Master's thesis, Universität Konstanz, 1997.

[20] S. Schiller, J. Schoser, C. Braxmaier, K. Bencheikh, U. Strößner, A. Peters, J. Mlynek, and P. de Natale. Single-frequency cw optical parametric oscillators: Devices and applications. In *Proceedings XIV Int. Conf. Laser Spectroscopy ICOLS99*, pages 217 – 226. World Scientific, Singapore, 1999.

[21] J. Schoser. Ein portabler Dauerstrich-Optisch-Parametrischer Oszillator für die Molekülspektroskopie. Master's thesis, Universität Konstanz, 1999.

[22] W. R. Bosenberg, A. Drobshoff, J. I. Alexander, L. E. Myers, and R. L. Byer. 93% pump depletion, 3.5 W continuous-wave, singly resonant optical parametric oscillator. *Opt. Lett.*, 21(17):1336–1338, 1996.

[23] M. A. Gubin, D. A. Tyurikov, A. S. Shelkovnikov, E. V. Kovalchuk, G. Kramer, and B. Lipphardt. Transportable He-Ne/CH_4 optical frequency standard and absolute measurements of its frequency. *IEEE J. Quantum Electron.*, 31(12):2177–2182, 1995.

[24] O. Acef, A. Clairon, L. Hilico, D. G. Rovera, G. Kramer, B. Lipphardt, A. Shelkovnikov, E. Koval'chuk, E. Petrukhin, D. Tyurikov, M. Petrovskiy, and M. Gubin. Absolute frequency measurements and intercomparisons of He-Ne/CH_4 (λ = 3.39 μm), CO_2/OsO_4 (λ = 10.6 μm) frequency stabilized lasers and Cs primary standard. In T. L. Nelson, editor, *Digest of the Conference on Precision Electromagnetic Measurements (1998, Washington, USA)*, pages 258–259. Institute of Electrical and Electronics Engineers, Piscataway, NJ, 1998.

[25] M. Gubin, A. Shelkovnikov, E. Kovalchuk, D. Krylova, E. Petrukhin, and D. Tyurikov. Present performance of the transportable double-mode He-Ne/CH_4 frequency standards. In *Proceedings of the 1999 Joint Meeting of The European Frequency and Time Forum and the IEEE International Frequency Control Symposium*, pages 710–713. Institute of Electrical and Electronics Engineers, New York, 1999.

[26] C. O. Weiss, G. Kramer, B. Lipphardt, and H. Schnatz. Optical frequency measurement by conventional frequency multiplication. In A. N. Luiten, editor, *Frequency Measurement and Control: Advanced Techniques and Future Trends*, volume 79 of *Topics in Applied Physics*, pages 215–247. Springer-Verlag GmbH, Berlin Heidelberg, 2001.

[27] D. J. M. Stothard, M. H. Dunn, and C. F. Rae. Hyperspectral imaging of gases with continuous-wave pump-enhanced optical parametric oscillator. *Opt. Express*, 12(5):947–955, 2004.

[28] M. A. Gubin, D. A. Tyurikov, A. N. Kireev, E. V. Koval'chuk, A. S. Shelkovnikov, and D. Depatie. New approaches towards high precise, compact methane optical frequency standard ($\lambda = 3.39\,\mu$m). In J. C. Bergquist, editor, *Proceedings of the Fifth Symposium on Frequency Standards and Metrology (October 15-19, 1995, Woods Hole, Massachusetts, USA)*, pages 305–309. World Scientific, Singapore, 1996.

[29] M. A. Gubin, A. N. Kireev, E. V. Koval´chuk, D. A. Turikov, and A. S. Shelkovnikov. Prospects for increasing the precision of optical frequency standards based on transitions in the methane molecule. *Quant. Electron.*, 26(10):166, 1996.

[30] D. J. Jones, S. A. Diddams, J. K. Ranka, A. Stentz, R. S. Windeler, J. L. Hall, and S. T. Cundiff. Carrier-envelope phase control of femtosec-

ond mode-locked lasers and direct optical frequency synthesis. *Science*, 288:635–639, 2000.

[31] Th. Udem, R. Holzwarth, and T. W. Hänsch. Optical frequency metrology. *Nature*, 416:233–237, 2002.

[32] H. R. Telle, G. Steinmeyer, A. E. Dunlop, J. Stenger, D. H. Sutter, and U. Keller. Carrier-envelope offset phase control: A novel concept for absolute optical frequency measurement and ultrashort pulse generation. *Appl. Phys. B*, 69:327–332, 1999.

[33] S. A. Diddams, D. J. Jones, J. Ye, S. T. Cundiff, J. L. Hall, J. K. Ranka, R. S. Windeler, R. Holzwarth, Th. Udem, and T. W. Hänsch. Direct link between microwave and optical frequencies with a 300 THz femtosecond laser comb. *Phys. Rev. Lett.*, 84(22):5102–5105, 2000.

[34] E. V. Kovalchuk, D. Dekorsy, A. I. Lvovsky, C. Braxmaier, J. Mlynek, S. Schiller, and A. Peters. Doppler-free spectroscopy of CH_4 using a cw optical parametric oscillator. In P. Gill, editor, *Proceedings of the 6th Symposium on Frequency Standards and Metrology (September 10-14, 2001, St. Andrews, UK)*, pages 513–515. World Scientific, Singapore, 2002.

[35] E. Kovalchuk, T. Schuldt, and A. Peters. A combination of cw-OPO and femtosecond frequency comb for optical frequency metrology. *Opt. Lett.*, 30(23):3141–3143, 2005.

[36] J.-Ph. Uzan. The fundamental constants and their variation: observational and theoretical status. *Rev. Mod. Phys.*, 75:403–455, 2003.

[37] S. Bize, S. A. Diddams, U. Tanaka, C. E. Tanner, W. H. Oskay, R. E. Drullinger, T. E. Parker, T. P. Heavner, S. R. Jefferts, L. Hollberg, W. M. Itano, and J. C. Bergquist. Testing the stability of fundamental constants with the $^{199}Hg^{+}$ single-ion optical clock. *Phys. Rev. Lett.*, 90(15): 150802, 2003.

[38] E. Peik, B. Lipphardt, H. Schnatz, T. Schneider, Chr. Tamm, and S. G. Karshenboim. Limit on the present temporal variation of the fine structure constant. *Phys. Rev. Lett.*, 93(17):170801, 2004.

[39] Eric R. Hudson, H. J. Lewandowski, Brian C. Sawyer, and Jun Ye. Cold molecule spectroscopy for constraining the evolution of the fine structure constant. *Phys. Rev. Lett.*, 96(14):143004, 2006.

[40] H. Müller, S. Herrmann, C. Braxmaier, S. Schiller, and A. Peters. Modern Michelson-Morley experiment using cryogenic optical resonators. *Phys. Rev. Lett.*, 91:020401, 2003.

[41] S. Herrmann, A. Senger, E. Kovalchuk, H. Müller, and A. Peters. Test of the isotropy of the speed of light using a continuously rotating optical resonator. *Phys. Rev. Lett.*, 95:150401, 2005.

[42] S. Herrmann, A. Senger, E. Kovalchuk, H. Müller, and A. Peters. Test of Lorentz Invariance using a continuously rotating optical resonator. *Lect. Notes Phys.*, 702:385–400, 2006.

[43] P. A. Franken, A. E. Hill, C. W. Peters, and G. Weinreich. Generation of optical harmonics. *Phys. Rev. Lett.*, 7(4):118–120, 1961.

[44] J. A. Giorgmaine and R. C. Miller. Tunable coherent parametric oscillation in LiNbO$_3$ at optical frequencies. *Phys. Rev. Lett.*, 14(24):973–976, 1965.

[45] S. A. Akhmanov, A. I. Kovrigin, A. S. Piskarskas, V. V. Fadeev, and R. V. Khokhlov. Observation of parametric amplification in the optical range. *Zh. Experim. Teor. Fiz. Pis'ma (USSR)*, 2:300–305, 1965.

[46] A. Yariv. *Quantum Electronics*. Wiley, New York, 1988.

[47] R. W. Boyd. *Nonlinear Optics*. Academic Press, San Diego, 2003.

[48] V. G. Dmitriev, G. G. Gurzadyan, and D. N. Nikogosyan. *Handbook of Nonlinear Optical Crystals*. Springer-Verlag, Berlin, 1999.

[49] D. A. Roberts. Simplified characterization of uniaxial and biaxial nonlinear optical crystals: a Plea for standardization of nomenclature and conventions. *IEEE Journal of Quantum Electronics*, 28(10):2057–2074, 1992.

[50] D. A. Kleinman. Nonlinear dielectric polarization in optical media. *Phys. Rev.*, 126(6):1977–1979, 1962.

[51] R. C. Miller, W. A. Nordland, and P. M. Bridenbaugh. Dependence of second-harmonic-generation coefficients of LiNbO$_3$ melt compositions. *J. Appl. Phys.*, 42(11):4145–4147, 1971.

[52] J. E. Midwinter and J. Warner. The effects of phase matching method and of uniaxial crystal symmetry on the polar distribution of second-order non-linear optical polarization. *Brit. J. Appl. Phys.*, 16:1135, 1965.

[53] G. D. Boyd and D. A. Kleinman. Parametric interaction of focused gaussian light beams. *J. Appl. Phys.*, 39(8):3597–3639, 1968.

[54] S. Schiller, K. Schneider, and J. Mlynek. Theory of an optical parametric oscillator with resonant pump and signal. *J. Opt. Soc. Am. B*, 16(9): 1512–1524, 1999.

[55] M. Ebrahimzadeh. Mid-infrared ultrafast and continuous-wave optical parametric oscillators. In Irina T. Sorokina and Konstantin L. Vodopyanov, editors, *Solid-State Mid-Infrared Laser Sources*, volume 89 of *Topics in Applied Physics*, pages 179–219. Springer-Verlag GmbH, Berlin Heidelberg, 2003.

[56] J. A. Armstrong, N. Bloembergen, J. Ducuing, and P. S. Pershan. Interactions between light waves in a nonlinear dielectric. *Phys. Rev.*, 127 (6):1918–1939, 1962.

[57] P. A. Franken and J. F. Ward. Optical harmonics and nanlinear phenomena. *Reviews of Modern Physics*, 35(1):23–39, 1963.

[58] U. Strößner. *Development of optical synthesizers*. PhD thesis, Universität Konstanz, 2001.

[59] G. D. Boyd, R. C. Miller, K. Nassau, W. L. Bond, and A. Savage. LiNbO$_3$: an efficient phase matchable nonlinear optical material. *Appl. Phys. Lett.*, 5(11):234–236, 1964.

[60] R. S. Weis and T. K. Gaylord. Lithium niobate: Summary of physical properties and crystal structure. *Appl. Phys. A*, 37(4):191–203, 1985.

[61] Francesco Segato. http://solidi4.padova.infm.it/research.html, 2000. LiNbO$_3$ Group Home Page, University of Padova, Italy.

[62] D. R. Weise. Aufbau und effiziente Frequenzkonversion eines schmal-bandigen Hochleistungs-Dauerstrich-Lasers. Master's thesis, Universität Konstanz, 1999.

[63] S. C. Abrahams, J. M. Reddy, and J. L. Bernstein. Ferroelectric lithium niobate. 3. Single crystal X-Ray diffraction study at 24 °C. *J. Phys. Chem. Solids*, 27:997, 1966.

[64] D. H. Jundt, G. A. Magel, M. M. Fejer, and R. L. Byer. Periodically poled LiNbO$_3$ for high-efficiency second-harmonic generation. *Appl. Phys. Lett.*, 59(21):2657–2659, 1991.

[65] M. Yamada and K. Kishima. Fabrication of periodically reversed domain structure for SHG in LiNbO$_3$ by direct electron beam lithography at room temperature. *Electron. Lett.*, 27(10):828–829, 1991.

[66] M. Yamada, N. Nada, M. Saitoh, and K. Watanabe. First-order quasi-phase matched LiNbO$_3$ waveguide periodically poled by applying an external field for efficient blue second-harmonic generation. *Appl. Phys. Lett.*, 62(5):435–436, 1993.

[67] W. K. Burns, W. McElhanon, and L. Goldberg. Second harmonic generation in field poled, quasi-phase-matched, bulk LiNbO$_3$. *IEEE Photon. Technol. Lett.*, 6(2):252–254, 1994.

[68] L. E. Myers, R. C. Eckardt, M. M. Fejer, R. L. Byer, W. R. Bosenberg, and J. W. Pierce. Quasi-phase-matched optical parametric oscillators in bulk periodically poled LiNbO$_3$. *J. Opt. Soc. Am. B*, 12(11):2102–2116, 1995.

[69] G. J. Edwards and M. Lawrence. A temperature-dependant dispersion equation for congruently grown lithium niobate. *Opt. Quantum Electron.*, 16:373, 1984.

[70] D. H. Jundt. Temperature-dependent Sellmeier equation for the index of refraction, n_e, in congruent lithium niobate. *Opt. Lett.*, 22(20):1553–1555, 1997.

[71] Y. R. Shen. *The Principles of Nonlinear Optics*. Wiley, New York, 1984.

[72] C. Fabre, P. F. Cohadon, and C. Schwob. Cw optical parametric oscillators: single mode operation and frequency tuning properties. *Quantum Semiclass. Opt.*, 9:165–172, 1997.

[73] R. C. Eckardt, C. D. Nabors, W. J. Kozlovsky, and R. L. Byer. Optical parametric oscillator frequency tuning and control. *J. Opt. Soc. Am. B*, 8(3):646–667, 1991.

[74] R. W. P. Drever, J. L. Hall, F. V. Kowalski, J. Hough, G. M. Ford, A. J. Munley, and H. Ward. Laser phase and frequency stabilization using an optical resonator. *Appl. Phys. B*, 31(2):97–105, 1983.

[75] D. Dekorsy. Doppler-freie Spektroskopie mit einem Optisch Parametrischen Oszillator. Master's thesis, Universität Konstanz, 2000.

[76] T. J. Kane and R. L. Byer. Monolithic, unidirectional single-mode Nd:YAG ring laser. *Opt. Lett.*, 10(2):65–67, 1965.

[77] T. Schuldt. Frequenzstabilisirter Nd:YAG-Laser für Weltraumanwendungen. Master's thesis, Universität Hamburg, 2003.

[78] H. Müller, S. Herrmann, T. Schuldt, M. Scholz, E. Kovalchuk, and A. Peters. Offset compensation by use of amplitude-modulated sidebands in optical frequency standards. *Opt. Lett.*, 28(22):2186–2188, 2003.

[79] M. Hercher and H. A. Pike. Tunable dye laser configurations. *Opt. Commun.*, 3(1):65–67, 1971.

[80] H. W. Kogelnik, E. P. Ippen, A. Dienes, and C. V. Shank. Astigmatically compensated cavities for cw dye lasers. *IEEE J. Quant. Electronics*, 8(3):373–379, 1972.

[81] J. L. Hall, L. Hollberg, T. Baer, and H. G. Robinson. Optical heterodyne saturation spectroscopy. *Appl. Phys. Lett.*, 39(9):680–682, 1981.

[82] R. L. Barger and J. L. Hall. Pressure shift and broadening of methane line at 3.39 μm studied by laser-saturated molecular absorption. *Phys. Rev. Lett.*, 22(1):4–8, 1969.

[83] T. W. Hänsch. Spectroscopic applications of tunable lasers. In A. Mooradian, T. Jaeger, and P. Stokseth, editors, *Tunable Lasers and Applications*, volume 3 of *Springer Series in Optical Sciences*, pages 326–339. Springer-Verlag, Berlin, 1976.

[84] Ye. V. Baklanov and V. P. Chebotayev. Narrow resonances of two-photon absorption of super-narrow pulses in a gas. *Appl. Phys.*, 12: 97–99, 1977.

[85] J. N. Eckstein, A. I. Ferguson, and T. W. Hänsch. High-resolution two-photon spectroscopy with picosecond light pulses. *Phys. Rev. Lett.*, 40 (13):847–850, 1978.

[86] F. Krausz, M. E. Fermann, T. Brabec, P. F. Curley, M. Hofer, M. H. Ober, Ch. Spielmann, E. Wintner, and A. J. Schmidt. Femtosecond solid-state lasers. *IEEE J. Quantum Electron.*, 28(10):2097–2122, 1992.

[87] Franz X. Kärtner, editor. *Few-cycle laser pulse generation and its applications*, volume 95 of *Topics in Applied Physics*. Springer-Verlag GmbH, Berlin Heidelberg, 2004.

[88] Th. Udem, J. Reichert, R. Holzwarth, T. Hänsch, and M. Kourogi. The measurement of large optical frequency differeces and the design of a new type of frequency chain. In *Proceedings of the 1999 Joint Meeting of The European Frequency and Time Forum and the IEEE International Frequency Control Symposium*, volume 2, pages 620–625. Institute of Electrical and Electronics Engineers, New York, 1999.

[89] Th. Udem, J. Reichert, R. Holzwarth, and T. W. Hänsch. Absolute optical frequency measurement of the cesium d_1 line with a mode-locked laser. *Phys. Rev. Lett.*, 82(18):3568–3571, 1999.

[90] Th. Udem, J. Reichert, R. Holzwarth, and T. W. Hänsch. Accurate measurement of large optical frequency differences with a mode-locked laser. *Opt. Lett.*, 24(13):881–883, 1999.

[91] Th. Udem, J. Reichert, R. Holzwarth, M. Niering, M. Weitz, and T. W. Hänsch. Measuring the frequency of light with mode-locked lasers. In A. N. Luiten, editor, *Frequency Measurement and Control: Advanced Techniques and Future Trends*, volume 79 of *Topics in Applied Physics*, pages 275–294. Springer-Verlag GmbH, Berlin Heidelberg, 2001.

[92] J. C. Knight, T. A. Birks, P. St. J. Russell, and D. M. Atkin. All-silica single-mode optical fiber with photonic crystal cladding. *Opt. Lett.*, 21 (21):1547–1549, 1996.

[93] J. K. Ranka, R. S. Windeler, and A. J. Stentz. Visible continuum generation in air-silica microstructure optical fibers with anomalous dispersion at 800 nm. *Opt. Lett.*, 25(1):25–27, 2000.

[94] J. Reichert, M. Niering, R. Holzwarth, M. Weitz, Th. Udem, and T. W. Hänsch. Phase coherent vacuum-ultraviolet to radio frequency comparison with a mode-locked laser. *Phys. Rev. Lett.*, 84(15):3232–3235, 2000.

[95] R. Holzwarth, Th. Udem, T. W. Hänsch, J. C. Knight, W. J. Wadsworth, and P. St. J. Russell. Optical frequency synthesizer for precision spectroscopy. *Phys. Rev. Lett.*, 85(11):2264–2267, 2000.

[96] J. Ye, L. S. Ma, and J. L. Hall. Molecular iodine clock. *Phys. Rev. Lett.*, 87(27):270801–1–4, 2001.

[97] M. Bellini and T. W. Hänsch. Phase-locked white-light continuum pulses: toward a universal optical frequency-comb synthesizer. *Opt. Lett.*, 25(14):1049–1051, 2000.

[98] J. D. Jost, J. L. Hall, and J. Ye. Continuously tunable, precise, single frequency optical signal generator. *Opt. Express*, 10(12):515–520, 2002.

[99] S. A. Diddams, Th. Udem, J. C. Bergquist, E. A. Curtis, R. E. Drullinger, L. Hollberg, W. M. Itano, W. D. Lee, C. W. Oates, K. R. Vogel, and D. J. Wineland. An optical clock based on a single trapped ^{199}Hg$^+$ ion. *Science*, 293:825–828, 2001.

[100] S. A. Diddams, L. Hollberg, L.-S. Ma, and L. Robertsson. Femtosecond-laser-based optical clockwork with instability $\leq 6.3 \times 10^{-16}$ in 1 s. *Opt. Lett.*, 27(1):58–60, 2002.

[101] P. Gill, G. P. Barwood, H. A. Klein, G. Huang, S.A. Webster, P. J. Blythe, K. Hosaka, S. N. Lea, and H. S. Margolis. Trapped ion optical frequency standards. *Meas. Sci. Technol.*, 14:1174–1186, 2003.

[102] Ch. Tamm, T. Schneider, and E. Peik. Trapped ion optical frequency standards for laboratory tests of alpha-variability. *Lect. Notes Phys.*, 648:247–261, 2004.

[103] M. Zimmermann, Ch. Gohle, R. Holzwarth, Th. Udem, and T. W. Hänsch. Optical clockwork with an offset-free difference-frequency comb: accuracy of sum- and difference-frequency generation. *Opt. Lett.*, 29 (3):310–312, 2004.

[104] O. D. Mücke, O. Kuzucu, F. N. C. Wong, E. P. Ippen, F. X. Kärtner, S. M. Foreman, D. J. Jones, L.-S. Ma, J. L. Hall, and J. Ye. Experimental implementation of optical clockwork without carrier-envelope phase control. *Opt. Lett.*, 29(23):2806–2808, 2004.

[105] S. M. Foreman, A. Marian, J. Ye, E. A. Petrukhin, M. A. Gubin, O. D. Mücke, F. N. C. Wong, E. P. Ippen, and F. X. Kärtner. Demonstration of a He-Ne/CH_4-based optical molecular clock. *Opt. Lett.*, 30(5):570–572, 2005.

[106] A. Amy-Klein, A. Goncharov, C. Daussy, C. Grain, O. Lopez, G. Santarelli, and C. Chardonnet. Absolute frequency measurement in the 28-THz spectral region with a femtosecond laser comb and a long-distance optical link to a primary standard. *Appl. Phys. B*, 78: 25–30, 2004.

[107] S. M. Foreman, D. J. Jones, and J. Ye. Flexible and rapidly configurable femtosecond pulse generation in the mid-IR. *Opt. Lett.*, 28(5):370–372, 2003.

[108] T. Fuji, A. Apolonski, and F. Krausz. Self-stabilization of carrier-envelope offset phase by use of difference-frequency generation. *Opt. Lett.*, 29(5):632–634, 2004.

[109] H. R. Telle, B. Lipphardt, and J. Stenger. Kerr-lens, mode-locked lasers as transfer oscillators for optical frequency measurements. *Appl. Phys. B*, 74:1–6, 2002.

[110] Fritz Riehle. *Frequency standards: basics and applications*. Wiley-VCH, Weinheim, 2004.

[111] F. Riehle and J. Helmcke. Optical frequency standards based on neutral atoms and molecules. In A. N. Luiten, editor, *Frequency Measurement and Control: Advanced Techniques and Future Trends*, volume 79 of *Topics in Applied Physics*, pages 95–129. Springer-Verlag GmbH, Berlin Heidelberg, 2001.

[112] A. A. Madej and J. E. Bernard. Single-ion optical frequency standards and measurement of their absolute optical frequency. In A. N. Luiten, editor, *Frequency Measurement and Control: Advanced Techniques and Future Trends*, volume 79 of *Topics in Applied Physics*, pages 153–195. Springer-Verlag GmbH, Berlin Heidelberg, 2001.

[113] P. Lemonde, Ph. Laurent, G. Santarelli, M. Abgrall, Y. Sortais, S. Bize, C. Nicolas, S. Zhang, A. Clairon, N. Dimarcq, P. Petit, A. G. Mann, A. N. Luiten, Sh. Chang, and Ch. Salomon. Cold-atom clocks on earth and in space. In A. N. Luiten, editor, *Frequency Measurement and Control: Advanced Techniques and Future Trends*, volume 79 of *Topics in Applied Physics*, pages 131–153. Springer-Verlag GmbH, Berlin Heidelberg, 2001.

[114] A. Husakou and J. Herrmann. Supercontinuum generation of higher-order solitons by fission in photonic crystal fibers. *Phys. Rev. Lett.*, 87 (20):203901–1 – 203901–4, 2001.

[115] J. Herrmann, U. Griebner, N. Zhavoronkov, A. Husakou, D. Nickel, J. C. Knight, W. J. Wadsworth, P. St. J. Russell, and G. Korn. Experimental evidence for supercontinuum generation by fission of higher-order solitons in photonic fibers. *Phys. Rev. Lett.*, 88(17):173901–1 – 173901–4, 2002.

[116] A. V. Husakou and J. Herrmann. Supercontinuum generation, four-wave mixing, and fission of higher-order solitons in photonic-crystal fibers. *J. Opt. Soc. Am. B*, 19(9):2171–2182, 2002.

[117] M. Scholz. Aufbau und Charakterisierung eines kryogenen Nd:YAG-Lasers. Master's thesis, Universität Konstanz, 2003.

[118] St. Seel, R. Storz, G. Ruoso, J. Mlynek, and St. Schiller. Cryogenic optical resonators: A new tool for laser frequency stabilization at the 1 Hz level. *Phys. Rev. Lett.*, 78(25):4741–4744, 1997.

[119] U. Strößner, J.-P. Meyn, R. Wallenstein, P. Urenski, A. Arie, G. Rosenman, J. Mlynek, St. Schiller, and A. Peters. Single-frequency continuous-wave optical parametric oscillator system with an ultrawide tuning range of 550 to 2830 nm. *J. Opt. Soc. Am. B*, 19(6):1419–1424, 2002.

[120] P. Gross, M. E. Klein, T. Walde, K.-J. Boller, M. Auerbach, P. Wessels, and C. Fallnich. Fiber-laser-pumped continuous-wave singly resonant optical parametric oscillator. *Opt. Lett.*, 27(6):418–420, 2002.

[121] S. Y. T. van de Meerakker, P. H. M. Smeets, N. Vanhaecke, R. T. Jongma, and G. Meijer. Deceleration and electrostatic trapping of OH radicals. *Phys. Rev. Lett.*, 94:023004, 2005.

Acknowledgements

with me the office, for his readiness to help and for his support every time I needed it. Besides that, I am very indebted to Thilo and Sven for the thorough reading of this thesis and many invaluable corrections and wording suggestions. Many thanks also goes to Malte Schmidt for his very helpful recommendations during the final thesis edition.

My heartfelt gratefulness goes to Stephan Götzinger, Thomas Aichele, Leonardo Menezes and Andrea Mazzei for unforgettable friendly climate outside the lab and many evenings spending together, for many conversations and for always being open for my questions and for assistance. The motivation they provided as well as our conversations relating to all sides of life, and our journeys, and observing the Solar Eclipse of 31. May 2003 will never be forgotten.

I would like to thank all people from the QOM, NANO and AMO groups at the Hausvogteiplatz, who worked here from the very beginning and who came recently for the nice friendly environment.

It is difficult to express my gratitude and all my love to my parents and my brother for supporting me through good and bad times, for their encouragement and real interest to help me and solve all my problems, and for their never-ending love. I would also like to thank my relatives and my parents in law for all the good they have done for me.

The last but not the least words of my acknowledgments I would like to dedicate to my family, my beloved wife Anna and my lovely children Dmitry and Tatiana. This work would not be possible without their tremendous patience and great love.

The endless support and assistance of my dear Anna and her encouragement and belief in me is one of the most important influences on the success of this work.

Selbständigkeitserklärung

Hiermit erkläre ich, die vorliegende Arbeit selbständig ohne fremde Hilfe verfasst und nur die angegebene Literatur und Hilfsmittel verwendet zu haben.

Ich habe mich anderwärts nicht um einen Doktorgrad beworben und besitze einen entsprechenden Doktorgrad nicht.

Ich erkläre die Kenntnisnahme der dem Verfahren zugrunde liegenden Promotionsordnung der Mathematisch-Naturwissenschaftlichen Fakultät I der Humboldt-Universität zu Berlin.

Berlin, den 22. Dezember 2006
Evgeny Kovalchuk